UNIVERSITÀ DI PARMA

UNIVERSITA' DEGLI STUDI DI PARMA

DOTTORATO DI RICERCA IN SCIENZE CHIMICHE

CICLO XXXVI

SMART ELECTROCHEMICAL BIOSENSORS FOR POINT-OF-CARE TESTING

Coordinatore:
Chiar.ma Prof.ssa Bacchi Alessia

Tutor:
Chiar.mo Prof. Giannetto Marco

Dottoranda: Chiara Giliberti

Anni Accademici 2020/2021 – 2022/2023

SUMMARY

1 *Biosensors for Point-of-Care Testing* 5

1.1 Introduction.....5

1.2 Classification of biosensors 7

1.3 Electrochemical sensors.....8

1.4 Amperometric sensors 10

1.5 Immobilization techniques of bioreceptors in biosensors....13

1.6 Nanostructured- materials for biosensing 15

1.6.1 Carbon Nanotubes (CNT) 15

1.6.2 Gold Nanoparticles (GNP) 17

1.6.3 Magnetic Particles.....18

1.7 Screen printed electrodes (SPE).....20

1.8 Point-Of-Care Testing (Poct) 21

1.9 Internet Of Things (Iot).....23

1.10 References.....26

***2* *Immunosensors for SARS-CoV-2-detection* 31**

2.1 Antigens and antibodies.....31

2.2 Classification of immunosensors.....33

2.2.1 Label-free immunosensors.....33

2.2.2 Labelled immunosensors 34

2.3 SARS-CoV-2 and Coronavirus Disease (COVID-19).....35

2.3.1 Spike protein 36

2.3.2 Nucleocapsid protein 37

2.4 SARS-CoV-2 immune response.....38

2.5 SARS-CoV-2 detection methods 39

2.6 References.....41

***3* *SARS-CoV-2 serological tests: state of the art* 44**

3.1 Aim of the study 45

3.2 Material and methods.....46

3.2.1 Materials 46

3.2.2 Buffer composition....47
3.2.3 Equipments....47
3.2.4 Serum specimens....50
3.2.5 Anti-N Immunosensor fabrication....51
3.2.6 Anti-S Immunosensor fabrication....52
3.2.7 Data acquisition and manipulation for anti-N and anti-S immunosensors....53
3.3 Results and discussion....55
3.3.1 Electrode surface immobilization....55
3.3.2 Anti-N Immunosensor setup....55
3.3.3 Evaluation of different parameters for anti-N immunosensors....56
3.3.4 Linearity assessment....59
3.3.5 Validation in clinical samples....61
3.3.6 Anti-S Immunosensor setup....62
3.3.7 Evaluation of different parameters for anti-S immunosensors....62
3.3.8 Linearity assessment....69
3.3.9 Validation in clinical samples....70
3.4 References....72
4 SARS-CoV-2 antigen testing **....76**
4.1 Aim of the study....79
4.2 Materials and Methods....81
4.2.1 Materials and Chemicals....81
4.2.2 Buffers Composition....82
4.2.3 Equipment....82
4.2.4 Immunoassay protocol....84
4.2.5 Experimental Design....85
4.2.6 Analytical Validation....85
4.2.7 SARS-CoV-2 Pseudovirus Generation....86
4.3 Results and discussion....87

4.3.1 Immunosensor setup 87
4.3.2 Comparison of different electrode platforms.....87
4.3.3 Evaluation of anti-S1 IgM and anti-S1 IgG as receptors 88
4.3.4 Immunosensor optimization 90
4.3.5 Linearity assessment 91
4.3.6 Cross-reactivity.....92
4.3.7 Whole Lentiviruses Expressing S1 protein analysis....93
4.3.8 Use of Machine Learning techniques for sample classification 93
4.4 References.....97
***5 Genosensors for cancer diagnosis by liquid biopsy*..... 100**
5.1 Genosensors working principle..... 100
5.1.1 Nucleic acids as capture probes..... 100
5.1.2 Electrochemical transduction 104
5.2 Liquid biopsy..... 105
5.2.1 Biomarkers for liquid biopsy 107
5.2.2 CtDNA detection technologies..... 109
5.3 Colorectal cancer (CRC) 110
5.4 G12D Single Nucleotide Variation (Snv)..... 111
5.5 Biosensors for ctDNA analysis in liquid biopsy..... 113
5.6 Aim of the study 116
5.7 Materials and methods 117
5.7.1 Materials 117
5.7.2 Buffers composition 118
5.7.3 PNA Synthesis..... 119
5.7.4 Genoassay procedure..... 120
5.8 Results and discussion..... 123
5.8.1 Magneto-genosensing assay setup 123
5.8.2 Evaluation of incubation time 124

5.8.3 Optimization of magneto magneto-genosensing assay 126
5.8.4 Linearity assessment 127
5.8.5 Performance of the readout instrumentation 130
5.8.6 Validation on gDNA samples 131
5.9 Supplementary materials 133
5.10 References 136
6 *Micropore nanoelectrodes* 143
6.1 Introduction 143
6.2 Materials and methods 146
6.2.1 Materials and chemicals 146
6.2.2 Equipment 146
6.2.3 Micropore nanoelectrodes preparation 147
6.3 Results and discussion 149
6.3.1 Fabrication protocol 149
6.3.2 Pore punching methods 151
6.3.3 Capping layer methods 152
6.3.4 Electropolymerization 154
6.3.5 Tests with beads 156
6.4 Conclusion and future outlooks 157
6.5 References 158

1 *Biosensors for Point-of-Care Testing*

1.1 INTRODUCTION

Chemical sensors are defined by the International Union of Pure and Applied Chemistry (IUPAC) as "devices that transform chemical information, ranging from concentration of a specific sample component to total composition analysis, into an analytically useful signal"[1]. They are typically based on two components: a chemical or molecular recognition system (receptor) and a physicochemical transducer. The receptor represents the recognition system which interacts with analytes, thus resulting in a change in physical properties detectable by the transducer. Furthermore, in the context of chemical sensors, a biosensor is defined as "a device that uses specific biochemical reactions mediated by isolated enzymes, immunosystems, tissues, organelles or whole cells to detect chemical compounds usually by electrical, thermal or optical signals" [2]. They are used to monitor molecular processes, like DNA interactions, enzymatic reactions, antigen/antibody complexes or cellular communication process[3]. Indeed, they proved useful in a wide range of applications such as environmental monitoring, disease detection, drug discovery, detection of pollutants, food safety and quality [4, 5].

Typically, they present different components[6]:

- Bioreceptor: a biological component that specifically recognizes the analyte, such as enzymes, nucleic acids, antibodies. The interaction process between receptor and analyte generating the signal is defined "bio-recognition".
- Transducer: the portion that can convert the bio-recognition between bioreceptor and analyte into a measurable signal, correlated to the amount of target molecule.

- Electronics: in this part the signal generated by the transducer is processed and prepared for the display. It performs signal conditioning, like amplification and conversion of the signal from analogue form into digital form. Once the signal is processed, it is quantified by the display, that is a user interpretation system, for example a computer. It is typically composed of hardware and software with the aim of generating accessible signal that can be tabular, numeric or an image.

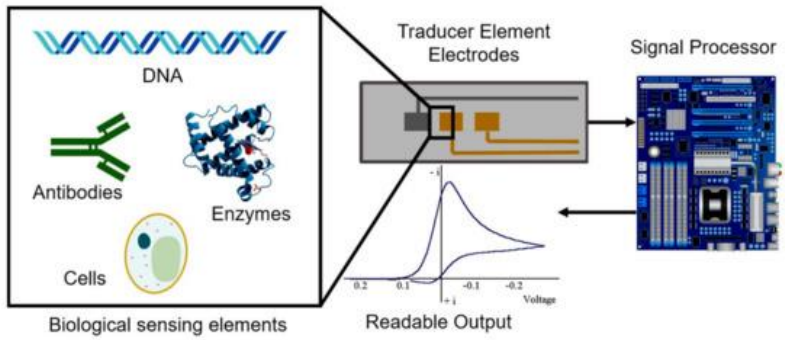

Figure 1.1: Structure and components of a biosensor. Reprinted with permission from Ref. 6 Copyright© 2018. MDPI, Basel. Switzerland.

An ideal biosensor system should be cost-effective, compact, specific, and possess the ability to sustain its functionality over an extended period. In addition to these characteristics, various analytical parameters are essential to consider for an ideal biosensor system, such as:[7]

- Selectivity: the ability of the bioreceptor to detect a class of compounds.
- Specificity: the ability to determine a single analyte in a complex sample.
- Sensitivity: the signal variation of signal obtained consequently to the change in concentration of the analyte.
- Limit of Detection (LOD): the lowest value of analyte concentration that gives a sensor response statistically different from the blank signal.

- Limit of Quantification (LOQ): the lowest concentration of analyte quantified with a specific degree of accuracy and precision.
- Linearity range: the interval in which the biosensor's response linearly correlates with the concentration of the analyte.
- Response Time: the time taken by the biosensor to provide a measurable signal from zero concentration to a step change in concentration.
- Hysteresis: the difference in output when a value is approached with increasing and a decreasing analyte concentration range.
- Reproducibility: it is verified when the same sample is measured multiple times and the biosensors results are consistent and accurate.
- Stability: ability to maintain functionality over time, crucial for continuous monitoring applications.
- Life cycle: time over which the sensor will operate.

1.2 CLASSIFICATION OF BIOSENSORS

Different criteria have been used to classify biosensors; the most commonly used are based on biorecognition element and signal transduction.[8,9]

Based on the biorecognition element, biosensors can be classified as:

- Enzymatic biosensors: among the most common biosensors classes, where the working principle is based on the catalytic reaction and binding potential of the enzyme. Their principle is to convert the enzyme-catalyzed non-detectable substrates into detectable species. In fact, enzyme reactions usually involve the release of measurables species, like ions, oxygen, etc. Among the most used enzymes for this kind of biosensors, there are oxidoreductases and hydrolase.
- Nucleic acid-based biosensors (genosensors): typically based on the generation of a double stranded DNA resulting from the interaction of two

single-strand DNA sequences. Normally, hydrogen bonds and Van der Waals interactions occur in these biosensors. They are characterized by high affinity, stability and specificity. Nucleic-acid mimics are also often used as receptors in biosensors due to their advantageous characteristics, like enhanced affinity, nuclease resistance, higher selectivity[10].

- Immunosensors: in this type of biosensors antibodies are embedded as bioreceptors allowing for high specificity of the molecular recognition of antigen to form a stable immune-complex. They have a wide application range due to their high sensitivity and selectivity, as well as the possibility to design recombinant antibodies.
- Microbial or whole-cell biosensors: based on luminescence reporter genes, they are widely used for medical applications.

According to classification based on transducers, biosensors are divided into electrochemical, optical, thermal, electronic and gravimetric.

1.3 ELECTROCHEMICAL SENSORS

Among the most investigated biosensors there are electrochemical sensors, where following the recognition event between bioreceptors and analytes, a variation in concentration of species occurs and is detected through electrochemical measurements. According to the transducer principle, they are furtherly divided into potentiometric, amperometric, conductometric and voltammetric biosensors.

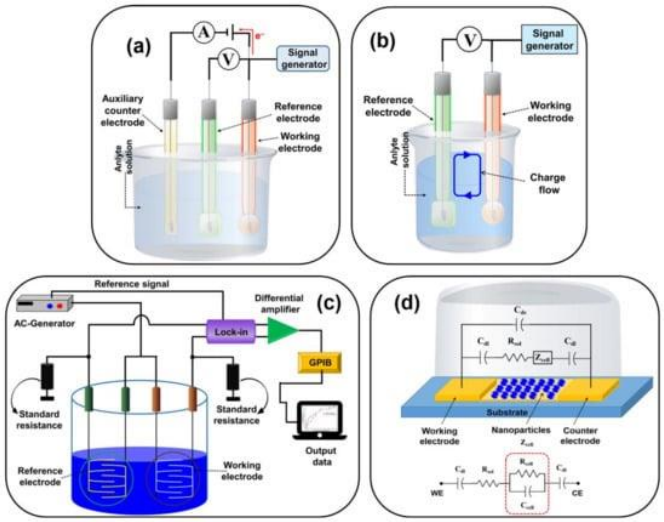

Figure 1.2: Schematic representation of (a) amperometric/voltametric (b) potentiometric, (c) conductometric biosensors, and (d) equivalent circuit of impedimetric biosensor. Reprinted with permission from Ref. 11 © 2023 MDPI, Basel, Switzerland.

Potentiometric sensors are typically based on a polymeric membrane integrated on Ion-Selective Electrodes (ISE) and Ion-Selective Field Effect Transistors (ISFET), and they measure the potential change at one electrode against another[11]. They have been widely exploited for key electrolytes testing such as H^+,NH_4^+, and other ions, as well as biomolecules including glucose, urea, penicillin, etc. [12,13].

Voltammetric biosensors measure the current when a controlled variation of potential is applied. In this context, in amperometric sensors a constant potential is applied, and the current produced by electrochemical oxidation or reduction of electroactive species is measured.

Impedimetric sensors are label-free biosensors. They can be used to quantify interactions between biomolecules. Indeed, changes in the dielectric constant or resistance are determined from interaction between target biomolecule and the receptor on the sensor surface.

Finally, conductimetric sensors measure the change in the electrical conductivity of a cell solution. Therefore, changes in conductivity can be observed in presence of electrochemical reactions.

1.4 AMPEROMETRIC SENSORS

Amperometric transduction allows to measure the current produced from electrochemical oxidation or reduction of the active species as a result of a constant or variable potential applied to the working electrode with respect to the reference electrode. In this way, they allow the specific detection by setting the potential for oxidation or reduction of the analyte. The driving force determining electron transfer reaction of electroactive species, leading to their gain (reduction) or loss (oxidation) of electrons, is the applied potential. The resulting current is a direct measure of the speed of the electron transfer reaction. The latter represents the recognition process and is proportional to the analyte concentration. Conversely, in voltammetric transduction, a current is measured during controlled variations of the potential[14 15].

These biosensors are usually based on two or three-electrode systems, composed of:

Working Electrode (WE): is where the reaction of oxidation or reduction takes place. Usually, it is composed of noble metals (gold, silver, platinum) or carbon-based material (glassy carbon, graphene, graphite). Its size is variable, depending on the application.

Reference Electrode (RE): it has a determined and stable potential. It is used to measure the electrochemical potential, given by the difference between WE and RE. The most used are Silver/Silver Chloride electrodes (Ag/AgCl), where an Ag wire is coated with AgCl and dipped into NaCl solution, and Saturated Calomel Electrode, with mercurous chloride (Hg_2Cl_2).

Counter or auxiliary Electrode (CE): it does not take part in the electrochemical reaction and is used to establish a current flow with the working electrode.

It is usually composed of an inert material, like gold, platinum, graphite or glassy carbon.

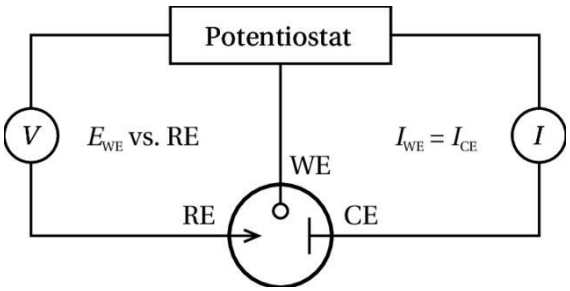

Figure 1.3: Scheme of a three-electrode electrochemical cell and potentiostat. Reprinted with permission from Ref. 16 © 2023 MDPI, Basel, Switzerland[16]

The electrolytic current flowing through the working electrode is recorded as a function of the applied potential.[17]

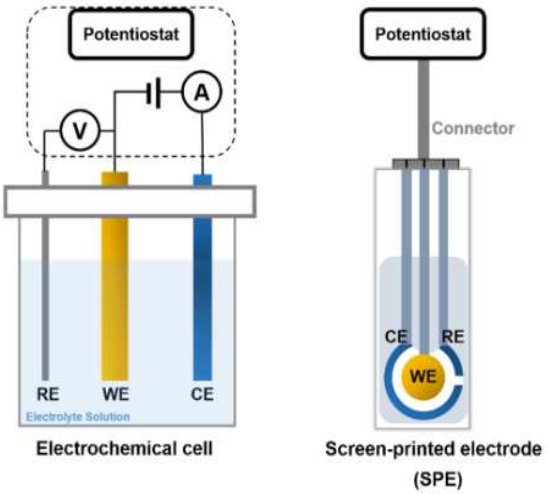

Figure 1.4: Three-electrode system with Reference Electrode (RE), Working Electrode (WE) and counter Electrode (CE) Reprinted with permission from Ref. 18 © 2020 MDPI, Basel, Switzerland[18].

In these systems, the total current that flows through the working electrode has two components: the faradic current and the capacitive current. The former follows the Faraday laws and depends on the electroactive compound discharge, the latter is generated by the presence of an electric double layer at the interface electrode-solution, resulting from the high concentration of the supporting

electrolyte in solution[19]. Since it is directly correlated to the active species and consequently to the analyte, the faradic current is the one of analytic interest. The capacitive current, instead, being caused by the presence of the supporting electrolyte, does not depend on the active species concentration, and determines a background noise of the current output[20].

Different electrochemical techniques can be applied using the three-electrode cell:

- Linear Sweep Voltammmetry: is the simplest voltammetric technique. Here the resulting response current is measured when a linear potential ramp.
- Cyclic Voltammetry: this technique is label-free and commonly used for studying redox processes, reaction intermediates, and the stability of reaction products. Here, the potential is varied in both forward (oxidation) and reverse (reduction) directions while monitoring the current for repeated cycles. The typical voltammogram from CV shows forward and reverse peaks, giving important information on the reversibility of the reaction involving the analyte.
- Chronoamperometry: current is measured as a function of time when a constant potential is applied between working and reference electrode.
- Differential Pulse Voltammetry: the waveform consists of small periodical potential pulses of constant amplitude superimposed to a linear scan. This technique is part of the pulsed methods, where the current is sampled twice for each pulse: the first point is registered before application of the pulse, the second at the end of the pulse, allowing the decay of capacitive current and a significant enhancement of signal. The calculated difference between the two registered currents is measured against the potential and gives a higher sensitivity with respect to other methods. In biosensors, this technique is widely used to detect and quantify biomolecules.

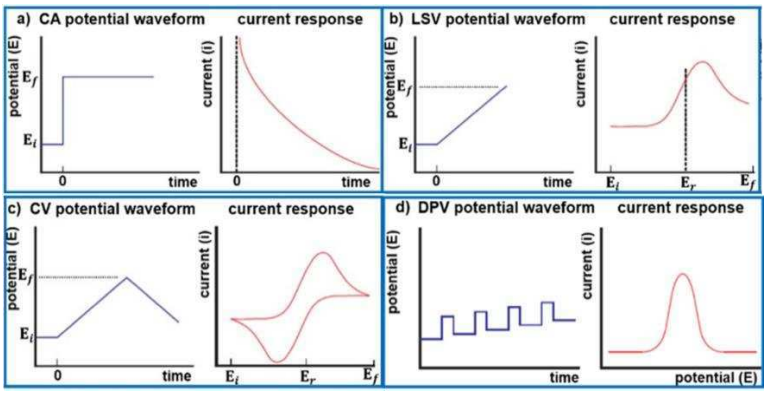

Figure 1.5: Electrochemical methods' waveform and current responses: chronoamperometry, differential pulse voltammetry, linear sweep voltammetry, cyclic voltammetry. Adapted with permission from Ref.21 © 2015, Taylor and Francis[21].

1.5 IMMOBILIZATION TECHNIQUES OF BIORECEPTORS IN BIOSENSORS

A crucial aspect in the construction of biosensors is the immobilization of the biorecognition element onto the electrode surface. Different techniques have been exploited to preserve the function, activity and structure after the biomolecules have been immobilized. They are divided into physical or reversible immobilization and chemical or irreversible immobilization[22].

In physical immobilization, biomolecules are attached to the surface without formation of chemical covalent bonds. They include physical adsorption and physical entrapment.

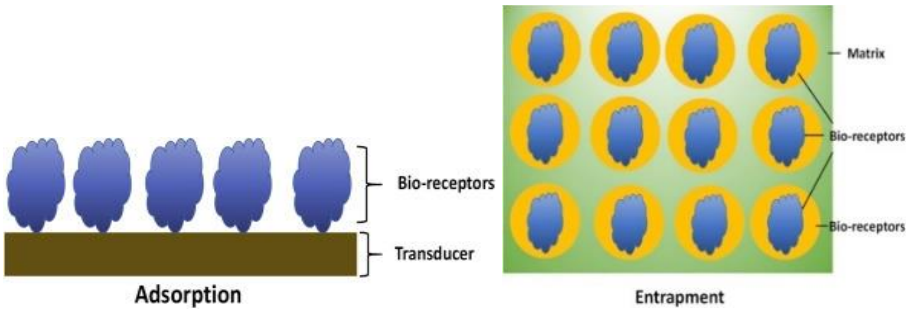

Figure 1.6: Representation of physical adsorption (Left) and physical entrapment (Right) Reprinted with permission from Ref. 12 © 2018 Elsevier Inc. All rights reserved[12]

- In physical adsorption, the bioreceptor can absorb directly on the surface by electrostatic interactions or weak attractive forces, like van der Waals

interactions, hydrogen or ionic bonding. It is advantageous due to the simple and economic process and reversibility, but the "weakness" of immobilization can make it sensitive to pH, temperature and ionic strength, leading to loss of efficiency and bioreceptor desorption.

- In physical entrapment, the bioreceptor is included within a porous matrix through covalent or non-covalent bonds. Different techniques are used in this process: electropolymerization, sol-gel process and microencapsulation [5,12].

In chemical immobilization, instead, covalent bonds are formed between the bioreceptor functional group and the electrode surface. These techniques are divided into direct covalent bonding and covalent cross-linking.

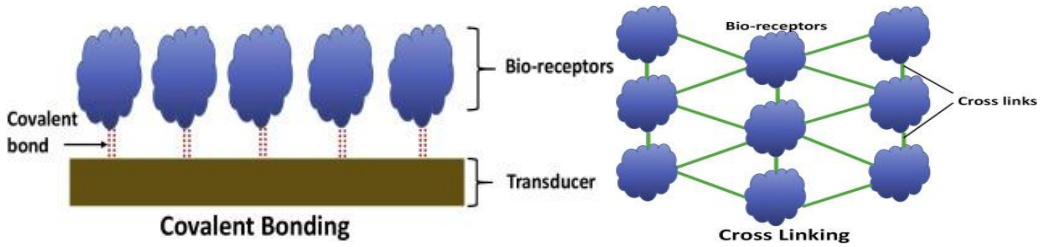

Figure 1.7: Representation of Covalent bonding (Left) and Cross Linking (Right) Reprinted with permission from Ref.12 © 2018 Elsevier Inc. All rights reserved[12].

Covalent bonding is among the most used immobilization techniques: it depends on the interaction between functional groups of the bioreceptor and reactive group of the surface, giving strong resistance to environmental changes. Different functional groups can be generated at the electrode surface to form covalent bonds, also by using magnetic particles or nanomaterials like carbon nanotubes.

Conversely, in cross-linking no support is involved, but with the introduction of polyfunctional reagents that act as linkers to connect the different molecules, bioreceptors are directly linked through formation of covalent bonds.

1.6 NANOSTRUCTURED- MATERIALS FOR BIOSENSING

In recent years, the integration of nanomaterials in biosensors has been strongly exploited due to the advantages of developing powerful analytical devices which are easy-to-handle, cost-effective, rapid, highly sensitive and selective.[23] Nanomaterials are chemical substances or materials with particle sizes between 1 to 100 nanometres in at least one dimension. They are classified, according to their dimensions, in 0D (nanoparticles), 1D (nanowires, nanotubes), 2D (nanosheets, thin-film multilayers) and 3D (nanocomposites) materials depending on how many dimensions of the materials are in the nanoscale. The use of these nanomaterials to develop analytical devices brought several advantages in different fields, like health monitoring[24], clinical diagnostics[25], food safety[26] and environmental monitoring[27].They can be used in electrochemical sensors for different applications, including sample preparation or preconcentration, bioreceptor immobilization and signal enhancement. [28]Different properties of nanomaterials make them a valuable tool for developing biosensors. In fact, due to their dimensions, they provide signal amplification, improve interactions with chemical and biological reagents and allow to immobilize specific moieties of biological reagents. Moreover, they possess highly tuneable size, charge, shape and physicochemical characteristics, thus allowing to adapt nanomaterials properties to different biosensors. Furthermore, one of the most important advantages is that they increase the surface area of the electrode platform, enhancing catalytic activity and sensing area. Here three different nanomaterials are discussed: gold nanoparticles, carbon nanotubes and magnetic particles.

1.6.1 Carbon Nanotubes (CNT)

Carbon-based materials are widely used to modify screen-printed electrodes due to their excellent properties[29]. Among them, carbon nanotubes are commonly used

as nanomaterials. They are hollow cylindrical tubes comprising of sp^2 hybridized graphene sheets. They are mainly divided into single-walled carbon nanotubes (SWCNT) and multi-walled carbon nanotubes (MWCNT).

SWCNT are formed by a single graphene sheet rolled up into a seamless cylinder with a diameter of 0.5-1.5 nm. Two or more cylindrical shells of graphene sheets, instead, form MWCNTs. These sheets are disposed around a central core held together by der Waals forces occurring between them, with a diameter higher than 100 nm [30].

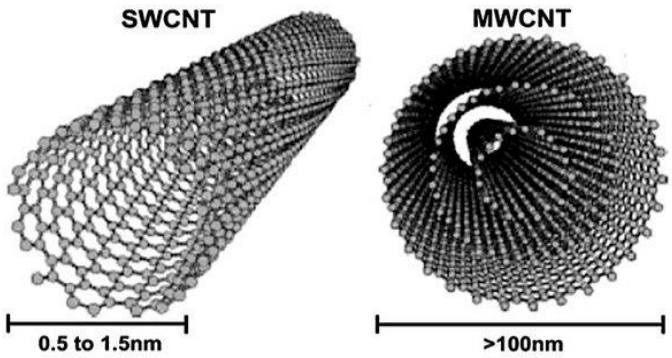

Figure 1.8: Representation of Single-walled carbon nanotubes (SWCNT) and multi-walled carbon nanotubes (MWCNT) Reprinted with permission from Ref. 29 © 2020 MDPI, Basel, Switzerland.

Different techniques for the synthesis of CNT have been reported like arc discharge, laser ablation and chemical vapour deposition[31]. They possess many desirable properties associated to their unique structure, functionality and morphology, such as excellent mechanical and electrical properties, chemical stability, high thermal conductivity, biocompatibility and good activity of electrocatalysis.

In particular, they have a high surface to volume ratio and enhanced electron transport properties, resulting in a bigger surface area and signal amplification when they are used for electrochemical biosensing. Moreover, they can be chemically functionalised to modify their properties or for the addition of biosensing elements. Indeed, CNTs can be functionalized by introducing chemical

groups at the π-conjugated skeleton with covalent binding, and by adsorption or wrapping with other molecules with non-covalent binding. Besides, the presence of carboxylic groups created by oxidation on their surface gives the chance to form nanocomposite materials by covalently binding several polymers, biomolecules and metallic particles. They are widely used in electrochemical biosensors, as the WE can be functionalized with CNT to enhance surface area for the loading of different molecules[32].

1.6.2 Gold Nanoparticles (GNP)

Noble metal nanoparticles are broadly used for electrochemical sensors and biosensors for *in vivo* and *in vitro* analysis due to their physical, chemical and electrochemical properties. They are very promising to improve sensitivity and selectivity of biosensors and can be used in medical field for early detection, cancer therapeutics[33,34], etc. In this context, gold nanoparticles are widely exploited for sensing thanks to different properties, and they can be obtained through simple preparation methods and fabrication process. One of the processes includes potentiostatic or potentiodynamic electrodeposition of nanogold starting from tetrachloroauric acid (HAuCl4)" [35]. Also, they possess high stability, great biocompatibility, wide electrochemical potential range and high catalytic affinity, thus allowing the miniaturization of sensing and biosensing platforms. [36,37.]

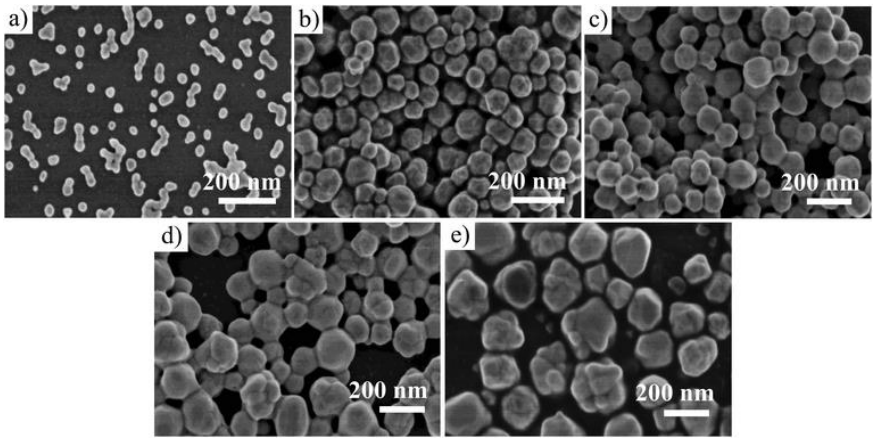

Figure 1.9: Scanning electron microscopy (SEM) images of the Au nanoparticles of different dimensions: (a) ~48 nm; (b) ~94 nm; (c) ~125 nm; (d) ~162 nm; (e) ~203 nm s Reprinted with permission from Ref. 37 © 2016. The Royal Society of Chemistry

For conjugation with bioelements, GNPs have been widely exploited as they are optimal substrates for the immobilization of bioreceptors on the electrode surface, due to the high affinity between sulphur and gold. In this way, proteins with aminoacids containing thiols, like cysteine and lysine, can be directly immobilized on the electrode surface. Moreover, the enhanced surface area allows the immobilization of a higher amount of receptor.

1.6.3 Magnetic Particles

Magnetic particles (MP), whose dimensions vary from nm to µm, are widely used in biosensing. In particular, iron oxides (γ-Fe_2O_3 and Fe_3O_4) are commonly used as they have highly active surface and chemical stability and they can be easily modified, allowing the functionalization with bioelements[38]. Among the several possible surface functionalization, carboxylic acid groups are exploited for the covalent binding of proteins, antibodies and other molecules.

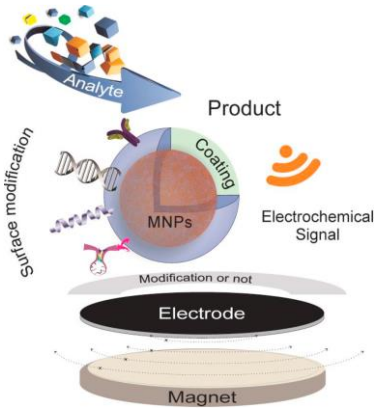

Figure 1.10: Schematic representation of application of Magnetic Nanoparticles (MNP) in electrochemical sensors. Reprinted with permission from Ref. 39 © 2021 Elsevier B.V. All rights reserved[39]

As they are able to respond in presence of a magnetic field and be dispersed upon removal of the magnet, MP allow easy separation of the solution and purification of biomolecules lowering the effect of matrix and impurities. Secondly, magnetic particles provide a large surface for the immobilization and the interactions of the bioreceptors, acting as effective solid supports for simple isolation, purification and pre-concentration of target analytes.

They have high sensitivity, reproducibility, ease of use and allow the reduction of the analysis times, making them ideal for highly sensitive and real-time measurement. In particular, they can be also integrated into devices aimed at developing Point-of-Care Testing bioassays.[40]

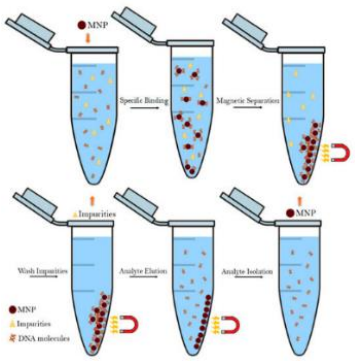

Figure 1.11: Schematic representation of magnetic separation of biomolecules with MP. Reprinted with permission from Ref. 39 © 2021 Elsevier B.V. All Rights reserved.

Magnetic particles can have different applications in bioassays:

- Sample enrichment and separation, as they provide easy separation with an external magnetic field and a specific interaction with biomolecules, avoiding non-specific absorption.
- Signal amplification, as they have a large surface area and mass.
- Signal read-out, as they can be used as magnetic labels to indicate the occurrence of interactions between molecules due to their good stability, ease of use and high signal-to-noise ratio.

All these nanomaterials are often exploited for the functionalization of miniaturized electrodes, for the development of portable devices.

1.7 SCREEN PRINTED ELECTRODES (SPE)

The need for analysis *in situ* led to the miniaturization of the equipment needed for electrochemical biosensors. In this context, screen-printed electrodes (SPE) have been developed, in which the three-electrode cell above descripted is miniaturized to obtain smaller devices. In SPEs, working, reference and counter electrodes are printed on a solid substrate, that is usually paper, ceramic, plastic or textile. [41] This technique consists of depositing a combination of layers of electrode material onto a flat substrate to obtain a compact device, where the diameter of WE is about 4 mm, as shown in *Figure 1.12*. This results in different advantages over the conventional three electrode cell: it is possible to have different electrode design, modifications and materials, in affordable, reproducible, low-cost and disposable devices. Furthermore, based on the small dimension of these electrodes a small amount of sample volume (about 25-50 µl) is required and this can be useful especially for assays in biomedical field.

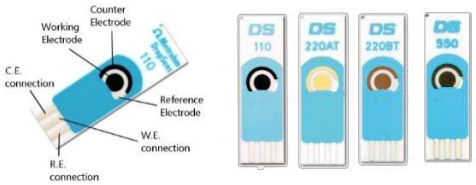

Figure 1.12: (Left)Representation of Screen-Printed Electrodes (SPE); (Right) Different types of Screen-Printed Electrodes. Images from https://www.metrohm.com/it_it.html

Various enhancements have been implemented to improve the analytical properties of SPE[42]: indeed, they can be functionalised with different materials or combination of them, such as carbon-based materials (CNT, graphene, carbon black), polymers, mediator nanoparticles and metallic nanoparticles, like gold and silver nanoparticles as well as magnetic beads. These nanomaterials can also have dimensions similar to the biological diagnosis elements, including proteins and DNA, whose composition can produce synergistic impacts, thus improving analytical properties of biosensors. All these features make SPE a valuable tool in the field of Point-of-Care Testing, as they allow to have *in-situ* and rapid analysis.

1.8 Point-Of-Care Testing (PoCT)

The concept of Point-of-Care Testing refers to all methods employing fast analysis and laboratory tests, giving a reliable output near the patient's bedside[43]. These tests do not need laboratory facilities to provide the results and they are used near the patient, whether it is a hospital, clinic, or at home to monitor diseases and therapies. They should be user-friendly with little or no sample treatment and easy to interpret results.

Different advantages and aspects are crucial for Point-of-Care Tests, such as:

- Assay Time: these tests should give rapid and time-saving results, as samples do not need to be processed and analyzed in dedicated laboratories.
- Cost: PoC tests should be cost-effective. In fact, instruments are smaller and more specific, materials that are used for these tests are cheap (chip, strips,

screen-printed electrodes). Indeed, if they are used for rapid screening, invasive and expensive tests could be avoided.

- Patient compliance: in-home and POC tests can reduce the need of hospital visits, travel expenses and they can be self-administered from the patients, thus leading to higher responsibilities and regularity.

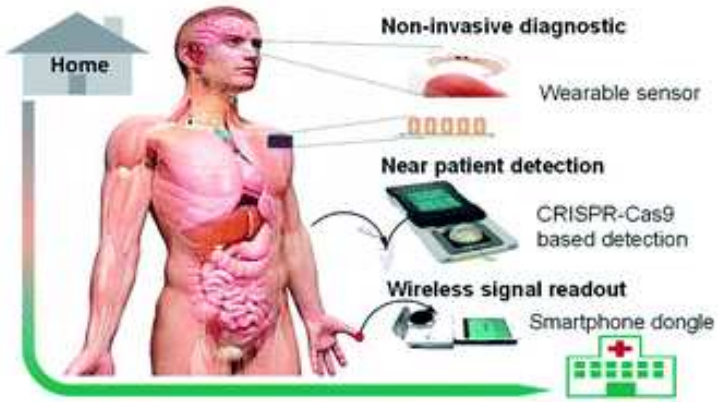

Figure 1.13: Point-of-Care Testing (POCT) graphic representation. Reprinted with permission from Ref. 43© The Royal Society of Chemistry.[43]

Efficient POCT devices are necessary for rapid and reliable analyte detection for disease diagnosis, monitoring, management, and predicting treatment response [44]. The World Health Organization (WHO) established a set of criteria to be met for the development of diagnostic tools, named *ASSURED*, acronym of Affordable, Sensitive, Specific, User friendly, Rapid and Robust, Equipment free and Deliverable to end users. These criteria have been recently revised and converted to *REASSURED*, with the addition of "Real-time connectivity" and "Ease of specimen collection". They have become the main reference for the development of biosensors, especially for POC tests in resource-limited areas [45,46].

In this context, electrochemical biosensors for diagnostics made great progress in the last years, as they allow for high sensitivity and low cost, but also miniaturization of POCT application [46]. In fact, the use of miniaturized electrodes,

like screen-printed electrodes, paper-based devices, wearable devices combined with low-cost portable equipment enable their use for Point-of-Care applications.

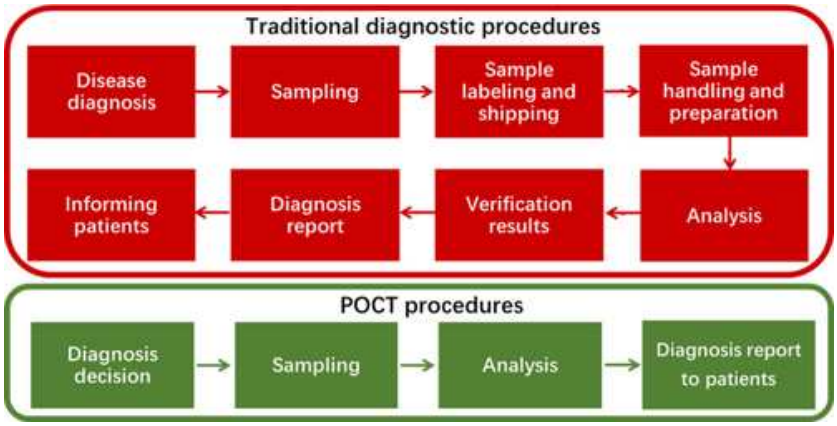

Figure 1.14: Comparison of the clinical application of the traditional diagnostic test in central laboratory and POCT. Reprinted with permission from Ref. 46 © 2021 Wiley VCH GmbH[46]

1.9 INTERNET OF THINGS (IOT)

Internet of Things (IoT) is defined as a system containing "smart objects" connected to the Internet and provided with capabilities of sensing, storing, processing as well as identifying and networking. These smart objects are nowadays ubiquitous: they can be home tools, like smart lightning, fridges, TVs, wearable and medical devices, smart energy networks, etc. In this way, the internet serves as a way to connect physical devices communicating between each other and/or with humans [47].

Normally, the IoT architecture includes different layers [48]:

- Smart device/sensor layer: using sensors it is possible to measure physical properties and convert them into signals accessible through an instrument, allowing real-time information to be detected and processed.
- Gateways and networks: the large amount of data produced needs high performance wired or wireless network infrastructure, that can be private, public or hybrid.

- Management service layer: information needs to be processed in terms of analytics, management of devices, security control and process modelling. In fact, it could be necessary to filter or process the information, but also to respond to emergency situations, like critical patient's conditions.
- Application layer: it is the real application field of these devices, like healthcare, environmental monitoring, emergency, lifestyle.

In this context, wireless sensors have been developed due to the increasing need for biochemical sensors combined with technical improvements in miniaturization of instruments, mobile communications and advanced chemical sensing in the field of security, healthcare, sport [49]. The aim is to develop a network of connected things that can interact and communicate between each other and that can react to sensed information about their surroundings, depending on the aim of the device.

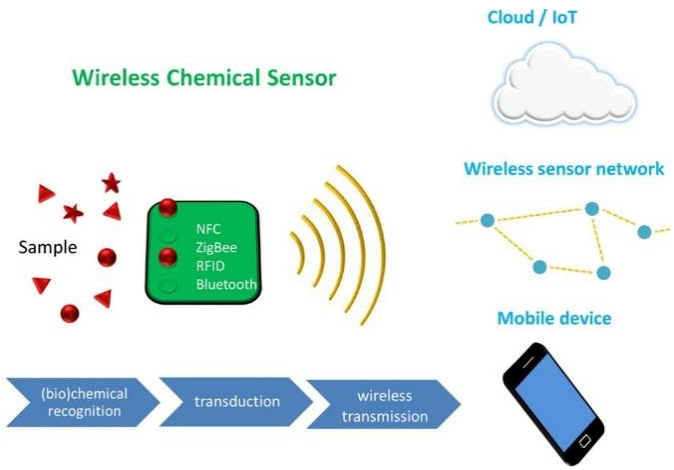

Figure 1.15: Schematic representation of the principle of Wireless Chemical Sensors and Internet of Things. Reprinted with permission from Ref. 49 © 2018 Elsevier B.V.[49]

Wireless and contactless technologies can define different aspects of the devices, like size, battery or power-supply requirements, real-time data or on-demand data, the distance they need to operate and their compatibility with smartphones. The latter is an important factor given the wide availability of such devices, hence protocols supported on smartphones are fast-growing, while technologies not

supported by smartphones are decreasing. In line with the Point-of-Care concept, thanks to these technologies it is possible to create portable instruments that can be moved according to the patient's needs. [49]Among chemical sensors, the electrochemical ones are usually employed in the wireless devices field, especially potentiometric and amperometric sensors.

1.10 REFERENCES

1. Hulanicki, A., Glab, S. & Ingman, F. Chemical sensors definitions and classification. *Pure Appl. Chem.* **63**, 1247–1250 (1991).

2. A. D. McNaught and A. Wilkinson. *IUPAC. Compendium of Chemical Terminology*. vol. online ver (1997).

3. Thévenot, D. R., Toth, K., Durst, R. A. & Wilson, G. S. Electrochemical biosensors: Recommended definitions and classification. *Biosens. Bioelectron.* **16**, 121–131 (2001).

4. Bhalla, N., Jolly, P., Formisano, N. & Estrela, P. Introduction to biosensors. 1–8 (2016) doi:10.1042/EBC20150001.

5. Naresh, V. & Lee, N. A review on biosensors and recent development of nanostructured materials-enabled biosensors. *Sensors (Switzerland)* **21**, 1–35 (2021).

6. Hernandez-Vargas, G. *et al.* Electrochemical biosensors: A solution to pollution detection with reference to environmental contaminants. *Biosensors* **8**, 1–21 (2018).

7. B. Magnusson and U. Örnemark. Eurachem Guide: The Fitness for Purpose of Analytical Methods – A Laboratory Guide to Method Validation and Related Topics. in *Eurachem Guide: The Fitness for Purpose of Analytical Methods – A Laboratory Guide to Method Validation and Related Topics* (2014).

8. Alhadrami, H. A. Biosensors: Classifications, medical applications, and future prospective. *Biotechnol. Appl. Biochem.* **65**, 497–508 (2018).

9. Karunakaran, C., Rajkumar, R. & Bhargava, K. *Introduction to Biosensors*. *Biosensors and Bioelectronics* (Elsevier Inc., 2015). doi:10.1016/B978-0-12-803100-1.00001-3.

10. Karkare, S. & Bhatnagar, D. Promising nucleic acid analogs and mimics: Characteristic features and applications of PNA, LNA, and morpholino. *Appl. Microbiol. Biotechnol.* **71**, 575–586 (2006).

11. Marques, A. C. *et al. Non-enzymatic lab-on-paper devices for biosensing applications*. *Comprehensive Analytical Chemistry* vol. 89 (Elsevier B.V., 2020).

12. Malhotra, B. D. & Ali, M. A. *Nanomaterials in Biosensors*. *Nanomaterials for Biosensors* (2018). doi:10.1016/b978-0-323-44923-6.00001-7.

13. Bansi Dhar Malhotra, M. A. A. Chapter 1 - Nanomaterials in Biosensors: Fundamentals and Applications. in *Nanomaterials for Biosensors* 1–74 (2018).

14. Grieshaber, D., MacKenzie, R., Vörös, J. & Reimhult, E. Electrochemical biosensors - Sensor principles and architectures. *Sensors* **8**, 1400–1458 (2008).

15. Labib, M., Sargent, E. H. & Kelley, S. O. Electrochemical Methods for the Analysis of Clinically Relevant Biomolecules. *Chem. Rev.* **116**, 9001–9090 (2016).

16. Wurster, B. Two-Dimensional Metal-Organic Networks as a New Class of Electrocatalysts. *Thesis* **6783**, (2015).

17. Gründler, P. *Chemical sensors: An introduction for scientists and engineers*. *Chemical Sensors: An Introduction for Scientists and Engineers* (2007). doi:10.1007/978-3-540-45743-5.

18. Wei, D. & Ivaska, A. Electrochemical biosensors based on polyaniline. *Chem. Analityczna* **51**, 839–852 (2006).

19. Mendoza, S., Bustos, E., Manríquez, J. & Godínez, L. A. Voltammetric Techniques. *Agric. Food Electroanal.* 21–48 (2015) doi: 10.1002/9781118684030.ch2.

20. Ciepiela, F. & Jakubowska, M. Faradaic and capacitive current estimation by means of Independent Components Analysis and 1 kHz sampling. *Talanta* **170**, 158–164 (2017).

21. Traynor, S. M. *et al.* Review—Recent Advances in Electrochemical Detection of Prostate Specific Antigen (PSA) in Clinically-Relevant Samples. *J. Electrochem. Soc.* **167**, 037551 (2020).

22. Nguyen, H. H. & Kim, M. An Overview of Techniques in Enzyme Immobilization. *Appl. Sci. Converg. Technol.* **26**, 157–163 (2017).

23. Maduraiveeran, G. & Jin, W. Nanomaterials based electrochemical sensor and biosensor platforms for environmental applications. *Trends Environ. Anal. Chem.* **13**, 10–23 (2017).

24. Khaliq, N. *et al.* Voltage-Switchable Biosensor with Gold Nanoparticles on TiO2Nanotubes Decorated with CdS Quantum Dots for the Detection of Cholesterol and H2O2. *ACS Appl. Mater. Interfaces* **13**, 3653–3668 (2021).

25. Li, F. *et al.* Ultrasensitive amperometric immunosensor for PSA detection

based on Cu2O@CeO2-Au nanocomposites as integrated triple signal amplification strategy. *Biosens. Bioelectron.* **87**, 630–637 (2017).

26. Li, J. & Bo, X. Laser-enabled flexible electrochemical sensor on finger for fast food security detection. *J. Hazard. Mater.* **423**, 127014 (2022).

27. Beduk, T., De Oliveira Filho, J. I., Ait Lahcen, A., Mani, V. & Salama, K. N. Inherent Surface Activation of Laser-Scribed Graphene Decorated with Au and Ag Nanoparticles: Simultaneous Electrochemical Behavior toward Uric Acid and Dopamine. *Langmuir* **37**, 13890–13902 (2021).

28. Liu, X., Huang, L. & Qian, K. Nanomaterial-Based Electrochemical Sensors: Mechanism, Preparation, and Application in Biomedicine. *Adv. NanoBiomed Res.* **1**, 2000104 (2021).

29. Siwal, S. S., Zhang, Q., Devi, N. & Thakur, V. K. Carbon-based polymer nanocomposite for high-performance energy storage applications. *Polymers (Basel).* **12**, 1–30 (2020).

30. Ribeiro, B., Botelho, E. C., Costa, M. L. & Bandeira, C. F. Carbon nanotube buckypaper reinforced polymer composites: A review. *Polimeros* **27**, 247–255 (2017).

31. Rathinavel, S., Priyadharshini, K. & Panda, D. A review on carbon nanotube: An overview of synthesis, properties, functionalization, characterization, and the application. *Mater. Sci. Eng. B* **268**, 115095 (2021).

32. Ferrier, D. C. & Honeychurch, K. C. Carbon nanotube (CNT)-based biosensors. *Biosensors* **11**, 1–33 (2021).

33. Rasheed, P. A. & Sandhyarani, N. Femtomolar level detection of BRCA1 gene using a gold nanoparticle labeled sandwich type DNA sensor. *Colloids Surfaces B Biointerfaces* **117**, 7–13 (2014).

34. Pothipor, C., Aroonyadet, N., Bamrungsap, S., Jakmunee, J. & Ounnunkad, K. A highly sensitive electrochemical microRNA-21 biosensor based on intercalating methylene blue signal amplification and a highly dispersed gold nanoparticles/graphene/polypyrrole composite. *Analyst* **146**, 2679–2688 (2021).

35. Giannetto, M. *et al.* An amperometric immunosensor for diagnosis of celiac disease based on covalent immobilization of open conformation tissue transglutaminase for determination of anti-tTG antibodies in human serum. *Biosens. Bioelectron.* **62**, 325–330 (2014).

36. Maduraiveeran, G., Sasidharan, M. & Ganesan, V. Electrochemical sensor and biosensor platforms based on advanced nanomaterials for biological and biomedical applications. *Biosens. Bioelectron.* **103**, 113–129 (2018).

37. Zhang, L. & Wang, Z. S. Gold nanoparticles as an ultrathin scattering layer for efficient dye-sensitized solar cells. *J. Mater. Chem. C* **4**, 3614–3620 (2016).

38. Xianyu, Y., Wang, Q. & Chen, Y. Magnetic particles-enabled biosensors for point-of-care testing. *TrAC - Trends Anal. Chem.* **106**, 213–224 (2018).

39. Mollarasouli, F., Zor, E., Ozcelikay, G. & Ozkan, S. A. Magnetic nanoparticles in developing electrochemical sensors for pharmaceutical and biomedical applications. *Talanta* **226**, 122108 (2021).

40. Choi, K. *et al.* Automated digital microfluidic platform for magnetic-particle-based immunoassays with optimization by design of experiments. *Anal. Chem.* **85**, 9638–9646 (2013).

41. García-Miranda Ferrari, A., Rowley-Neale, S. J. & Banks, C. E. Screen-printed electrodes: Transitioning the laboratory in-to-the field. *Talanta Open* **3**, (2021).

42. Paimard, G., Ghasali, E. & Baeza, M. Screen-Printed Electrodes: Fabrication, Modification, and Biosensing Applications. *Chemosensors* **11**, (2023).

43. Qin, J., Wang, W., Gao, L. & Yao, S. Q. Emerging biosensing and transducing techniques for potential applications in point-of-care diagnostics. *Chem. Sci.* **13**, 2857–2876 (2022).

44. Prattis, I. *et al.* Graphene for Biosensing Applications in Point-of-Care Testing. *Trends Biotechnol.* **39**, 1065–1077 (2021).

45. Land, K. J., Boeras, D. I., Chen, X. S., Ramsay, A. R. & Peeling, R. W. REASSURED diagnostics to inform disease control strategies, strengthen health systems and improve patient outcomes. *Nat. Microbiol.* **4**, 46–54 (2019).

46. Zhang, Y. & Zhou, N. Electrochemical Biosensors Based on Micro-fabricated Devices for Point-of-Care Testing: A Review. *Electroanalysis* **34**, 168–183 (2022).

47. van Deursen, A. J. A. M., van der Zeeuw, A., de Boer, P., Jansen, G. & van Rompay, T. Development and validation of the Internet of Things Skills Scale (IoTSS). *Inf. Commun. Soc.* **25**, 1883–1899 (2022).

48. Patel, K. K., Patel, S. M. & Scholar, P. G. Internet of Things-IOT: Definition,

Characteristics, Architecture, Enabling Technologies, Application & Future Challenges. *Int. J. Eng. Sci. Comput.* **6**, 1–10 (2016).

49. Kassal, P., Steinberg, M. D. & Steinberg, I. M. Wireless chemical sensors and biosensors: A review. *Sensors Actuators, B Chem.* **266**, 228–245 (2018).

2 Immunosensors for SARS-CoV-2-detection

Immunosensors are biosensors based on the interaction between antigens (Ag) and antibodies (Ab) on a transducer surface.[1] The binding event is then converted into a measurable signal, allowing for detection of analytes at low-concentration. Both antibodies and antigens can be immobilized onto the transducer to detect respectively antigens or antibodies. Due to the high specificity of their interaction it is possible to detect a wide range of biomolecules, including bacteria, viruses, proteins, nucleic acids, and biomarkers [2]. They are typically user-friendly, low-cost, small-sized, portable and with small sample volume needed for the analysis, allowing for a wide range of applications. [3]

2.1 ANTIGENS AND ANTIBODIES

Antibodies, or immunoglobulins (Ig), are glycoproteins capable of recognizing and binding antigens. They are characterized by a "Y" shape, containing four polypeptide chains: two heavy chains (HC) and two light chains (LC) connected by disulfide bonds. [1]

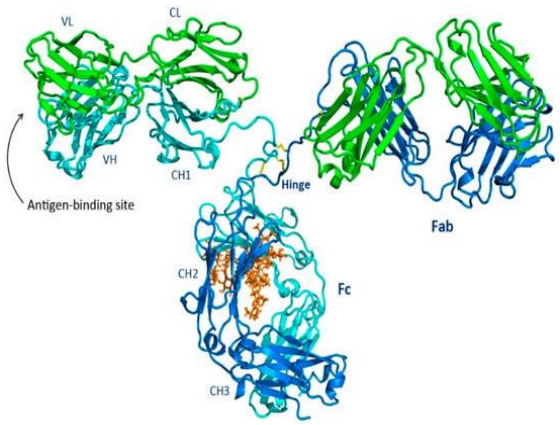

Figure 2.1: Schematic Structure of an antibody. Reprinted with permission from Ref. 4 © 2019 MDPI, Basel, Switzerland[4].

Immunoglobulins present a variable region on the top of the structure, and a constant region. The variable portion, with 110-130 aminoacids, includes the

terminal portion of light and heavy chains and gives the antibody its specificity for antigen binding. There are three functional regions in every antibody: two Fragment antigen binding domains (Fabs) and the Fragment crystallizable (Fc) domain, linked by a hinge region which allows a wide range of flexibility. Each Fab has identical antigen-binding sites for the specific target antigen. The Fc region, instead, binds to receptor molecules to mediate the activation of the immune system.[4] Depending on the constant region structure and their immune function, antibodies are divided into five classes: IgM, IgG, IgA, IgD, and IgE.

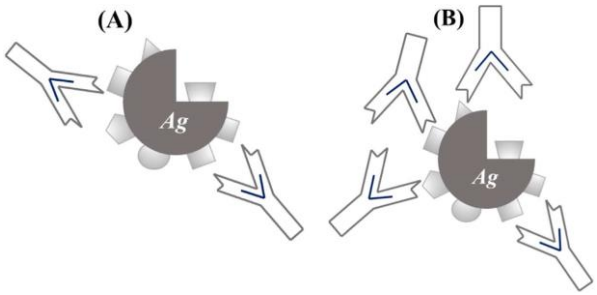

Figure 2.2: Representation of monoclonal (A) and polyclonal antibodies (B) Reprinted with permission from Ref.1

Antibodies can be classified also as monoclonal and polyclonal, depending on the epitope recognized, which is the region of the antigen bound by the antibody. The former can specifically recognise a single epitope, giving a higher specificity and avoiding cross-reactivity, while the latter can recognize and bind multiple epitopes of the antigen, showing a wider immunological response. Polyclonal antibodies are produced from different B-lymphocyte lines as a mixture of immunoglobulins, while monoclonal antibodies are a product of one clone of B-lymphocyte [5]. Antigens, on the other hand, are molecules or substances recognised by the immune system which trigger an immune response. Each antigen has distinct surface features (epitopes) resulting in specific responses from the immune system.

2.2 *CLASSIFICATION OF IMMUNOSENSORS*

Based on the detection approach, immunosensors are divided into label-free and labelled assays. In the first case, the presence of an analyte is detected directly through biochemical reactions occurring on a transducer surface. Conversely, in labelled assays, the analyte is sandwiched between a capture agent and a species conjugated with a marker, that can be an enzyme, quantum dot, fluorophore, or radioisotope, to generate a signal.[3]

2.2.1 Label-free immunosensors

Label-free immunosensors can detect physical or chemical changes deriving from the formation of the immunocomplex without the need for labelling [6]. Therefore, the advantage is that they facilitate rapid, real-time analysis, especially in clinical applications. [7]

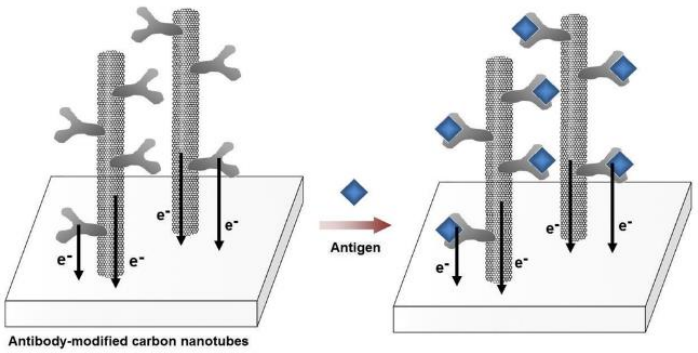

Figure 2.3: Representation of working principle of label-free immunosensors. Reprinted with permission from Ref. 7 © 2007 MDPI[7]

On the other hand, non-specific adsorption can occur, significantly affecting their response leading to false positives or false negatives. The non-specific binding of the antigen or other molecules on the surface can increase the background signal, leading to lower sensitivity. Usually, to fix this issue, different blocking agents are employed, like surfactants (e.g., Tween 20, polyethylene glycol), casein, bovine serum albumin (BSA), and thionic compounds for gold surfaces.

2.2.2 Labelled immunosensors

In labelled immunosensors[8] the capture antibody is immobilized onto the sensor surface to detect the antigen, while a secondary antibody is usually conjugated with a signal-generating label, the latter being an enzyme, metal ions, fluorescent dyes, nanomaterials.

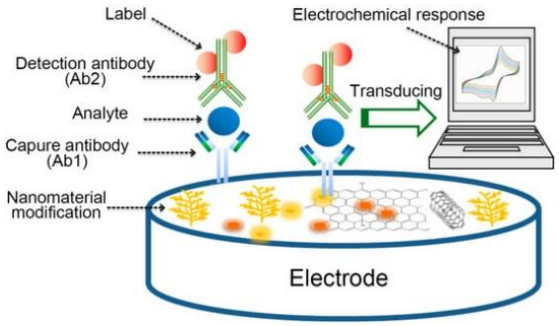

Figure 2.4: Representation of working principle of labelled immunosensors. Reprinted with permission from Ref. 8 © 2019 MDPI, Basel, Switzerland[8]

They have different advantages with respect to label-free immunosensors, such as a higher sensitivity and specificity. They can be divided into competitive and non-competitive immunosensors.

In the first case the analyte in the sample competes with a labelled analyte to access the limited number of antibody-binding sites. Typically, an antibody is immobilized on the surface and a solution of labelled antigen at known concentration is added to compete with the antigens in the samples. The signal obtained is inversely proportional to the concentration of the analyte[9]. They are usually employed for small molecules with one epitope and low molecular weight[10].

For macromolecular compounds with higher molecular weight and more epitopes, instead, non-competitive immunosensors are more advantageous. In these immunosensors, also called "sandwich" immunoassays, a capture (or primary) antibody is immobilized onto the sensor surface to bind the antigen and a labelled (secondary) antibody binds the immunocomplex, giving the detectable signal. In

this case the electrochemical response directly relies on the presence and the amount of the analyte in the sample[3].

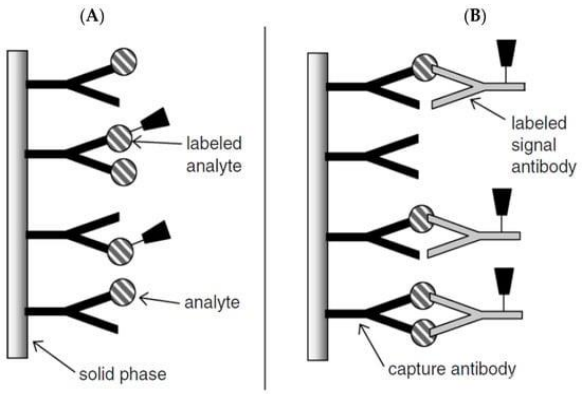

Figure 2.5: Representation of working principle of competitive and non-competitive immunosensors. Reprinted with permission from © 2019 by the authors. Licensee MDPI, Basel, Switzerland.[3]

These immunosensors are widely used for Point-of-Care testing applications, as their characteristics allow to have smart, portable and user-friendly devices. They are used in clinical fields, like biomarkers determination, virus detection [11,12], serological tests[13] or trace contaminants monitoring[14].

2.3 SARS-CoV-2 AND CORONAVIRUS DISEASE (COVID-19)

In December 2019 a new coronavirus infection was found in Wuhan, China, resulting in a pandemic which was declared in March 2020 and affected more than 200 countries in the world.[15] The virus causing the COVID-19 disease was identified as Severe Acute Respiratory Syndrome Coronavirus 2 (SARS-CoV-2)[16]. SARS-CoV-2 can be transmitted through the respiratory tract, via cough and saliva.

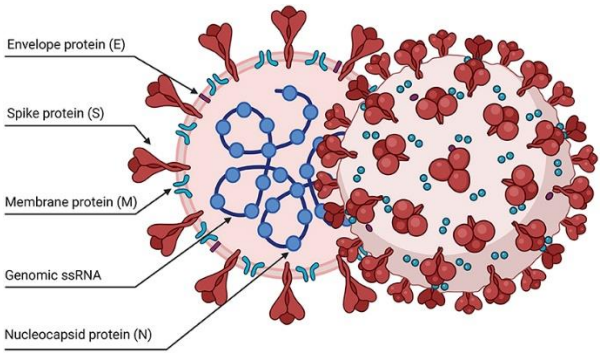

Figure 2.6: Representation of SARS-CoV-2 structure. Reprinted with permission from Ref. 17 © 2022, Frontiers in Virology [17]

This virus belongs to the family of β-Coronaviruses, a group of enveloped viruses, pathogenic, with a positive single stranded RNA genome contained in a helical nucleocapsid. The genome is about 30 kilobases. It contains four structural proteins, which are Spike (S), Envelope (E), Membrane (M), and Nucleocapsid (N). Among these proteins, Spike and Nucleocapsid proteins are the main immunogens, as they induce a strong immune response in hosts. Both N and S proteins and their portions, indeed, have been used as capture antigens to develop different tests aimed at the detection of anti-SARS-CoV-2 antibodies in serum.

2.3.1 Spike protein

Spike protein is a transmembrane structural glycoprotein containing two main subunits: S1 and S2. It plays a substantial role in the pathogenesis of COVID-19, as it binds to the host cell through its Receptor Binding Domain (RBD), triggering the infection.

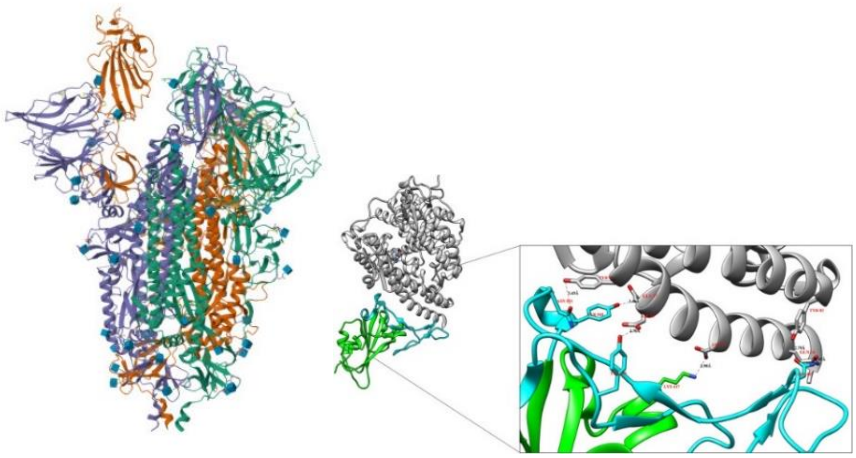

Figure 2.7: Representation of SARS-CoV-2 Spike protein (left) from RCSB Protein Databank; S1 subunit with RBD (Right) Reprinted with permission from Ref. 18 © 2022 Springer Nature B.V. [18]

In particular, the RBD interacts with the human receptor Angiotensin-converting enzyme 2 (ACE2)[18]. S2 subunit, instead, works as the fusion protein to help the virion fusion with the mammalian cell membrane. During this process, S protein undergoes different conformational changes to help the entry into the host cell. Due to its important role in the pathogenesis and immune response of COVID-19 disease, Spike protein has been selected as the main antigen target for vaccine development and among the most used target for antigen tests[19,20]

2.3.2 Nucleocapsid protein

The role of this protein is to package the viral genome RNA into a helical ribonucleocapsid complex[21]. Moreover, it mediates viral assembly by interacting with membrane protein and viral genome. It is highly conserved in the coronaviruses genomes and is one of the most abundant proteins. It is very important as it serves as immunodominant antigen in host immune responses, thus representing a diagnostic marker to determine the presence of the virus or antibodies directed against it.

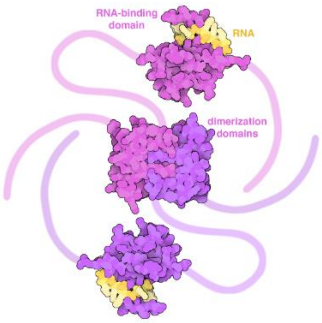

Figure 2.8: Representation of SARS-CoV-2 Nucleocapsid protein. From pdb101.rcsb

Moreover, as this protein is highly conserved and abundantly expressed during SARS-CoV-2 infections, several antigen tests [22–24]for determination of the virus are based on N protein detection[19].

2.4 SARS-CoV-2 IMMUNE RESPONSE

As SARS-CoV-2 has resulted to be highly contagious and the symptomatology is not very specific and similar to a common flu, early detection is very important to control its spreading [25]. To this end, rapid and specific tests for the diagnosis were needed to detect the presence of the virus and its components as well as assessing immunization status through detection of antibodies in serological tests.

Once the virus enters the target cell, the host immune system recognizes the whole virus or its surface epitopes, triggering the innate or adaptive immune response[26,27].

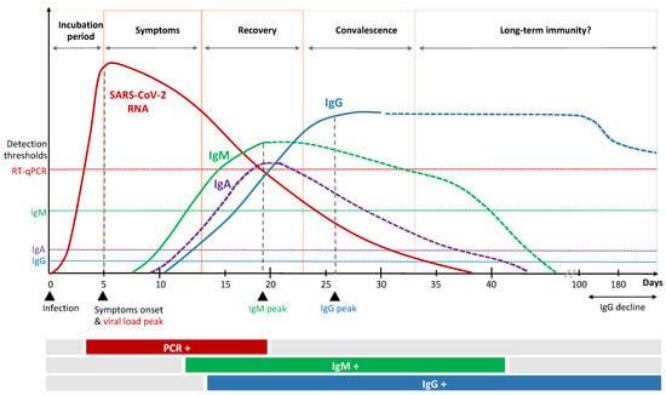

Figure 2.9: Representation of immune response to SARS-CoV-2 Reprinted with permission from © 2021 by the authors. Licensee MDPI, Basel, Switzerland[27]

Generally, after the infection, antibodies against nucleocapsid and spike protein are produced. Immune response against SARS-CoV-2 is very similar to that against other coronavirus infections and involves IgA, IgG and IgM production. Antibodies targeting the receptor binding domain of the Spike protein are important for viral neutralization, since they prevent virus binding to the human receptor and entering the host cell[28]. Most patients show SARS-CoV-2-specific antibodies responses shortly after the infection that can last for weeks or months. In particular, IgA response occurs first with a peak very early on and then decreases. Production of IgM and IgG antibodies is reported to take place almost simultaneously, from 7 to 14 days after symptoms onset [29].

Therefore, IgG and IgM against SARS-CoV-2 nucleocapsid and spike protein can be detected by serological screening. In particular, anti-N immunoglobulins indicate a previous or current SARS-CoV-2 infection, while anti-S antibodies can also provide information about the response to the vaccine[30].

2.5 SARS-CoV-2 DETECTION METHODS

Different methods have been developed to detect the presence of SARS-CoV-2 or of antibodies against it.

The quantitative reverse transcription Polymerase Chain Reaction (RT-qPCR)[25] is considered the gold standard for the detection of SARS-CoV-2 as it is accurate, specific and it can detect very low concentrations of RNA copies, allowing for early detection of the virus. With this method, the presence of nucleic acids is revealed by targeting and amplifying virus-specific genes, giving a quantitative result. Due to the high demand for rapid diagnosis and detection techniques, other tests have been developed. In particular, serological and antigen tests have been widely used to detect the presence of the virus or antibodies. In the first case, blood or serum samples are analyzed to detect specific antibodies, IgG or IgM, directed against

Spike or Nucleocapsid protein, while in antigen tests SARS-CoV-2 specific antibodies or other affinity ligands, like synthetic peptides, are exploited as receptors to bind the viral proteins or RNA in samples of saliva or nasopharyngeal swabs.

For these tests, different techniques have been used, like Lateral Flow Immunoassays (LFIA) and Enzyme-linked Immunosorbent Assays (ELISA), [31]. ELISA assays have higher specificity and sensitivity, but longer response time. Conversely, LFIA tests give a qualitative response in a short time and grant a high portability and ease of use, however they have shown poor robustness determined by false positive and negative results[25].: These tests have been widely used in non-hospital settings as rapid-diagnostic tests. In this context, several biosensors[32] have been developed to assess the immunization status of patients or the presence of the virus. Therefore, to overcome the limitations of traditional clinical and at home testing, much attention has been dedicated to novel biosensing technologies that through unique features can help to tackle the spreading of a pandemic.

2.6 REFERENCES

1. Felix, F. S. & Angnes, L. Electrochemical immunosensors – A powerful tool for analytical applications. *Biosens. Bioelectron.* **102**, 470–478 (2018).
2. Gil Rosa, B. *et al.* Multiplexed immunosensors for point-of-care diagnostic applications. *Biosens. Bioelectron.* **203**, 114050 (2022).
3. Mollarasouli, F., Kurbanoglu, S. & Ozkan, S. A. The role of electrochemical immunosensors in clinical analysis. *Biosensors* **9**, 1–19 (2019).
4. Chiu, M. L., Goulet, D. R., Teplyakov, A. & Gilliland, G. L. Antibody structure and function: The basis for engineering therapeutics. *Antibodies* **8**, (2019).
5. Pohanka, M. Monoclonal and polyclonal antibodies production - Preparation of potent biorecognition element. *J. Appl. Biomed.* **7**, 115–121 (2009).
6. Samuel, V. R. & Rao, K. J. A review on label free biosensors. *Biosens. Bioelectron. X* **11**, 100216 (2022).
7. Vestergaard, M., Kerman, K. & Tamiya, E. An overview of label-free electrochemical protein sensors. *Sensors* **7**, 3442–3458 (2007).
8. Zhang, Z., Cong, Y., Huang, Y. & Du, X. Nanomaterials-based electrochemical immunosensors. *Micromachines* **10**, (2019).
9. Fowler, J. M., Wong, D. K. Y., Brian Halsall, H. & Heineman, W. R. *Recent developments in electrochemical immunoassays and immunosensors*. *Electrochemical Sensors, Biosensors and their Biomedical Applications* (Elsevier Inc., 2008). doi:10.1016/B978-012373738-0.50007-6.
10. Janik-Karpinska, E. *et al.* Immunosensors—The Future of Pathogen Real-Time Detection. *Sensors* **22**, 1–20 (2022).
11. Giannetto, M., Bianchi, M. V., Mattarozzi, M. & Careri, M. Competitive amperometric immunosensor for determination of p53 protein in urine with carbon nanotubes/gold nanoparticles screen-printed electrodes: A potential rapid and noninvasive screening tool for early diagnosis of urinary tract

carcinoma. *Anal. Chim. Acta* **991**, 133–141 (2017).

12. Fabiani, L. *et al.* Magnetic beads combined with carbon black-based screen-printed electrodes for COVID-19: A reliable and miniaturized electrochemical immunosensor for SARS-CoV-2 detection in saliva. *Biosens. Bioelectron.* **171**, (2021).
13. Torrente-Rodríguez, R. M. *et al.* SARS-CoV-2 RapidPlex: A Graphene-Based Multiplexed Telemedicine Platform for Rapid and Low-Cost COVID-19 Diagnosis and Monitoring. *Matter* **3**, 1981–1998 (2020).
14. Fang, L. *et al.* Recent progress in immunosensors for pesticides. *Biosens. Bioelectron.* **164**, 112255 (2020).
15. Naqvi, A. A. T. *et al.* Insights into SARS-CoV-2 genome, structure, evolution, pathogenesis and therapies: Structural genomics approach. *Biochim. Biophys. Acta - Mol. Basis Dis.* **1866**, 165878 (2020).
16. Hu, B., Guo, H., Zhou, P. & Shi, Z. L. Characteristics of SARS-CoV-2 and COVID-19. *Nat. Rev. Microbiol.* **19**, 141–154 (2021).
17. Pizzato, M. *et al.* SARS-CoV-2 and the Host Cell: A Tale of Interactions. *Front. Virol.* **1**, 1–29 (2022).
18. Borkotoky, S., Dey, D. & Hazarika, Z. Interactions of angiotensin-converting enzyme-2 (ACE2) and SARS-CoV-2 spike receptor-binding domain (RBD): a structural perspective. *Mol. Biol. Rep.* **50**, 2713–2721 (2023).
19. Pierce-ruiz, C. *et al.* Quantification of SARS-CoV-2 spike and nucleocapsid proteins using isotope dilution tandem mass spectrometry. (2021).
20. Karakuş, E., Erdemir, E., Demirbilek, N. & Liv, L. Colorimetric and electrochemical detection of SARS-CoV-2 spike antigen with a gold nanoparticle-based biosensor. *Anal. Chim. Acta* **1182**, (2021).
21. Bai, Z., Cao, Y., Liu, W. & Li, J. Structure , Biological Functions , and a Potential Target for Drug. *Viruses* **13**, 1–13 (2021).

22. Diao, B. *et al.* Accuracy of a nucleocapsid protein antigen rapid test in the diagnosis of SARS-CoV-2 infection. *Clin. Microbiol. Infect.* **27**, 289.e1-289.e4 (2021).
23. Yano, T. aki *et al.* Ultrasensitive detection of SARS-CoV-2 nucleocapsid protein using large gold nanoparticle-enhanced surface plasmon resonance. *Sci. Rep.* **12**, 1–8 (2022).
24. Miyamura, S. *et al.* Rapid, high-sensitivity detection of biomolecules using dual-comb biosensing. *Sci. Rep.* **13**, 1–14 (2023).
25. Lino, A., Cardoso, M. A., Gonçalves, H. M. R. & Martins-Lopes, P. SARS-CoV-2 Detection Methods. *Chemosensors* **10**, (2022).
26. Shah, V. K., Firmal, P., Alam, A., Ganguly, D. & Chattopadhyay, S. Overview of Immune Response During SARS-CoV-2 Infection: Lessons From the Past. *Front. Immunol.* **11**, 1–17 (2020).
27. Koch, T., Mellinghoff, S. C., Shamsrizi, P., Addo, M. M. & Dahlke, C. Correlates of vaccine-induced protection against sars-cov-2. *Vaccines* **9**, 1–17 (2021).
28. Lou, B. *et al.* Serology characteristics of SARS-CoV-2 infection since exposure and post symptom onset. *Eur. Respir. J.* **56**, (2020).
29. Poland, G. A., Ovsyannikova, I. G. & Kennedy, R. B. SARS-CoV-2 immunity: review and applications to phase 3 vaccine candidates. *Lancet* **396**, 1595–1606 (2020).
30. Prendecki, M. *et al.* Effect of previous SARS-CoV-2 infection on humoral and T-cell responses to single-dose BNT162b2 vaccine. *Lancet* **397**, 1178–1181 (2021).
31. Suleman, S. *et al.* Point of care detection of COVID-19: Advancement in biosensing and diagnostic methods. *Chem. Eng. J.* **414**, 128759 (2021).
32. Imran, S., Ahmadi, S. & Kerman, K. Electrochemical biosensors for the detection of sars-cov-2 and other viruses. *Micromachines* **12**, 1–23 (2021).

3 SARS-CoV-2 serological tests: state of the art

In the context of COVID-19 epidemiological monitoring, serological tests are aimed at detection of antibodies in infected patients after exposure to SARS-CoV-2. As for biosensors for the detection of SARS-CoV-2 antibodies, the virus structural proteins, namely Nucleocapsid (N) or Spike (S) proteins or their components, are exploited as receptors so that they can detect and bind antibodies (IgG-IgM) in patients' biological body fluids[1]. In particular, anti-N antibodies can be detected in currently or previously infected patients, while anti-S antibodies can also be detected in patients after vaccination and provide information on the immune response.

Countless electrochemical immunosensors have been developed to assess SARS-CoV-2 developed immunity. Just for example, Torrente-Rodrìguez developed RapidPlex , a SARS-CoV-2 multiplexed graphene-based electrochemical platform to detect specific biomarkers in both blood and saliva, in particular anti-Spike antibodies (S1-IgM and S1-IgG), Nucleocapsid protein and C-reactive protein, associated with inflammation[2]. This platform consists of laser-engraved graphene electrodes with antigens and antibodies immobilized on them to provide information on different aspects: viral infection due to the presence of nucleocapsid protein, immune response, detectable through antibodies, and disease severity, given by the level of C-reactive protein. Yakoh et al.[3] developed a label-free paper-based electrochemical platform targeting SARS-CoV-2 antibodies without the specific requirement of a reading antibody. In presence of SARS-CoV-2 antibodies the conversion of a redox indicator is inhibited, resulting in a decreased current response. This electrochemical sensor was tested in real serum samples from patients with good results. In addition, the proposed format was also extended to detect the antigen, i.e., Spike protein from SARS-CoV-2.

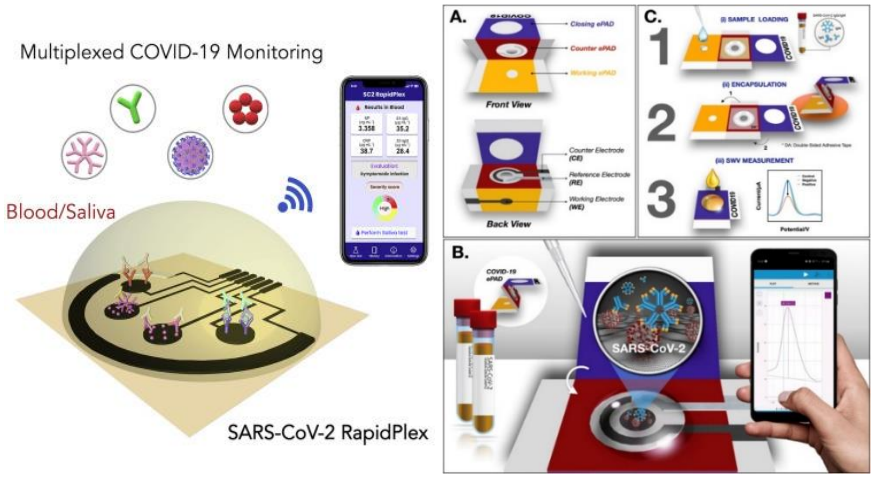

Figure 3.1: (Left) SARS-CoV-2 RapidPlex: multiplexed graphene-based electrochemical platform to detect S1-IgM, S1-IgG, N protein and C-Reactive protein; reprinted with permission from Ref.2 © 2020 Elsevier Inc. (Right) Label-free paper-based electrochemical platform to detect SARS-CoV-2 antibodies. Reprinted with permission from Ref.3. © 2020 Elsevier B.V. All rights reserved.

3.1 AIM OF THE STUDY

In this context, this study aimed at developing smart, portable and cloud-connected immunosensors to assess natural or vaccine-induced SARS-CoV-2 immunity. In particular, immunosensors aimed at detecting and discriminating IgM and IgG anti-N antibodies and IgG anti-S antibodies were developed for testing human serum. In fact, both anti-N and anti-S antibodies are detectable in infected subjects, while only anti-Spike antibodies are developed as a result of the vaccination. The developed immunosensors, therefore, will monitor the immune response of both infected and vaccinated subjects. They are based on the use of screen-printed electrodes functionalized with gold nanoparticles (GNP), carbon nanotubes (CNT), or a combination of them (CNT-GNP). In particular, the antigen receptor was immobilized on the electrode surface to bind the specific antibodies and an enzyme-labelled secondary antibody was used to generate the analytical signal, in a sandwich assay format. Alkaline phosphatase (AP) was used as enzyme label to generate the electroactive species, detectable through voltammetric measurements. In particular, in the readout step, the not electroative enzyme

substrate, hydroquinone diphosphate (HQDP), undergoes dephosphorylation operated by AP and is converted to electroactive hydroquinone (HQ); the electrochemical oxidation of HQ to benzoquinone (BQ), generates the signal of analytical interest, detected with SPE by differential pulse voltammetry (DPV); the signal is proportional to the amount of generated hydroquinone, which in turns depends on the amount of AP labels of the secondary antibody binding the target antibodies recognized by the antigen receptor .

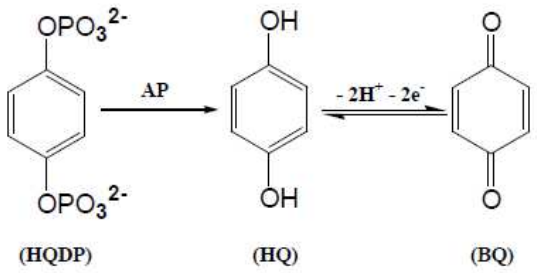

Figure 3.2 : AP-promoted dephosphorylation of HQDP and subsequent electrochemical oxidation of HQ to BQ

The signal was obtained using a smart, compact and battery powered potentiostat equipped with a Wi-fi protocol and compatible with the Internet of Things concept due to is portability, storage of data and small-size [4].

3.2 MATERIAL AND METHODS

3.2.1 Materials

Sodium chloride (NaCl), potassium chloride (KCl), potassium dihydrogen phosphate (KH_2PO_4), disodium hydrogen phosphate (Na_2HPO_4), Trizma® Base, sodium hydroxide (NaOH), hydrochloric acid (37%w/v) (HCl), magnesium chloride ($MgCl_2$), potassium ferrocyanide ($K_4[Fe(CN)_6]$), N-(3-dimethyl)-N'-ethylcarbodiimide hydrochloride (EDC), N-Hydroxysuccinimide (NHS), 4-morpholineethanesulfonic acid monohydrate (MES), Tween® 20 and plasma from bovine were purchased from Merck (Milan, Italy). Sars-CoV-2 Nucleocapsid His T protein, goat Anti-Human IgG

conjugated with alkaline phosphatase (Anti-Hu-IgG-AP) and goat Anti-Human IgM conjugated with alkaline phosphatase (Anti-Hu-IgM-AP) were purchased from Thermo Fisher Scientific (Milan, Italy). Sars-CoV-2 Nucleocapsid antibody IgG (anti-N-IgG) and IgM (anti-N-IgM), Sars-CoV-2 Spike protein S1, Sars-CoV-2 Spike S1 IgG (anti-S1-IgG) and IgM (anti-S1-IgM) antibodies, Sars-CoV-2 Spike protein RBD mFc Tag (RBD-Fc), MonoRab™ AntiMouse IgG (RAM) were purchased from GenScript (Leiden, Netherlands). Hydroquinone diphosphate (HQDP), SWCNT-SPEs (DropSens DRP-110SWCNT), GNP-SPEs (DropSens DRP-110GNP) and SWCNT/GNP-SPEs (DropSens DRP-110CNT-GNP) were purchased from Metrohm Italiana s.r.l. (Origgio, Italy).

3.2.2 Buffer composition

Phosphate Buffer Saline (PBS) at pH = 7.4 was prepared in distilled water with the following composition: 137 mM NaCl, 2.7 mM KCl, 1.2 mM KH_2PO_4, 8 mM Na_2HPO_4. PBS-T was prepared by addition of the surfactant Tween® 20 to PBS to reach a final concentration of 0.05% (w/v). TRIS buffer (pH = 7.4) and reading buffer (pH=9.8) were prepared in distilled water with the following composition: 100 mM Trizma Base, 20 mM $MgCl_2$. The pH was adjusted with 1M HCl. TRIS-T was prepared by addition of the surfactant Tween® 20 to TRIS to reach a final concentration of 0.05% (w/v). MES buffer was prepared dissolving 0.1 M MES in distilled water and adjusting the pH with NaOH to 5.0.

3.2.3 Equipments

Cyclic voltammetry (CV) experiments were carried out using a benchtop potentiostat, Autolab PGSTAT 204 (Metrohm Italiana s.r.l., Origgio, Italy) for the characterization of the functionalized SPEs. The CV measurements were carried out with a scan rate of 100 mV/s in a potential window ranging from -0.3 to 0.6 V, using 5 mM potassium ferrocyanide as a redox probe, dissolved in 0.1 M KCl.

As for the readout of the immunosensors' analytical response, the amperometric signal was generated as a result of the formation of the immunocomplex between the target and secondary antibodies, labelled with AP. The readout step was carried out by drop-casting 50 µL of a 1 mg/mL solution of HQDP dissolved in the reading buffer and performing a DPV measurement after a 150 seconds incubation with the enzyme substrate. A Wi-Fi portable potentiostat[4] , devised for PoCT or home testing, was designed and realized by electronic engineers from our research team and used for the data acquisition.

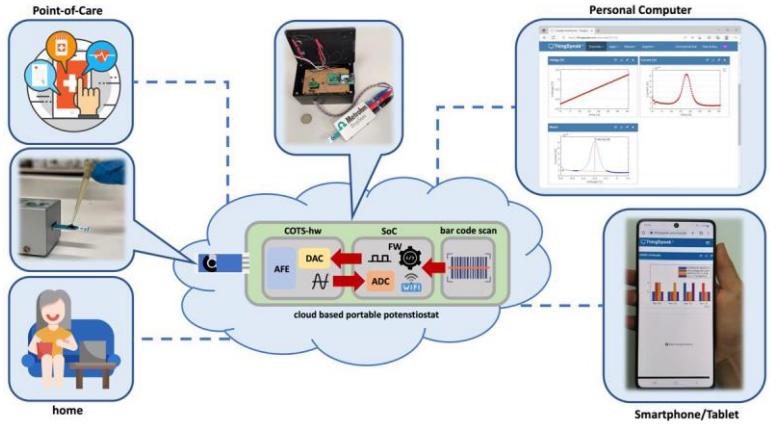

Figure 3.3: Schematic representation of the immunosensors integrated with the IoT-Wi-Fi portable potentiostat

The system architecture comprises an *Internet of Things* (**IoT**) compliant fashion, a compact, battery- powered, hardware device for the edge computing with a cloud ecosystem to improve the storage possibilities and processing capabilities for the implementation of complex functions. The *cloud* is connected to a web service accessible through common web browsers available on PCs or mobile devices, providing user interaction and visualization in a simple and intuitive way, without the need to install custom apps or software. Both serological tests require a configuration phase to set the electrical parameters of the device (e.g., cell conditioning voltage) and the implementation of a suitable calibration function for the processing of the measurement data. The system is configured only via the

dedicated web interface, whereas the calibration can be performed either onboard or by exploiting the computing power of the cloud. Once the calibration procedure is complete, the obtained parameters are stored on the cloud and made available for subsequent download. This solution allows the device to easily switch between configurations, without having to be recalibrated each time a different analysis is performed. This behaviour increases the system flexibility, since the same compact hardware device can be moved to different locations and perform different types of analyses. The hardware device includes an analog section (COTS-hw) designed for exploiting COTS (Commercial-Off-The-Shelf) components and a board assembled with a CC3200 System-on-Chip (SoC) from Texas Instruments, including an Arm Cortex M4 MCU and a Wi-Fi transceiver. The former implements the cell conditioning and signal amplification functions, while the latter is dedicated to data processing and wireless communication. Furthermore, the system is equipped with a bar code optical scanner (Newland EM3080-W) for user identification with health card before proceeding with the serological test. During the signal acquisition, according to the DPV method, an Analog Front-End (AFE) circuit generates a suitable voltage waveform (V_{bias}) between the working and the reference electrodes (WE and RE, respectively) of the electrochemical cell. The signal conditioning circuit is based on a pair of 16-bit Digital to Analog Converters (DACs) and features voltage accuracy, which affects the V_{bias} waveform similar to bench-top instruments, acquiring a total of 342 measurement points. In this work, a potential scan ranging from −0.5 to 0.3 V was applied to the electrochemical cell to perform the current measurements.

A bias voltage V_{bias} of −0.5 V is forced for cell preconditioning and, after 30 s, the DPV scan input is sent to the cell. The high and low values are progressively increased with 5 mV steps between successive periods. Under these conditions, a scan rate of 25 mV/s was applied, based on an optimized DPV waveform[5]. The

output voltage is then processed to calculate the current peak related to the target analyte concentration. The implemented algorithm performs baseline correction to detect the current peaks, even in the presence of baseline drift[6]. Based on the calibration parameters downloaded from the cloud, the device can perform qualitative analysis providing a positive or negative result, or quantitative analysis measuring the concentration of the target analyte. The possibility of performing onboard data processing allows the device to operate even in areas not covered by a Wi-Fi connection. Once a Wi-Fi link is available, the data are transmitted to the cloud for storage and visualization. This architecture also ensures great flexibility: indeed, the onboard elaboration can be replaced with the on-cloud processing, given the specific application and the requirements in terms of power consumption and the computational resources needed.

3.2.4 Serum specimens

Blood samples from either SARS-CoV-2 infected or vaccinated subjects were purchased from Ospedale San Raffaele (OSR), Milan, Italy. Vaccinated subjects were healthcare professionals belonging to OSR who were offered the Comirnaty mRNA BNT162b2 vaccine within the first two months of 2021. A set of prepandemic sera (i.e., withdrawn during 2018 and stored at the OSR biobank) were used as negative samples. Subjects were part of the *Covidiagnostix* study approved by the Institutional Ethical Review Boards (CE:199/INT/2020). Blood samples from vaccinated subjects were drawn at approximately 21 days after receiving the second dose[7].A working standard (WS) prepared by pooling 52 samples from vaccinated subjects and whose concentration is expressed as *Binding Antibody Units per mL* (BAU/mL) was used for calibration[8].

3.2.5 Anti-N Immunosensor fabrication

3.2.5.1 Receptor protein immobilization on CNT-GNP-SPE

Nucleocapsid protein was diluted in PBS to a reach a concentration of 15 µg/mL and 25 µL of this solution were drop-casted overnight on CNT-GNP SPE at +4°C. After chemisorption of receptor on GNPs occurred, SPEs were rinsed with PBS-T followed by PBS buffer.

3.2.5.2 Blocking with BSA

To avoid non-specific binding, a blocking step was carried out by incubation of a 25 µL drop of plasma from bovine at room temperature for 30 minutes. Finally, a washing step was carried out by rinsing the SPEs with TRIS-T followed by TRIS buffer.

3.2.5.3 One-pot incubation of sample and secondary antibody solution

For analysis of anti-N antibodies, a solution at the desired concentration in TRIS was mixed with a solution containing 10 µg/mL Anti-Hu-IgM-AP or Anti-Hu-IgG-AP and human serum diluted by a factor 1:50. Alternatively, for analysis of serum sample containing anti-N, the sample was diluted a 1:50 factor in a TRIS solution containing 10 µg/mL anti-Hu-AP. The solution containing anti-N antibodies or serum specimen and secondary antibody was drop-casted for 1 hour on the surface of the modified CNT-GNP SPE. At the end of the incubation, a washing step with TRIS-T followed by TRIS was carried out.

3.2.5.4 Voltammetric readout

The readout step was carried out by drop-casting 50 µl of a 1 mg/ml solution of HQDP dissolved in reading buffer and, after 150s incubation of the enzyme substrate, a DPV measurement was performed between -0.5 V and +0.1 V with the following parameters:

step potential= +0.00495 V

modulation amplitude= +0.04995 V

modulation time= 0.102 s

interval time= 0.4 s.

3.2.6 Anti-S Immunosensor fabrication

3.2.6.1 Receptor protein immobilization on CNT-SPE

As for the first receptor tested, namely the Sars-CoV-2 Spike protein, before the immobilization the carboxylic functions of CNT-SPEs were activated for coupling reaction by drop-casting 50 µL of a solution of 0.2 M EDC and 0.05 M NHS in MES buffer for 30 minutes, followed by rinsing with distilled water. Then, a solution containing the receptor diluted at the desired concentration was prepared in PBS buffer and 50 µL were directly incubated on CNT-SPEs surface. After incubation, electrodes were rinsed with PBS-T and PBS buffer.

For the immobilization of the second receptor tested, namely Sars-CoV-2 Spike protein RBD mFc Tag (RBD-Fc), carboxylic groups of CNT-SPEs were previously activated as before mentioned. Then, a solution of RAM secondary antibody diluted in PBS to a final concentration of 20 µg/mL was incubated on the SPE surface overnight. After incubation, a washing step with PBS-T followed by PBS was performed. To perform receptor immobilization, 25 µL of a 3.75 µg/mL solution of RBD-Fc were drop-casted and left for 1 hour, after which a washing step with PBS-T and PBS was carried out.

3.2.6.2 Blocking

The SPE surface was treated with a 30 minutes incubation of a 25 µL drop of plasma from bovine to block potentially occurring non-specific interactions. A final washing step was carried out by rinsing the SPE with TRIS-T followed by TRIS.

3.2.6.3 One-pot incubation of sample and secondary antibody solution

To perform analysis of serum containing anti-S of the IgG isotype, the sample was diluted by a 1:10 factor in a TRIS solution containing 45 µg/ml anti-Hu-IgG-AP. The solution containing anti-S and secondary antibody was drop-casted for 1 hour on the surface of the modified CNT -SPE. At the end of the incubation, a washing step with TRIS-T followed by TRIS buffer was carried out.

3.2.6.4 Voltammetric readout

The readout step was carried out by drop-casting 50 µL of a 1 mg/ml solution of HQDP dissolved in reading buffer and after 150s incubation of the enzymatic substrate a DPV measurement was performed between -0.5 V and +0.3 V with the same waveform exploited for anti-N immunosensors (see 1.2.5.4).

3.2.7 Data acquisition and manipulation for anti-N and anti-S immunosensors

The analytical performance of the immunosensors was assessed in human serum matrix. For this purpose, sera from the pre-pandemic period were spiked with commercial monoclonal anti-N antibodies in the case of the anti-N immunosensor. Concerning the anti-S immunosensor, a 20,000 BAU/mL anti-S WS[8] was gradually diluted in the same pre-pandemic matrix up to 500 BAU/mL. Firstly, validation of the immunosensors developed for SARS-CoV-2 anti-N and anti-S antibodies detection and quantification was performed, according to the Eurachem Guide[9]. For this purpose, LOD, LOQ, linearity and precision were calculated, performing three replicated measurements for each level explored. As for LOD and LOQ, 10 replicate measurements of blank samples, i.e., matrices containing no detectable analyte, were carried out; LOD was calculated as $3*s_0/\sqrt{n}$ and LOQ as $10*s_0/\sqrt{n}$, where s_0 is the blank standard deviation and n is the number of replicate measurements. Concerning the evaluation of linearity, the regression residuals

were calculated, the mean of which over the linearity range was not significantly different from zero ($p > 0.05$). The precision was measured on two levels, i.e., the lower and upper levels of the calibration curve for each immunosensor. The selectivity of the immunosensors was assessed in human serum in terms of the matrix effect. The evaluation of both of the diagnostic tests was carried out in human COVID-19 serum samples from infected subjects provided by the OSR, following the diagnostic guidelines for epidemiological data[10] for the validation of the immunosensors with clinical specimens in terms of sensitivity, specificity and accuracy.

3.3 RESULTS AND DISCUSSION

3.3.1 Electrode surface immobilization

To evaluate the effective immobilization of receptors on the electrode platform, for both the developed immunosensors, cyclic voltammograms were recorded, using ferrocyanide as a redox probe and monitoring signals after immobilization of the different receptors (N protein and RBD-Fc). As shown in Figure 3.4, a progressive decrease in the diffusion current during the sequential functionalization of the SPEs occurs.

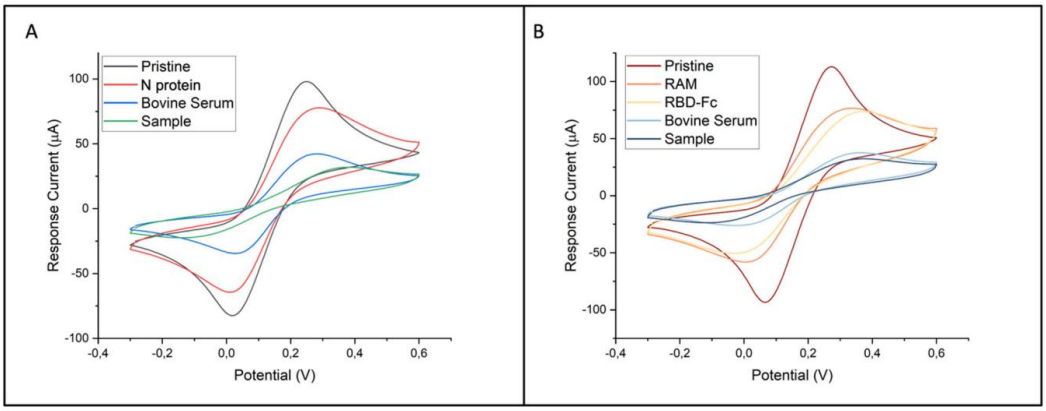

Figure 3.4: Cyclic voltammograms acquired after each functionalization step for (A) anti-N immunosensor on SWCNT/GNP-SPEs and (B) anti-S immunosensor on SWCNT-SPEs using ferrocyanide as redox probe for the characterization of SPEs functionalization.

3.3.2 Anti-N Immunosensor setup

As for anti-N antibodies, both IgG and IgM antibodies were detected. The immunochemical setup involves the nucleocapsid protein as the receptor, used to recognize and bind specific antibodies, i.e., IgG and IgM anti-N antibodies. These antibodies are, in turn, bound by the anti-Human secondary antibodies (Anti-Hu-IgG-AP; Anti-Hu-IgM-AP) in the constant portion (Fc).

Hence, the antigen is immobilized onto the SPE surface, then a mixture of the human target antibodies and secondary antibodies is incubated on the

immunosensor surface. The last step consists of the addition of the enzyme substrate to obtain the signal of analytical interest.

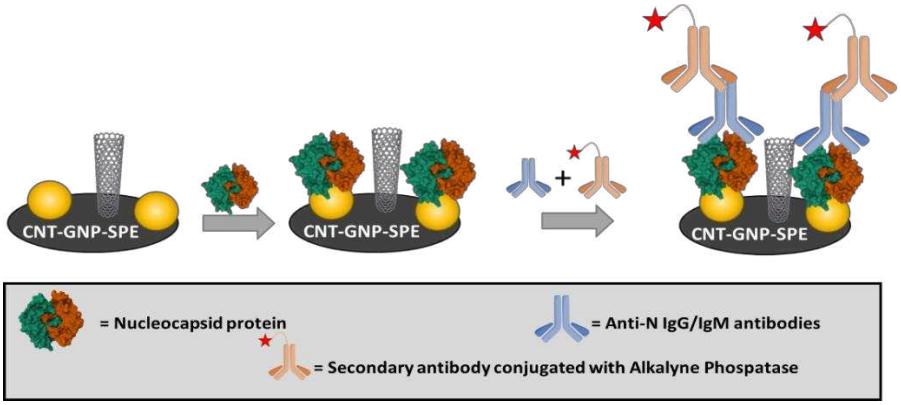

Figure 3.5 Protocol for development of anti-N immunosensor

As shown in Figure 3.5, the immunoassay only involves few steps and the sample incubation lasts one hour, thus allowing to consider these immunosensors time-effective, user-friendly and compatible with Point-of-Care tests as they also have small dimensions and a portable device for the readout.

3.3.3 Evaluation of different parameters for anti-N immunosensors

3.3.3.1 Nucleocapsid concentration

In order to obtain a proper functionalization of the SPE surface and to maximize the response signals, different concentrations of nucleocapsid protein were tested. Initially, to exclude the presence of non-specific binding, SPEs without antigen and anti-N antibodies incubation were separately evaluated: in both cases, signals were negligible, as shown in Figure 3.6

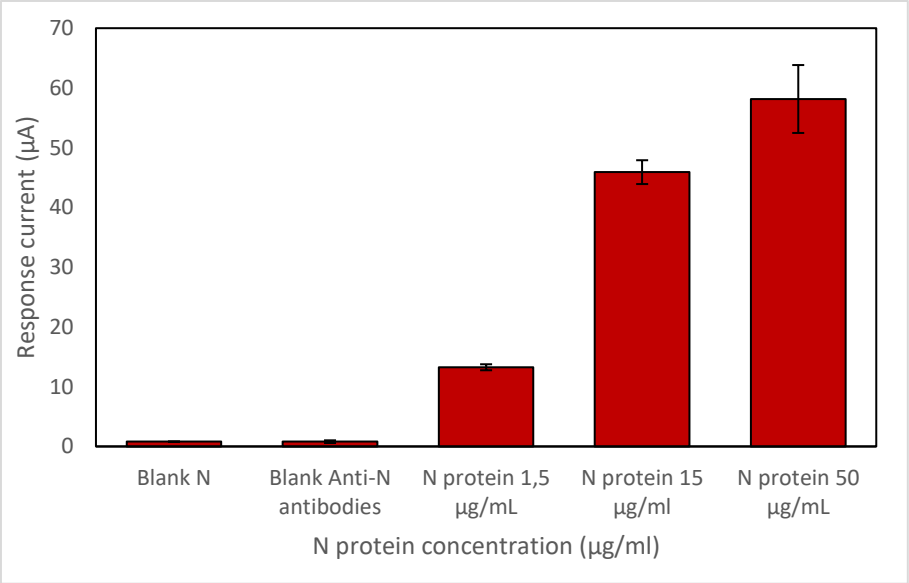

Figure 3.6: Effect of different nucleocapsid concentrations on response current

Subsequently, different N protein concentrations were considered: 1,5 µg/ml, 15 µg/ml and 50 µg/mlAnti-N antibodies and Anti-Hu-AP concentrations were kept at 5 µg/ml and 1 µg/ml, respectively, for these tests. Based on the current peak, the best results were obtained with the highest explored concentration but considering the data dispersion (standard deviation) the response at 50 µg/ml resulted to be not statistically different *($p>0.05$)* from the intermediate concentration; thus, it was decided to fix the concentration of 15 µg/ml N protein for all subsequent experiments.

3.3.3.2 Effect of serum dilution and Anti-Hu-AP concentration

After finding the best conditions for nucleocapsid protein concentration, the effect of the matrix on the analytical response was considered. To this end, it was chosen to test the results obtained by diluting the anti-N antibody standards in commercial human serum. Within the serum matrix there may be interfering elements, in particular other antibodies of IgG isotype, typically present in high concentrations

in serological samples[11]. They are different in a few aminoacidic residues present in the constant portion domains and in the hinge region, compared to those directed against nucleocapsid, thus causing possible interferences in the binding with the secondary antibody. Due to interference with other antibodies, a limited number of secondary antibodies is available to bind and recognize specific anti-N IgG and IgM: for this reason, both serum dilution and higher concentration of Anti-Hu-IgG-AP and Anti-Hu-IgM-AP were considered.

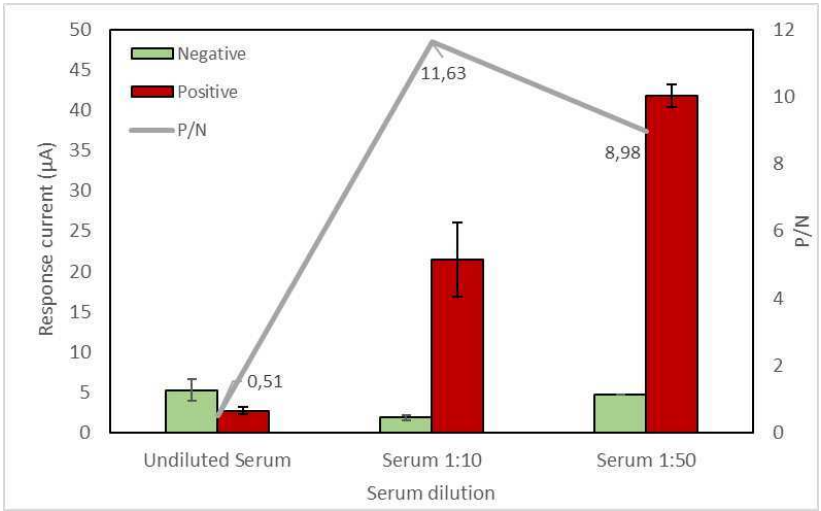

Figure 3.7: Effect of serum dilution on response current

In particular, three different conditions for serum were evaluated: undiluted serum, 1:10 and 1:50 diluted serum in TRIS buffer (Figure 3.7). The positive/negative ratio corresponding to the undiluted serum replicates resulted lower than 1 and had minimal current values and high dispersion. As for 1:10 and 1:50 dilution, the positive/negative ratio in the first case was higher. However, it should be noticed that the relative signal dispersion obtained on three replicates per level was significantly higher for 1:10 dilution (RSD>10%) and the positive peak intensity was significantly lower than 1:50 dilution. Hence, a 1:50 dilution factor for serum was considered for the following experiments.

Under the best conditions obtained for serum dilution, the secondary antibody concentration was considered for both IgG and IgM (Figure 3.8). In particular, two levels for each of them were considered, i.e., 10 µg/ml and 20 µg/ml: in both cases, the best combination between highest P/N ratio and lower RSD values was found with the lower concentration of the Anti-Hu-AP.

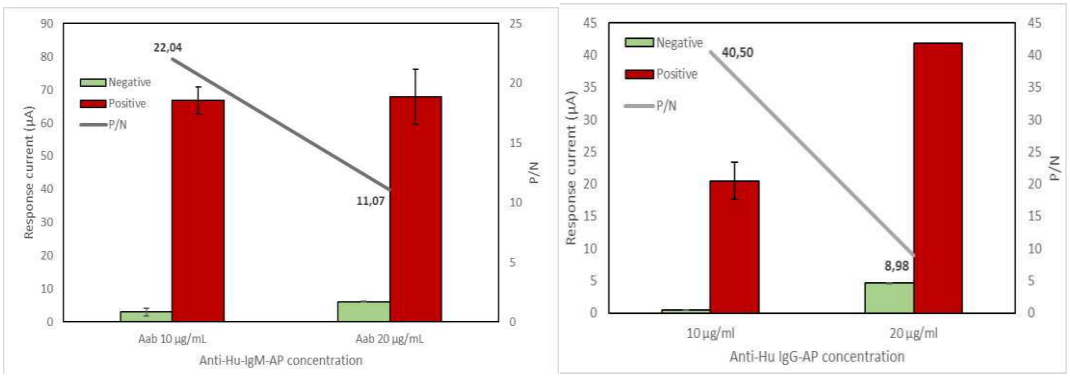

Figure 3.8: Effect of different concentration of Anti-Hu-IgM-AP (left) and Anti-Hu-IgG-AP (right)

3.3.4 Linearity assessment

To assess the linearity of anti-N immunosensors for the detection of IgG and IgM antibodies, two different electrode platforms were considered: GNP-SPE (Figure 3.9) and SWCNT/GNP-SPE (Figure 3.10). All the calibration lines were acquired in 1:50 diluted serum.

In particular, with GNP-SPE electrodes and anti-N IgM antibodies, concentrations from 0,5 to 10 µg/ml were explored, obtaining a linear response between 0,75 and 5 µg/ml. In this case LOD and LOQ of 0,18 and 0,56 µg/ml were observed, respectively. Regarding the same platform with anti-N IgG antibodies, the explored range was 0.75-10 µg/ml, with a linear response between 1 and 5 µg/ml. In this case, calculated LOD and LOQ were 0.21 and 0.6 µg/ml, respectively.

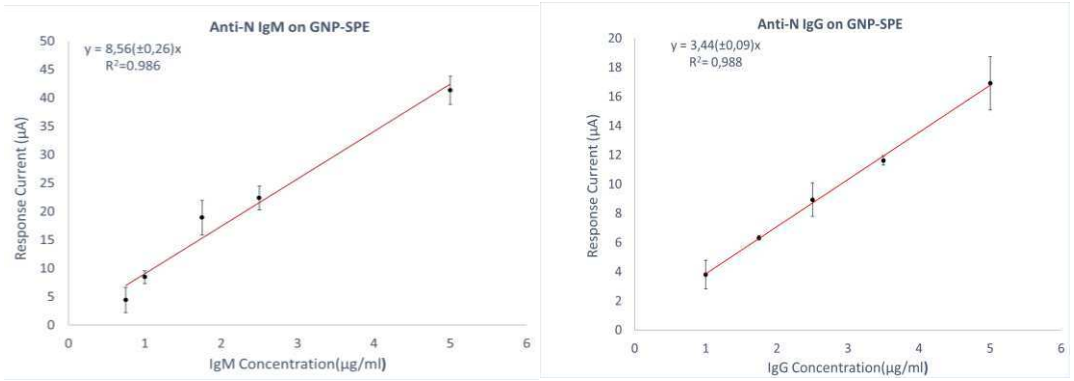

Figure 3.9: Linear response for different concentrations of Anti-N IgM antibodies (left) and Anti-N IgG antibodies (right) on SWCNT-SPEs

As for SWCNT-GNP/SPE, the combination of gold nanoparticles and carbon nanotubes gives a significant improvement on the performance of the immunosensors: in fact, GNPs are involved into receptor immobilization, while carbon nanotubes increase the surface area of the electrode, promoting the electron transfer and amplification of the signal.

Anti-N IgM antibodies were tested in a range from 0,25 µg/ml to 1,75 µg/ml, with a linear response between 0,25 and 1,5 µg/ml. Lower values of LOD and LOQ (0,05 µg/ml and 0.16 µg/ml, respectively) were obtained in comparison with GNP-SPE.

Regarding anti-N IgG antibodies, a range between 0,25 and 5 µg/ml was explored: linearity was observed between 0,25 and 2,5 µg/ml, with LOD and LOQ levels of 0,06 and 0,19 µg/ml.

As a result, for both anti-N IgG and IgM antibodies better performances were obtained with the combination of CNT and GNP electrodes in terms of sensitivity and precision, thus permitting to select them for the following experiments.

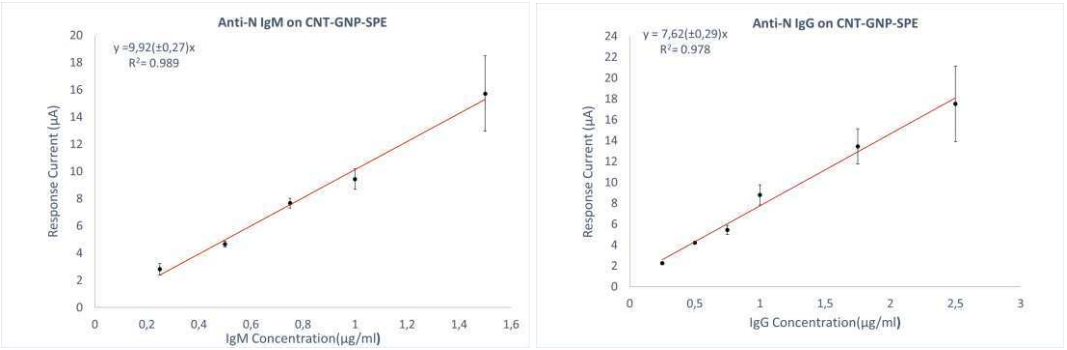

Figure 3.10: Linear response for different concentrations of Anti-N IgM antibodies (left) and Anti-N IgG antibodies (right) on CNT-GNP SPEs

3.3.5 Validation in clinical samples

Validation on real samples was carried out using clinical serum samples provided by OSR and tested with Roche Elecsys® Anti-SARS-CoV-2 chemiluminescence immunoassay, used as the reference instrument to evaluate the right classification of the samples. For the immunoassay developed for anti-N antibodies detection, 21 serum samples were tested, including 10 negative patients (anti-N concentration <1 AU/mL assessed on Elecsys Anti-SARS-CoV-2) and 11 SARS-CoV-2 positive patients (anti-N concentration > 1 AU/mL assessed on Elecsys Anti-SARS-CoV-2). Even though the number of samples tested was quite limited to perform a clinical validation, it was possible to correctly classify all of the samples, as shown in Figure 3.11, giving excellent performances in terms of selectivity, accuracy and sensitivity, close to 100%.

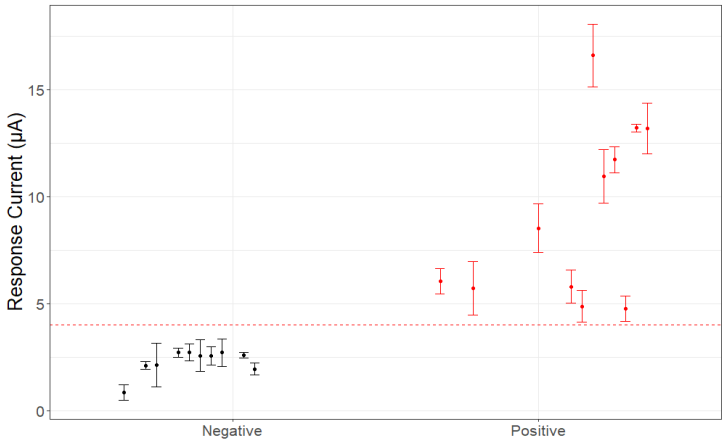

Figure 3.11: Scatterplot of current responses resulted from serum samples containing anti-N IgG antibodies.

3.3.6 Anti-S Immunosensor setup

As for anti-S antibodies, an immunosensor was developed to determine IgG in serum samples. It is worth noticing that, in this case, the test is aimed at detecting antibodies expressed both upon SARS-CoV-2 infection and as effect of vaccination[12]. Analogously to the immunosensors developed for anti-N antibodies, the assay is based on the immobilization of the antigen receptor onto the electrode surface to detect antibodies in serum samples, which are in turn recognised from a secondary antibody conjugated with AP, to generate the analytical signal.

3.3.7 Evaluation of different parameters for anti-S immunosensors

3.3.7.1 Receptor immobilization

For the detection of anti-S antibodies, two different receptors were tested.

Initially, the S1 protein, which is a subunit of the Spike protein involved into the binding with anti-S antibodies, was immobilized onto the electrode surface of CNT-SPEs after activation with coupling reagents (Figure 3.12). Then, a premixed solution of serum samples and AP-labelled secondary antibodies was incubated for 1 hour for the recognition between the immobilized antigen and target antibodies,

followed by generation of the voltametric signal, thanks to the addition of the AP substrate.

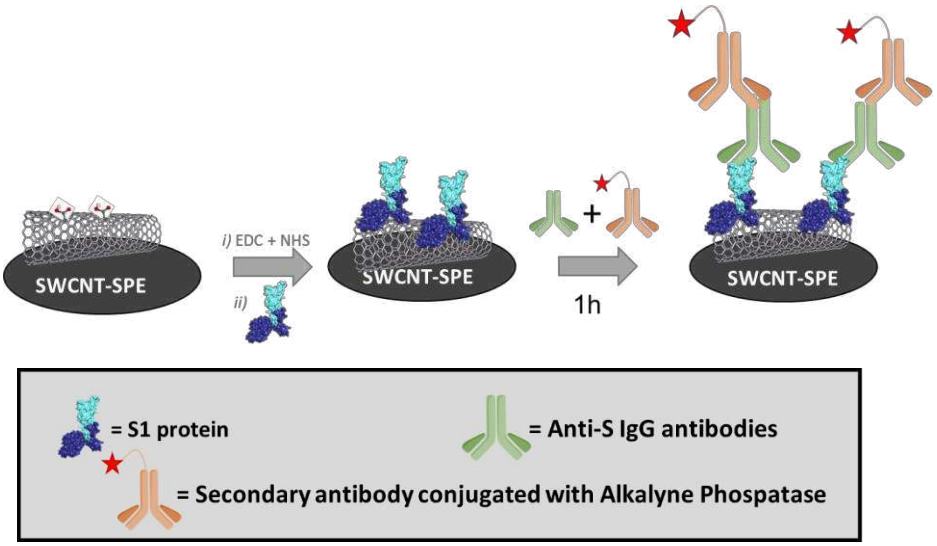

Figure 3.12: Protocol for development of anti-S immunosensor with S1 receptor

The S1 protein concentration was initially tested at 10, 15 and 20 µg/mL in the presence of anti-S1-IgG monoclonal antibodies (5 µg/mL) and anti-Hu-IgG-AP (2 µg/mL) on SWCNT-SPEs. Best response was observed for 15 µg/mL, as shown in Figure 3.13, which was then used for further experiments.

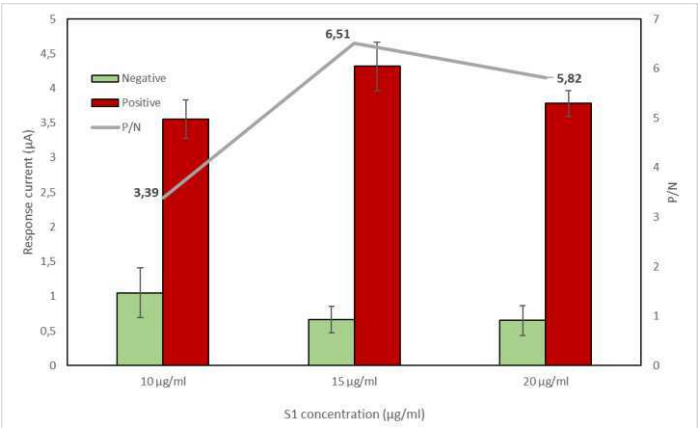

Figure 3.13: Effect of different S1 concentration on response current and P/N ratio

However, after evaluating different parameters, a strong matrix effect was observed analysing serum samples containing anti-S antibodies. In particular, different electrode platforms were tested, and several blocking agents were exploited (casein, fetal bovine serum, powdered milk). These data can probably be explained by hypothesizing that S1 receptor interacts with species present in the serum samples, giving non-specific signal and not significantly differences between negative and positive samples with a high concentration of anti-S IgG antibodies, as reported in Figure 3.14.

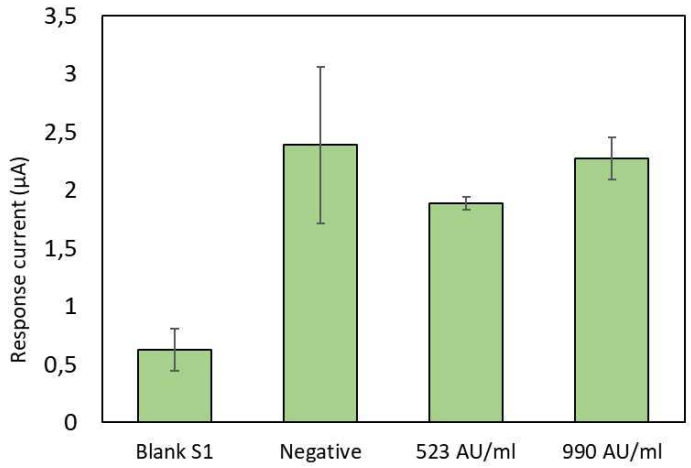

Figure 3.14: Different serum samples tested with S1 receptor causing matrix effect.

In order to overcome this problem, we focused our attention on a different receptor, namely RBD-Fc, in which the Receptor Binding Domain of SARS-CoV-2 (RBD) is conjugated to a Fc mouse moiety, that can be immobilized onto the surface by means of a rabbit-anti-mouse secondary antibody (RAM). For this setup, represented in Figure 3.15, RAM is covalently immobilized on previously activated SWCNT SPEs, then RBD-Fc is incubated so that the Fc moiety can be recognised and interact with RAM. Subsequently, a premixed solution of serum samples containing anti-S antibodies and Anti-Hu IgG-AP is incubated to finally generate the analytical signal, when HQDP is added.

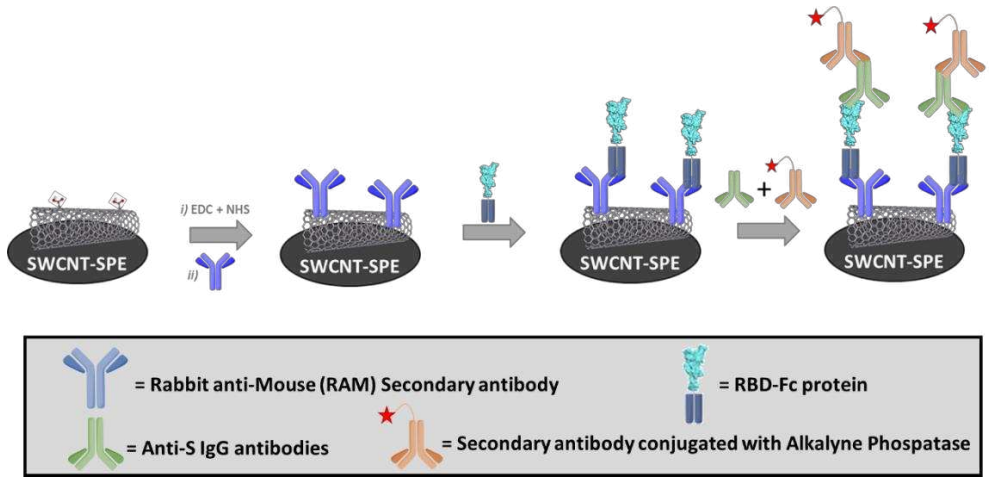

Figure 3.15: Protocol for development of anti-S immunosensor with RBD-Fc receptor

3.3.7.2 Electrode platform and RAM effect

In this immunosensor setup, the RBD-Fc is anchored to the surface using a secondary antibody. To this end, two different electrode platforms (GNP-SPEs and SWCNT-SPEs) were tested immobilizing the RBD-Fc protein directly or indirectly *via* RAM.

The best combination resulted in the use of SWCNT -SPEs and RAM on the surface. In fact, significantly lower signals with negligible P/N ratio were obtained without the use of RAM. Besides, it is worth noticing that probably the immobilization given by GNP is not efficient or it causes a wrong orientation of the receptor, thus determining a weak interaction with antibodies (see Figure 3.16).

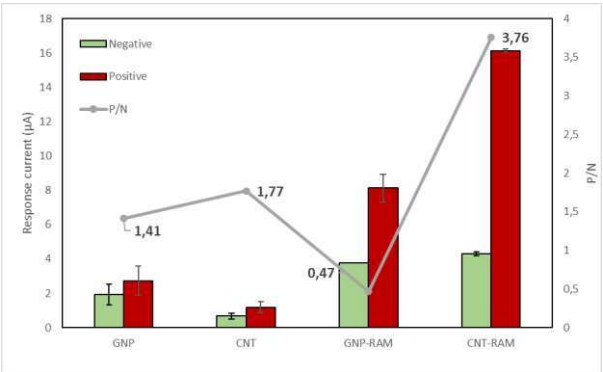

Figure 3.16: Effect of different electrode platforms (CNT-GNP) and RAM antibody

3.3.7.3 Effect of RBD-Fc and RAM concentration

Once it was established which was the best electrode platform and strategy for the immobilization of the receptor, different concentrations for both RAM and RBD-Fc were considered. In the first case, concentration ranging from 10 to 50 µg/ml were tested, while the receptor antigen was kept at 7.5 µg/ml. The best response was obtained at 20 µg/mL (see Figure 3.17).

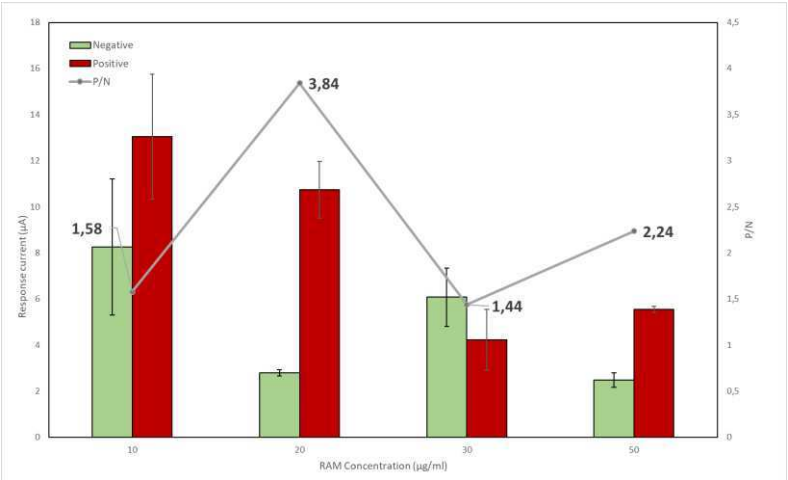

Figure 3.17: Effect of RAM-antibody concentration on P/N ratio and response current

Under these conditions, the RBD-Fc concentration was explored ranging from 1.88 to 30 µg/ml on SWCNT-SPEs. Figure 3.18 shows as best results were obtained at 3.75 µg/ml: in fact, it was observed that at lower concentrations probably it is not possible to interact with all the available RAM interaction sites, while a signal decrease was noticed at higher concentrations, probably due to over-crowding of antibody-binding sites.

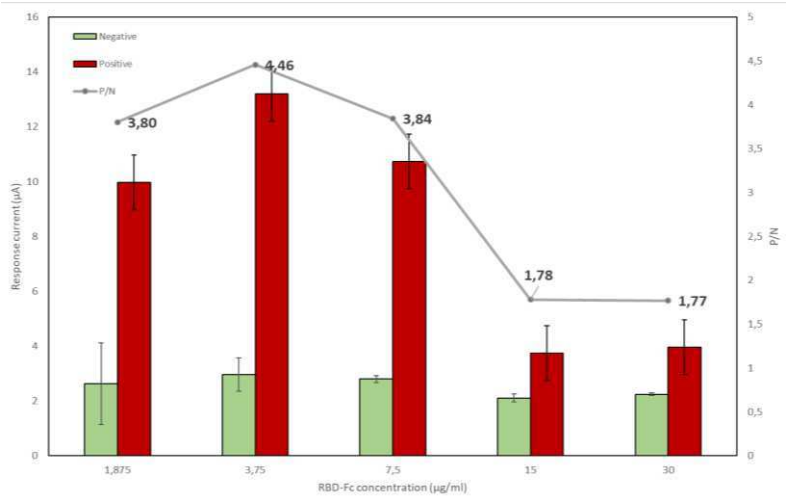

Figure 3.18: Effect of different RBD-Fc concentrations on P/N ratio and response current

3.3.7.4 Effect of serum dilution and Anti-HU-IgG-AP concentration

Different serum dilution factors were tested, using the same pooled working standard provided by OSR and exploited for anti-N immunosensor from vaccinated subjects[8] as positive samples and pooled human sera from the prepandemic period as negative controls. The dilution was carried out using TRIS buffer with three factors tested, namely 1:25, 1:10 and 1:5. Best results were observed using a 1:10 dilution factor (see Figure 3.19).

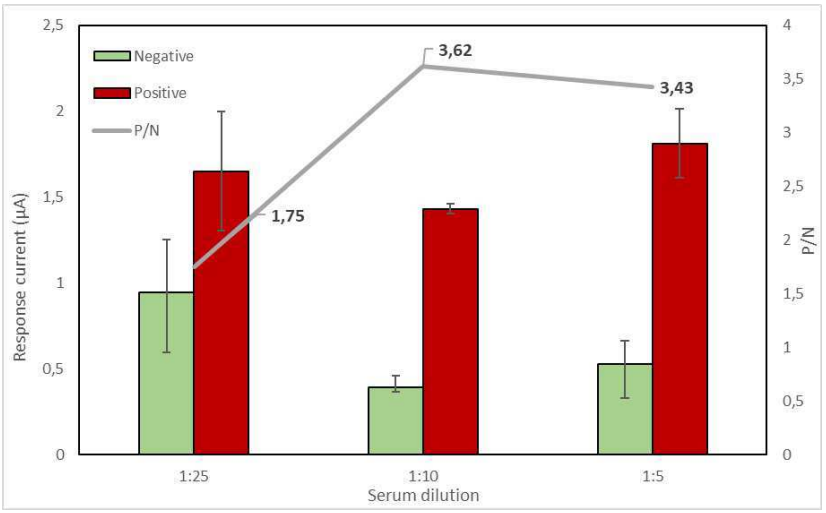

Figure 3.19: Effect of different serum dilution on P/N ratio and response current

Under the best conditions obtained for serum dilution, the effect of Anti-Hu-IgG-AP concentration was evaluated by exploring the response at 20, 30, 40 and 45 µg/ml. The highest P/N ratio was obtained with the maximum concentration tested, as shown in Figure 3.20, therefore the secondary antibody concentration used for subsequent experiments was set at 45 µg/ml.

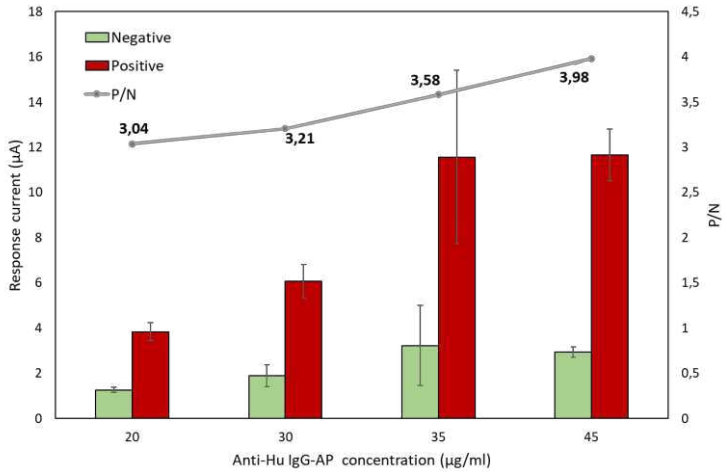

Figure 3.20: Effect of different Anti-Hu-IgG-AP concentrations on P/N ratio and response current

The absence of non-specific signals was assessed under these conditions, carrying out measurements in absence or in presence of the RBD-Fc receptor. No significant signals were observed for blank RBD-Fc and negative samples and the responses were both significantly different from the positive sample (550 AU/ml), thus confirming that no interactions were taking place between the receptor and matrix components, as reported in Figure 3.21.

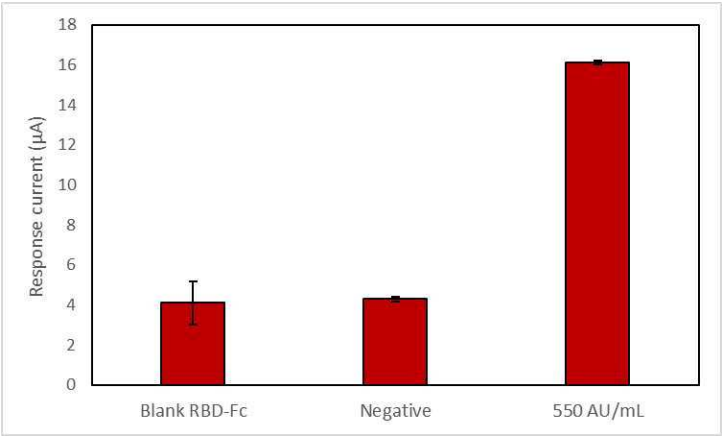

Figure 3.21: Effect of serum samples using RBD-Fc receptor.

3.3.8 Linearity assessment

To evaluate the linearity of the anti-S immunosensor based on RBD-Fc receptor, different anti-S-IgG levels were tested in samples ranging from 500 to 2000 BAU/ml. Tests were performed on SWCNT-SPEs using 1:10-diluted samples. A linear response was obtained from 500 to 1500 BAU/ml (see Figure 3.22), with LOD and LOQ values of 210 and 233 BAU/ml, respectively. Precision assessed at lower and upper concentration levels of the calibration resulted in RSD values of 9% and 7%, respectively. Taking into account the low presence of IgM positive clinical samples and that IgG are the most relevant antibodies for the evaluation of the immune response induced by vaccination, the study continued on the detection of the anti-S-IgG antibody isotype.

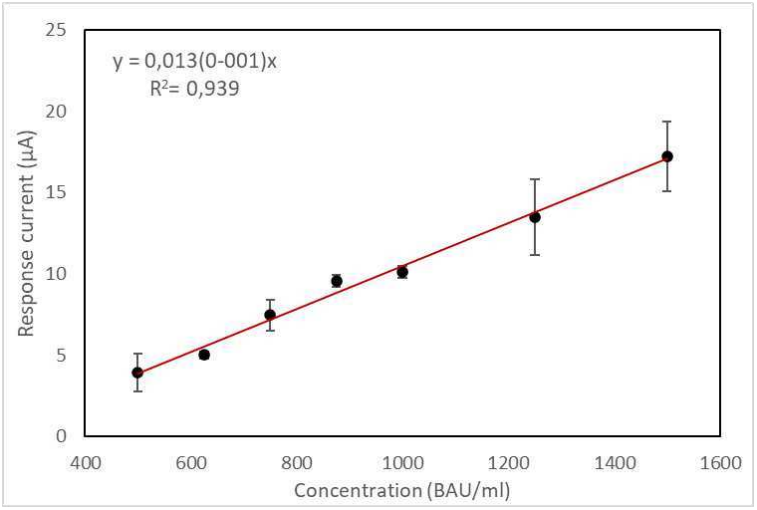

Figure 3.22: Linear response of anti-S antibodies in different concentration of serum samples

3.3.9 Validation in clinical samples

As for validation in clinical samples of the anti-S immunosensor, the recovery rate of the assay was evaluated by exploiting samples obtained by diluting the WS with pre-pandemic human serum. From the undiluted WS (20000 BAU/mL) three solutions at concentrations of 600, 800 and 1100 BAU/mL were prepared. Concentrations values found from the developed immunosensor were 570 BAU/mL, 854 BAU/mL and 1023 BAU/mL, resulting in recovery values of 95%, 106% and 93%.

Analysis of single-patient serum specimens was also performed on six samples from subjects previously infected by SARS-CoV-2. The resulting anti-S concentrations calculated using the calibration curve were compared with the titers obtained at OSR using the Roche Elecsys® chemiluminescence immunoassay. A good correlation (R^2=0.87) between the two devices was obtained, as shown in Figure 3.23, taking into account that they shared the same protein target (RBD protein). It is also worth noticing that this correlation level is remarkable considering the lack of standardization among devices produced by different manufacturers. To this end, different studies showed that when comparing devices based on both

different technologies and different S-protein targets (i.e., monomeric soluble form, trimeric form, RBD motif) the correlation factors were as low as R^2=0.13[8]. Therefore, the developed immunosensor was proven as a valuable tool for monitoring of the immune response to SARS-CoV-2 infection and vaccine-induced immunity.

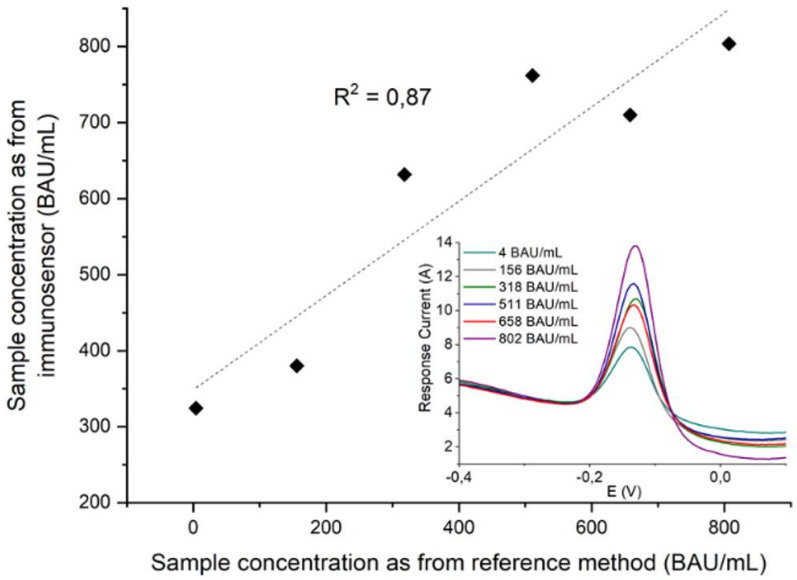

Figure 3.23: Correlation between anti-S IgG in serum samples measured by the immunosensor and corresponding values obtained by reference chemiluminescence immunoassay instrument.

This work led to the publication of a research article:

- Fortunati, S.; Giannetto, M.; Giliberti, C.; Bolchi, A.; Ferrari, D.; Locatelli, M.; Bianchi, V.; Boni, A.; De Munari, I.; Careri, M. Smart Immunosensors for Point-of-Care Serological Tests Aimed at Assessing Natural or Vaccine-Induced SARS-CoV-2 Immunity. *Sensors* **2022**, *22*, 5463. https://doi.org/10.3390/s22145463

3.4 REFERENCES

1. Rahman, M. M. Progress in Electrochemical Biosensing of SARS-CoV-2 Virus for COVID-19 Management. *Chemosensors* **10**, (2022).
2. Torrente-Rodríguez, R. M. *et al.* SARS-CoV-2 RapidPlex: A Graphene-Based Multiplexed Telemedicine Platform for Rapid and Low-Cost COVID-19 Diagnosis and Monitoring. *Matter* **3**, 1981–1998 (2020).
3. Yakoh, A. *et al.* Paper-based electrochemical biosensor for diagnosing COVID-19: Detection of SARS-CoV-2 antibodies and antigen. *Biosens. Bioelectron.* **176**, 112912 (2021).
4. Bianchi, V. *et al.* IoT and Biosensors: A Smart Portable Potentiostat with Advanced Cloud-Enabled Features. *IEEE Access* **9**, 141544–141554 (2021).
5. Giannetto, M. *et al.* An integrated IoT-Wi-Fi board for remote data acquisition and sharing from innovative immunosensors. Case of study: Diagnosis of celiac disease. *Sensors Actuators B Chem.* **273**, 1395–1403 (2018).
6. Bianchi, V. *et al.* A Wi-Fi Cloud-Based Portable Potentiostat for Electrochemical Biosensors. *IEEE Trans. Instrum. Meas.* **69**, 3232–3240 (2020).
7. Ferrari, D. *et al.* Long-term antibody persistence and exceptional vaccination response on previously SARS-CoV-2 infected subjects. *Vaccine* **39**, 4256–4260 (2021).
8. Ferrari, D. *et al.* Harmonization of six quantitative SARS-CoV-2 serological assays using sera of vaccinated subjects. *Clin. Chim. Acta* **522**, 144–151 (2021).
9. B. Magnusson and U. Örnemark. Eurachem Guide: The Fitness for Purpose of

Analytical Methods – A Laboratory Guide to Method Validation and Related Topics. in *Eurachem Guide: The Fitness for Purpose of Analytical Methods – A Laboratory Guide to Method Validation and Related Topics* (2014).

10. Zhu, W., Zeng, N. & Wang, N. Sensitivity, specificity, accuracy, associated confidence interval and ROC analysis with practical SAS® implementations. *Northeast SAS Users Gr. 2010 Heal. Care Life Sci.* 1–9 (2010).

11. Objectives, L. 18.4: B Lymphocytes and Antibodies - Biology LibreTexts. 1–6.

12. Poland, G. A., Ovsyannikova, I. G. & Kennedy, R. B. SARS-CoV-2 immunity: review and applications to phase 3 vaccine candidates. *Lancet* **396**, 1595–1606 (2020).

13. (WHO), W. H. O. Testing for SARS-CoV-2 infection and immunity. 30 (2021).

14. Chen, Q. *et al.* Diagnostic technologies for COVID-19: a review. *RSC Adv.* **10**, 35257–35264 (2020).

15. Corman, V. M. *et al.* Detection of 2019 novel coronavirus (2019-nCoV) by real-time RT-PCR. *Eurosurveillance* **25**, (2020).

16. Hsiao, W. W. W. *et al.* Recent advances in novel lateral flow technologies for detection of COVID-19. *Biosensors* **11**, 1–26 (2021).

17. You, M. *et al.* Household Fluorescent Lateral Flow Strip Platform for Sensitive and Quantitative Prognosis of Heart Failure Using Dual-Color Upconversion Nanoparticles. *ACS Nano* **11**, 6261–6270 (2017).

18. Etienne, E. E., Nunna, B. B., Talukder, N., Wang, Y. & Lee, E. S. Covid-19 biomarkers and advanced sensing technologies for point-of-care (Poc) diagnosis. *Bioengineering* **8**, 1–27 (2021).

19. Martín, J., Tena, N. & Asuero, A. G. Current state of diagnostic, screening and surveillance testing methods for COVID-19 from an analytical chemistry point

of view. *Microchem. J.* **167**, 106305 (2021).

20. Lino, A., Cardoso, M. A., Gonçalves, H. M. R. & Martins-Lopes, P. SARS-CoV-2 Detection Methods. *Chemosensors* **10**, (2022).

21. Fortunati, S. *et al.* Smart Immunosensors for Point-of-Care Serological Tests Aimed at Assessing Natural or Vaccine-Induced SARS-CoV-2 Immunity. *Sensors* **22**, (2022).

22. Farzin, L., Sadjadi, S., Sheini, A. & Mohagheghpour, E. A nanoscale genosensor for early detection of COVID-19 by voltammetric determination of RNA-dependent RNA polymerase (RdRP) sequence of SARS-CoV-2 virus. *Microchim. Acta* **188**, (2021).

23. Sadique, M. A. *et al.* Highly Sensitive Electrochemical Immunosensor Platforms for Dual Detection of SARS-CoV-2 Antigen and Antibody based on Gold Nanoparticle Functionalized Graphene Oxide Nanocomposites. *ACS Appl. Bio Mater.* (2022) doi:10.1021/acsabm.2c00301.

24. Seo, G. *et al.* Rapid Detection of COVID-19 Causative Virus (SARS-CoV-2) in Human Nasopharyngeal Swab Specimens Using Field-Effect Transistor-Based Biosensor. *ACS Nano* **14**, 5135–5142 (2020).

25. Fabiani, L. *et al.* Magnetic beads combined with carbon black-based screen-printed electrodes for COVID-19: A reliable and miniaturized electrochemical immunosensor for SARS-CoV-2 detection in saliva. *Biosens. Bioelectron.* **171**, (2021).

26. No Title. https://thingspeak.com/ https://thingspeak.com/.

27. Donofrio, G. *et al.* A simplified sars-cov-2 pseudovirus neutralization assay. *Vaccines* **9**, 1–12 (2021).

28. Giannetto, M., Bianchi, M. V., Mattarozzi, M. & Careri, M. Competitive

amperometric immunosensor for determination of p53 protein in urine with carbon nanotubes/gold nanoparticles screen-printed electrodes: A potential rapid and noninvasive screening tool for early diagnosis of urinary tract carcinoma. *Anal. Chim. Acta* **991**, 133–141 (2017).

29. Pallesen, J. *et al.* Immunogenicity and structures of a rationally designed prefusion MERS-CoV spike antigen. *Proceedings of the National Academy of Sciences of the United States of America* vol. 114 E7348–E7357 (2017).

30. Sriwilaijaroen, N. & Suzuki, Y. Molecular basis of the structure and function of H1 hemagglutinin of influenza virus. *Proc. Japan Acad. Ser. B Phys. Biol. Sci.* **88**, 226–249 (2012).

31. Zeng, X. T., Zhang, C., Kwong, J. S. W., Sun, X. & Li, Y. P. Software for network meta-analysis: A usage-based comparative study. *Chinese J. Evidence-Based Med.* **14**, 1270–1275 (2014).

32. Bianchi, V. *et al.* IoT and Biosensors: A Smart Portable Potentiostat with Advanced Cloud-Enabled Features. *IEEE Access* **9**, 141544–141554 (2021).

4 SARS-CoV-2 antigen testing

SARS-CoV-2 infection diagnosis is based on two different types of tests: Nucleic Acid Amplification Testing (NAAT), which detects viral genetic material, and Immunochemical Antigen Testing, for the detection of viral proteins, like nucleocapsid or spike protein[1].

In both cases, swab tests are used to sample upper respiratory fluids or saliva. In the context of NAAT testing, quantitative reverse transcription Polymerase Chain Reaction (RT-qPCR), is considered the "gold standard" for infection diagnosis[2], due to its high sensitivity and reliability. For this analysis, the biological sample is collected to isolate RNA. After isolation, the RNA is converted into cDNA with a reverse transcription, then amplification of specific viral regions detected by specific primers and probes occurs. The amplificated sequences are subsequently detected by a fluorescence signal.

Primers and probes specific for SARS-CoV-2 recommended by World Health Organization also contain Nucleocapsid (N) and Spike (S) genes[3]. NAAT results are usually available within 24 hours: the time required for testing is until 4 hours, but transport and sample management can significantly lengthen analysis time.

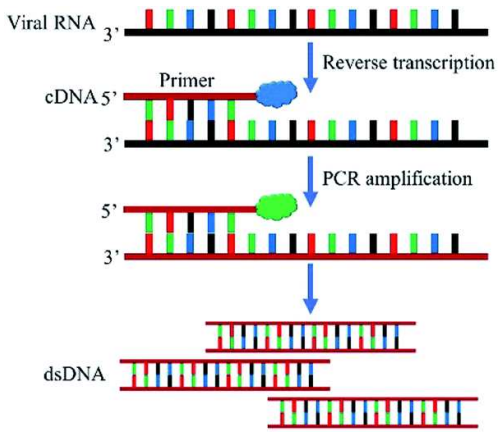

Figure 4.1: Scheme of Real-Time Polymerase Chain Reaction (RT-PCR). Reprinted with permission from Ref.2 © The Royal Society of Chemistry 2020

For antigen testing, upper respiratory samples are analysed to detect viral proteins and diagnose ongoing SARS-CoV-2 infection. These tests can diagnose the infection "on-site" within first 5-7 days of symptoms. They are available both for professional and self-testing use and time required for analysis is significantly lower than RT-PCR, as only 15-30 minutes are usually required for results. In addition, antigen tests are remarkably cheaper, if compared with NAAT, even though they present relatively lower sensitivity and specificity. Among them, Lateral Flow Immunoassays (LFIA) are widely and extensively used.

In LFIA, specific antibodies are immobilized onto a paper-like membrane at two different sites[4], corresponding to control zone and test zone. The sample moves through the conjugate pad, which contains antibodies specific to the target antigen and conjugated to colloidal gold or latex microspheres for naked-eye detection [5,6]. These tests offer a rapid, low-cost and user-friendly solution for SARS-CoV-2, but there are different aspects to consider, like low accuracy and specificity in addition to the fact that they only give a qualitative response[7].

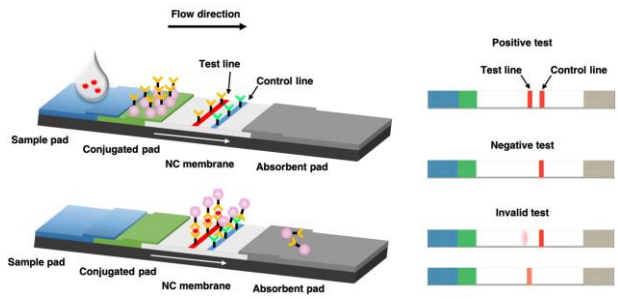

Figure 4.2: Scheme of Lateral Flow Immunoassay for antigen detection. Reprinted with permission from Ref. 4 © 2021 MDPI, Basel, Switzerland.

In this context, also different nanoparticles-based biosensors were developed to detect SARS-CoV-2 proteins. They present different advantages with respect to LFIA, as they are easy-to-use, fast-responsive, cheap, suitable for PoCT and with higher sensitivity and specificity[8]. Different receptors have been exploited giving high variety of suitable biosensors to detect several target analytes, like nucleic

acids, antibodies and antigens[9–11]. The latter have been widely explored to detect SARS-CoV-2 N and S proteins with different transduction methods, like voltammetry, SPR, Field-Effect-Transistors.

For example, Seo et al.[12] reported a field-effect transistor (FET)-based biosensing device to detect SARS-CoV-2 in clinical samples. This sensor is based on graphene sheets coated with a specific antibody for S protein, giving a change in current intensity in presence of the target. They obtained a LOD of 1 fg/ml in buffer and successfully detected SARS-CoV-2 in culture medium with a LOD of 1.6x101 pfu/ml and in clinical samples (LOD: 2.42 × 102 copies/mL), even though it was carried out only on three samples. Besides, it does not result suitable for on-site Point-of-Care testing environments as it requires benchtop and not portable equipment.

Fabiani et al.[13]developed an immunoassay based on magnetic beads and screen-printed electrodes to detect S and N protein in untreated saliva samples, reaching a detection limit of 19 ng/ml and 8 ng/ml, respectively. The assay was also tested using cultured virus in biosafety level 3 and in saliva clinical samples, comparing the data using the nasopharyngeal swab specimens tested with Real-Time PCR, and correctly classifying 22/24 samples. They used a PALM SENS portable and cable-connected potentiostat for the readout, making the immunosensor suitable for PoCT, even though managing the use of magnetic beads can require specific equipment.

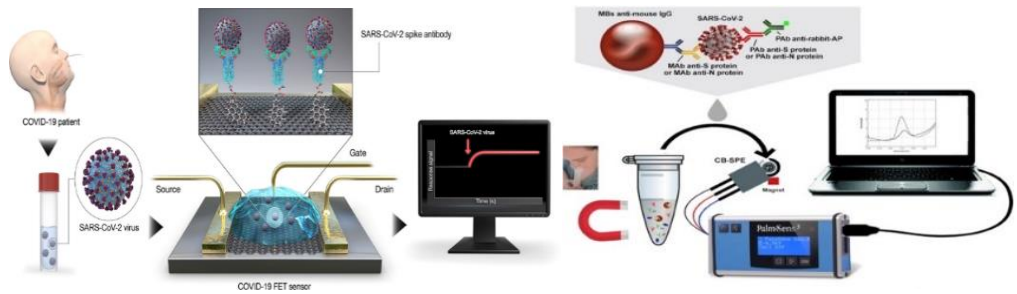

Figure 4.3: (Left) FET-based biosensor to detect SARS-CoV-2 in saliva samples. Reprinted with permission from Ref. 10 © 2020 American Chemical Society (Right): immunoassay based on magnetic beads and SPEs to detect N and S proteins from SARS-CoV-2 in untreated saliva samples. Reprinted with permission from Ref. 11 © 2020 Elsevier B.V. All rights reserved.

4.1 AIM OF THE STUDY

In order to detect SARS-CoV-2 infection, an electrochemical immunosensor based on screen printed electrodes functionalized with gold nanoparticles (GNP-SPEs) was designed to detect S1 subunit of Spike Protein. This immunosensor is based on a sandwich setup, in which a monoclonal IgM specific for S1 (mA-S1) was immobilized onto the surface to recognize and bind the S1 target, which is, in turn, bound by anti-S1 rabbit polyclonal antibody (pA-S1). The sample is mixed also with a secondary goat anti-rabbit reading antibody, labelled with alkaline phosphatase (GAR-AP) recognizing the Fc portion of the polyclonal antibody pA-S1. All the immunochemical reactions take place in a single incubation step. The AP enzyme label enables the generation of the analytic signal when the enzyme substrate is added, as shown in Figure 4.4.

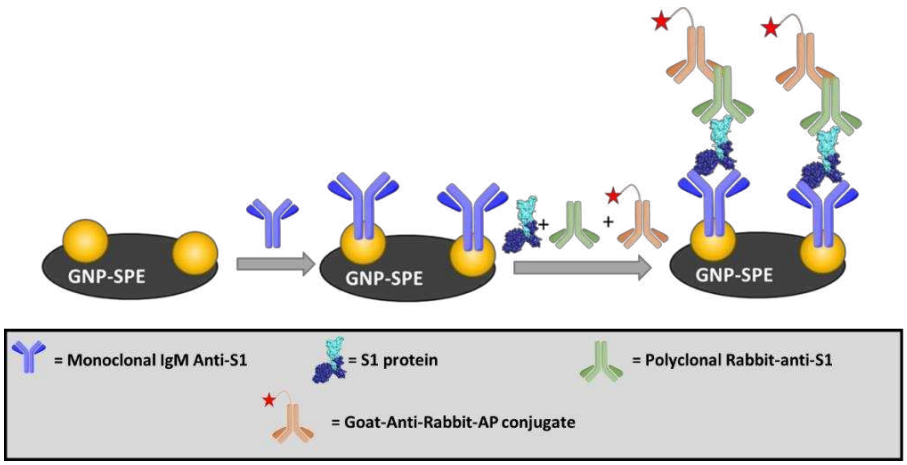

Figure 4.4: Protocol for immunoassay development for SARS-CoV-2 S1 protein detection

Analytical validation of the immunosensor was performed in Viral Transfer Medium (VTM) matrix, typically used for desorption of nasopharyngeal swabs, showing high specificity with respect to viral proteins of other pathogens, usually occurring in clinical samples as potentially interfering species. Furthermore, the developed immunosensor was tested on Lentiviruses expressing the SARS-CoV-2 spike protein

on their surface, thus demonstrating its ability to detect the whole virus in nasopharyngeal swab tests.

The immunosensor was connected to a portable device using Wi-Fi for signal readout and *on-cloud* data processing, which enables Machine Learning (ML) features[14]. This potentiostat is connected through a Wi-Fi protocol with the Thingspeak cloud service, which consists of an IoT data analytics platform with the capability to use MATLAB for data analysis[15], thus allowing to integrate techniques in a single solution that does not require additional external devices.

ML techniques are suitable for classifying true positive and true negative samples with high accuracy (>90%), without the need for pre-processing of the data. Moreover, they allow to process the voltammograms acquired through Differential Pulse Voltammetry (DPV) over a wider potential range than the traditional calculation of the current peak. This results in a simplification of the acquisition set-up and on-board processing. In fact, the training phase, which is necessary only once, can be performed on the cloud platform due to a higher computation power than the one available on a microcontroller unit (MCU) platform. This model can be directly coded in C language and implemented on the MCU platform. In addition, the processing of the data acquired during the test phase is carried out on board, resulting in an easier test process for all the users. These characteristics determine the implementation of acquisition and processing actions on low-cost, low-power MCU platform, resulting in more flexibility and higher usability.

In this context, this device, implemented on a portable, wireless and standalone instrumentation, has proved suitable for the integration of ML algorithms to improve accuracy in the classification of responses for the detection of the SARS-CoV-2 spike protein.

4.2 MATERIALS AND METHODS

4.2.1 Materials and Chemicals

Sodium chloride (NaCl), potassium chloride (KCl), potassium dihydrogen phosphate (KH_2PO_4), disodium hydrogen phosphate (Na_2HPO_4), Trizma® Base, magnesium chloride ($MgCl_2$), N-(3-dimethyl)-N'-ethylcarbodiimide hydrochloride (EDC), N-Hydroxysuccinimide (NHS), 4-morpholineethanesulfonic acid monohydrate (MES), Tween® 20, bovine serum albumin (BSA) were purchased from Merck (Milan, Italy). SARS-CoV-2 S1 subunit, SARS-CoV-2 Spike S1 Antibody (hIgM2001; mA-S1), Human Chimeric and H1N1 (A/California/04/2009) Hemagglutinin (HA) were purchased from GenScript (Piscataway, NJ, USA). SARS-CoV-2 Spike Protein S1 Polyclonal antibody (pA-S1) and Goat anti-Rabbit secondary antibody conjugated with alkaline phosphatase (GAR-AP) were purchased from Invitrogen, ThermoFisher Scientific (Waltham, MA, USA). Viral Transport Medium (VTM) with CDC formula was purchased from Capricorn Scientific (Ebsdorfergrund, Germany). Recombinant Coronavirus Spike Protein MERS-CoV-S1 was purchased from Biovision (Milpitas, CA, USA). Hydroquinone diphosphate (DRP HQDP) was purchased from Metrohm Italiana s.r.l. (Origgio, Italy). p8.74 packaging and pREV pseudotyping vectors were obtained from Addgene (Teddington, UK). DMEM was purchased from Euroclone s.p.a. (Milan, Italy). Eagle's Minimal Essential Medium (EMEM) and fetal bovine serum were purchased from Gibco, ThermoFisher Scientific (Carlsbad, CA, USA). Polyethylenimine (PEI) transfection reagent was from Polysciences, Inc. (Warrington, PA, USA). 0.45 µm filters were obtained from Millipore, Merk (Darmstadt, Germany). HEK 293T cells (CRL-1573) were from American Type Culture Collection (ATCC, Manassas, VA, USA).

4.2.2 Buffers Composition

Composition of different buffers is listed below:

Phosphate Buffer Saline (PBS): 137mM NaCl, 2.7mM KCl, 1.2mM KH_2PO_4, 8mM Na_2HPO_4 in distilled water (pH = 7.4)

PBS-t: same composition as PBS, with the addition of the surfactant Tween® 20 with a final concentration of 0.05% (w/v).

TRIS buffer: 0.1 M Trizma Base, 0.02 M $MgCl_2$ in distilled water (pH= 7.4; for reading buffer pH=9.8).

TRIS-t same composition as TRIS buffer with addition of the surfactant Tween® 20 with a final concentration of 0.05% (w/v).

MES buffer: 0.1 M MES in distilled water (pH=5.00)

4.2.3 Equipment

Immunosensors were assembled on single-walled carbon nanotubes-modified screen-printed carbon electrodes (SWCNT-SPEs; DropSens DRP-110SWCNT) or gold nanoparticles modified screen-printed carbon electrodes (GNP-SPEs; DropSens DRP-110GNP), purchased from Metrohm Italiana Srl (Origgio, Varese, Italy). The size of the SPEs was 3.4*1.0*0.05 cm, with a working electrode diameter of 4 mm. Reference electrode and electric contacts were made of silver, whereas the counter electrode was made of carbon. All electrochemical measurements were performed using the smart potentiostat developed in this work. It is a portable wireless device that uses the Wi-Fi protocol to connect to a cloud environment for data processing and visualization. The main feature of this device is that it does not need to rely on external devices (e.g., PC, tablets or smartphones) for operation.

The device consists of a custom Analog Front End (AFE) interfaced with a microcontroller that embeds a Wi-Fi network processor (i.e., CC3200 by Texas Instruments). Its dimensions are 12 x8x6 cm (LxWxH) for a weight of 200 g. The

device can be powered by two 1.5V AA batteries. The AFE contains different components: a TransImpedance Amplifier (TIA) with a programmable gain to sense the cell current, a 16-bit Digital to Analog Converter (DAC) for the conditioning potentials and a 14-Analog to Digital (ADC) to acquire data and send them to the microcontroller. The implementation is intended to minimize the number of required components and the power consumption. For example, with five acquisitions per day and two 1.5 V, 2700 mAh AA batteries, an autonomy of about 3.8 years can be achieved. A barcode reader is interfaced with the serial port of the microcontroller to match the personal ID with the acquired data. Samples can be processed on the edge to reduce energy consumption or sent to a cloud so that they can be processed.

Hybrid solutions can also be implemented with onboard pre-processing. The cloud service selected is ThingSpeak, an IoT analytics platform based on a MATLAB engine, although connection to other services can be implemented. Thingspeak has been also used for the configuration, storage and visualization of data thanks to an integrated custom web application. Thanks to the Wi-Fi connection, no Internet gateway or dedicated network infrastructure is required. It is worth noting that thanks to the possibility of performing data processing either on the local microcontroller or the remote cloud service, it is possible to choose the best compromise between higher computing power or lower energy consumption, depending on the considered application. For instance, it is possible to form complex and demanding computations such as training a ML algorithm completely autonomously from third-party devices or software, obtaining a compact, integrated and flexible approach which is particularly suitable for a PoCT context.

4.2.4 Immunoassay protocol

4.2.4.1 Receptor immobilization

As for receptor immobilization, two different electrodes platform were tested, namely SWCNT-SPEs and GNP-SPEs. In the first case, carboxylic group were previously activated with a solution containing 0.2 M EDC and 0.05 M NHS in MES buffer. 25 µl of this solution were drop-casted on SPEs and incubated for 30 minutes, followed by washing step with water. As for GNP-SPEs, direct immobilization was performed.

mA-S1 antibodies were diluted in PBS buffer to have a final concentration of 15 µg/ml and 25 µl of solution were drop casted on the SPEs platforms overnight at +4 °C. After immobilization of the receptor on the substrates, electrodes were rinsed with PBS-T and PBS buffer.

4.2.4.2 Blocking

To prevent non-specific binding, a blocking treatment was carried out by drop-casting 25 µl of a 20 mg/ml solution of BSA dissolved in PBS on the electrode surface. After 30 min of incubation, the electrodes were washed with TRIS-t and TRIS buffer.

4.2.4.3 One-pot incubation of sample and secondary antibody solution

The SARS-CoV-2 S1 protein was diluted by a selected factor in a solution containing TRIS and Viral Transport Medium in a 1:1 ratio and then mixed with a previously prepared solution containing pA-S1 and GAR-AP to reach a final concentration of 1 µg/ml and 2 µg/ml, respectively. 25 µl of the final solution were drop casted on each electrode and incubated for 1h, after which a washing step with TRIS-t and TRIS was performed.

4.2.4.4 Voltammetric readout

The readout step was carried out by drop-casting 50 µl of a 1 mg/mL solution of HQDP dissolved in reading buffer and, after 150 s of incubation of the enzymatic substrate, a DPV measurement was performed between -0.5 V and +0.1 V with the following parameters:

step potential = + 0.00495 V

modulation amplitude = + 0.04995 V

modulation time = 0.102 s

interval time = 0.4 s.

4.2.5 Experimental Design

A two factors and three levels (3^2) Full Factorial Design (FFD) was implemented in order to optimize the experimental conditions for the development of the immunoassay. The response variable was the P/N signal ratio (P = positive sample; N = negative sample) and the experimental factors evaluated were the concentrations of SARS-CoV-2 Spike S1 IgM Antibody (mA-S1) and SARS-CoV-2 Spike Protein S1 Polyclonal antibody (pA-S1). ANOVA tests were carried out to evaluate the significance of the effects of the two factors on the analytical response. Each of the experiments was replicated three times and acquired under randomized sequence. All statistical calculations were performed using the Statistics for Data Analysis V.28 software package (SPS Srl, Bologna, Italy).

4.2.6 Analytical Validation

Validation of the developed immunosensor was performed according to Eurachem Guidelines[16]. Measurements were carried out on solutions containing 1:1 diluted VTM spiked with SARS-CoV-2 S1 target antigen at different concentrations. Limit of detection (LOD), limit of quantification (LOQ), linearity and precision in terms of

repeatability were calculated performing three replicated measurements for each level explored. As for LOD and LOQ, 10 replicate measurements of blank samples, i.e., matrices containing no detectable analyte, were carried out. LOD was calculated as $3*s_0/\sqrt{n}$ and LOQ as $10*s_0/\sqrt{n}$, where s_0 is the blank standard deviation and n is the number of replicate measurements. Precision was measured on two levels, i.e., lower and upper levels of the calibration curve and expressed as Relative Standard Deviation (RSD).

4.2.7 SARS-CoV-2 Pseudovirus Generation

Lentiviral vector-based SARS-CoV-2 spike pseudoviruses were generated as previously described[17] with minor modifications. Briefly, HEK 293T cells were transfected in T175 cm^2 flasks with:

- 25 µg of pLV-EF1-(turboGFP-Luc2)-WPRE transfer vector
- 15 µg of p8.74 packaging vector
- 13 µg of pseudotyping vector coding for spike glycoprotein [Wuhan-Hu-1 (B.1 Lineage; China)]
- 5 µg of pREV

The mixture (58 µg of total DNA) was diluted in 3 ml of complete DMEM without serum, and 145 µl of 1 mg/mL PEI in PBS was added (ratio DNA/PEI 1:2.5). After at least 15 min incubation at room temperature, 4 volumes of complete DMEM without serum were added, and the transfection solution was transferred to the cell monolayer. They were incubated for 6 h at 37 °C and 5% CO_2 in a humidified incubator, then the mixture was replaced with 25 ml of fresh complete EMEM with addition of 10% FBS and incubated for 48 h at 37 °C and 5% CO_2. The flask was then frozen at -80 °C; transfected cell supernatant (TCS) containing spike pseudovirus was clarified via centrifugation at 3500 rpm for 5 min at 4 °C, filtered through a 0.45 µm filter, aliquoted, titered by limited dilution, and stored at -80 °C.

4.3 RESULTS AND DISCUSSION

4.3.1 Immunosensor setup

The study aimed at developing an immunosensor to detect the presence of S1 protein in nasopharyngeal swabs. To this end, an electrochemical immunosensor based on the immobilization of a monoclonal antibody (mA-S1) directed against S1 subunit of Spike protein was designed. In particular, different receptors and electrode platforms were tested in order to obtain the highest discrimination between positive and negative samples. After immobilization of the receptor, a one-pot protocol was applied, with the incubation of a solution containing the sample and a premixed solution of the polyclonal rabbit antibodies pA-S1 (able to recognise and bind different epitopes of S1 protein) and GAR-AP as a secondary antibody to bind the Fc portion of pA-S1 and give the signal of analytical interest. Furthermore, a Viral Transport Medium (VTM) was used as matrix to mimic the real sample, considering that VTM is conventionally exploited for the desorption of samples deriving from nasopharyngeal swabs. The DPV signals were generated upon addition of HQDP[18]as AP substrate, namely, and the readout was carried out using the previously described[19]smart portable potentiostat. The enzymatic and electrode reactions involved in the generation of the signal are the same previously discussed in section 3.1 (Chapter 3).

4.3.2 Comparison of different electrode platforms

Two different electrode platforms were evaluated for the immobilization of mA-S1, namely CNT-SPEs and GNP-SPEs. In the first case, the immobilization of the receptor is performed covalently by a coupling reaction between the lysine residues of mA-S1 and the activated carboxylic groups of CNTs. As for GNP, a direct chemisorption

of the cysteine residues of the antibody receptor, based on strong sulphur-gold interaction is established.

To this end, IgG-mA-S1 was immobilized on both the electrode substrates with a concentration of 10 µg/ml, while pA-S1 and GAR-AP were used at a concentration of 10 µg/ml and 2 µg/ml, respectively. For positive samples, SARS-CoV-S1 protein was kept at a concentration of 15 µg/ml.

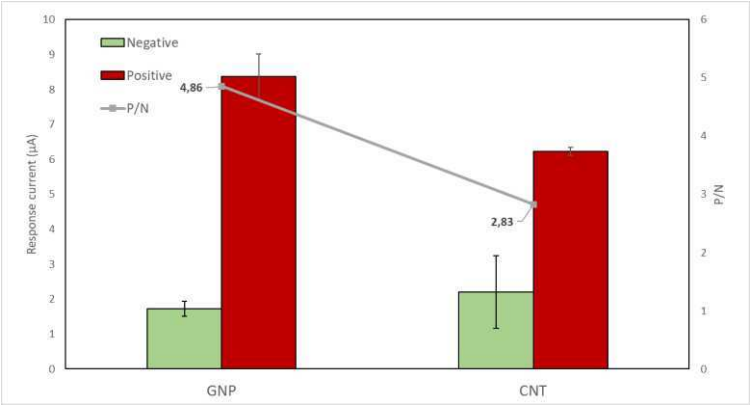

Figure 4.5: Evaluation of two different electrode substrates (GNP, CNT)

Figure 4.5 shows that the best P/N was obtained using GNP-SPE substrate, which was kept for the following experiments. This result is ascribable to a better orientation of the receptor on GNP-SPEs.

4.3.3 Evaluation of anti-S1 IgM and anti-S1 IgG as receptors

After determining the best electrode substrate, two different receptors for the immunoassay were considered: a monoclonal antibody of IgM isotype (IgM mA-S1) and a monoclonal antibody of IgG type (IgG-mA-S1), both able to recognize S1 subunit. The immobilization of the receptors on GNP-SPEs was carried out at 10 µg/ml, whereas pA-S1 and GAR-AP were used at a concentration of 10 µg/ml and 2 µg/ml, respectively. The highest P/N signal ratio was obtained using IgM receptor, as reported in Figure 4.6. This result can be explained considering that IgM are pentameric immunoglobulins, so they contain a greater amount of binding sites

than IgG, which is a monomeric antibody. Moreover, it is also likely that the epitope recognized by IgM, other than that recognized by IgG, is less masked by the antibody pa-S1 and therefore more available to the binding.

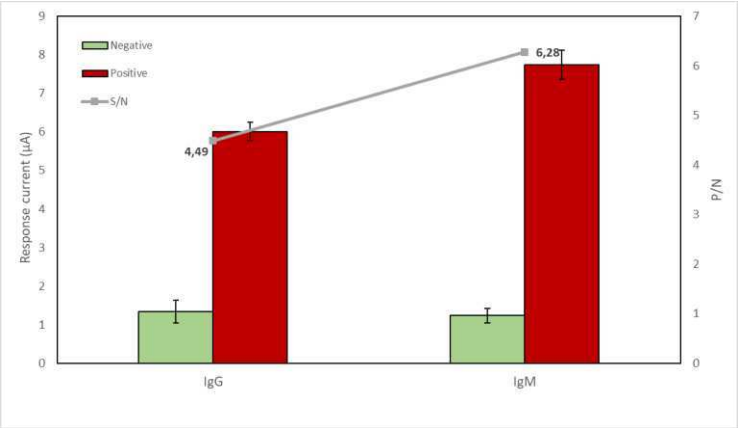

Figure 4.6: Evaluation of two different mA-S1 isotypes (IgG vs IgM) as receptors for the immunoassay

To verify the effective immobilization of the receptor, SPEs not functionalized with IgM were tested while keeping pA-S1 and GAR-AP at 10 and 2 µg/ml, respectively. As shown in figure 4.7, receptor-blank signal is not significantly different from the blank *(p<0,05)* under these conditions, thus demonstrating the effectiveness of the receptor immobilization and the absence of non-specific binding phenomena.

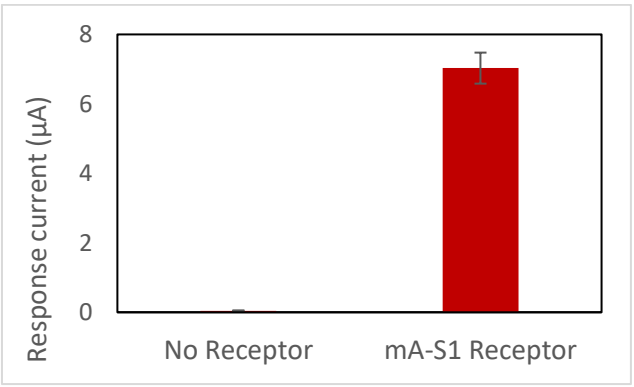

Figure 4.7: Tests on SPE without receptor for evaluation of non-specific binding

4.3.4 Immunosensor optimization

To evaluate the best experimental conditions, once the type of receptor and electrode platform was established, a two-factor and three-level (3^2) Full Factorial Design was performed. Factors A and B were concentrations of mA-S1 IgM and pA-S1, respectively. The P/N signal was optimized as response variable.

As for factor A, the three explored levels were 5,10 and 15 µg/ml, while for factor B they were 1,5 and 10 µg/ml. A two-way ANOVA with Bonferroni post-hoc test proved the statistical significance of all the effects of IgM mA-S1 *(p<0,01)* and pA-s1 *(p<0,05)* as well as their interaction *(p<0,01)*, as shown in the interaction plot reported in Figure 4.8.

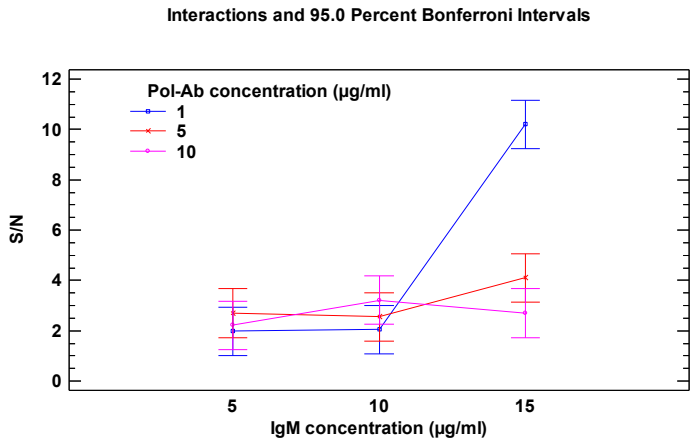

Figure 4.8: ANOVA interaction plot showing the effect of mA-S1 and pA-S1 on P/N

The P/N ratio was correlated with the explored factors by multiple regression, thus obtaining the response function (1) and the corresponding response surface (Figure 4.9). The optimal values of A and B factors found by equation (1) were 1 µg/ml for the pA-S1 and 15 µg/ml for mA-S1 IgM receptor, corresponding to the highest P/N ratio = 8.09

$$P/N = 2.0231 - 0.289467 \cdot A + 0.235617 \cdot B + 0.0501 \cdot A^2 - 0.0751311 \cdot A \cdot B + 0.0289352 \cdot B^2 \quad (1)$$

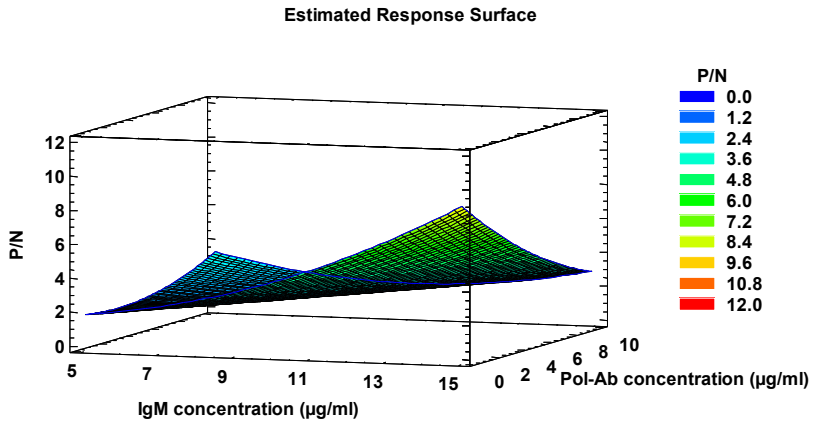

Figure 4.9: Response surface for mA-S1 and pA-S1 effect on P/N

4.3.5 Linearity assessment

Once assessed the optimized concentrations of mA-S1 IgM and pA-S1, the analytical performance of the immunosensor was evaluated. The experiments were performed in VTM to simulate the real sample.

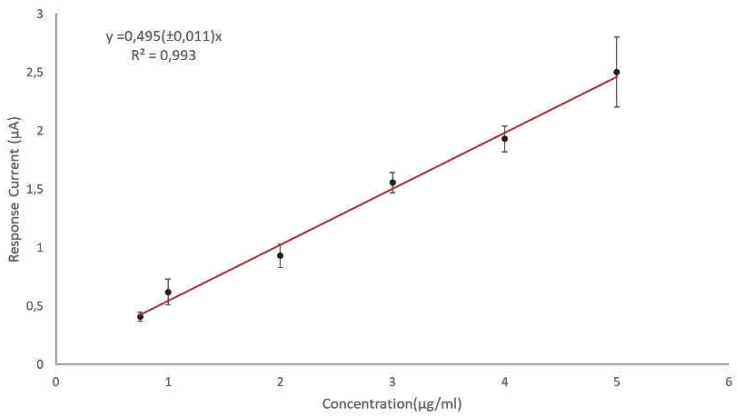

Figure 4.10: Calibration curve with different concentrations of SARS-CoV-S1 protein

The range between 0,25 and 10 µg/ml was explored, showing linearity between 0,5 and 5 µg/ml (see Figure 4.10), with LOD and LOQ values of 12 and 40 ng/ml, respectively. Good precision was observed at lower and upper levels, with RSD values always lower than 10% (n=3).

4.3.6 Cross-reactivity

To evaluate the specificity of the immunosensor for SARS-CoV-2 S1 protein, two different viral antigens were tested: Hemagglutinin (HA) from swine-origin influenza A (H1N1) virus and Spike Protein S1 from Middle East respiratory syndrome (MERS) Coronavirus. H1N1 Hemagglutinin is a protein involved in the binding of human receptor and it is a target for neutralizing antibodies, whereas MERS Spike protein takes part into the viral binding to the host cells and into the fusion of the virus with the cell membrane, playing an important role in infection. In both cases, similar symptoms to COVID-19 disease are developed[20,21].

Cross-reactivity experiments were carried out by comparing the responses obtained at 40 ng/ml for all the viral antigens with the blank signal (negative). As shown in Figure 4.11, no cross-reactivity phenomena were observed, since the signals acquired with S1-MERS and HA H1N1 resulted to be not significantly different from the blank (negative), thus proving the high specificity of the developed immunosensor.

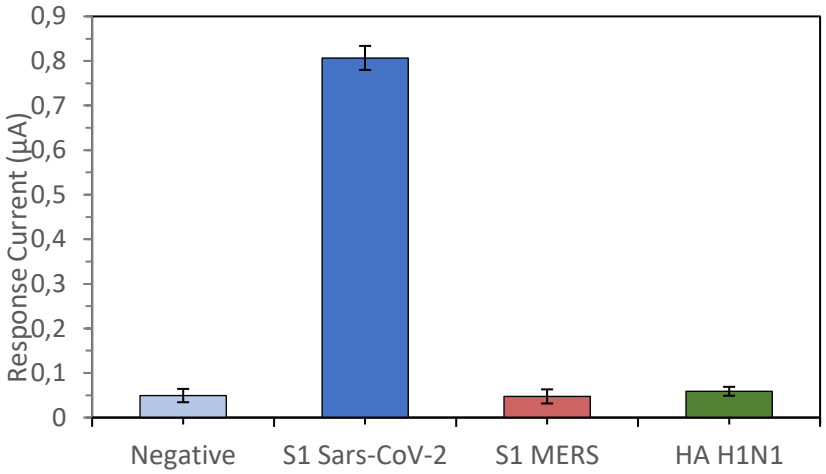

Figure 4.11: Cross-reactivity tests using Hemagglutinin from H1N1 and S1 Spike Protein from MERS

4.3.7 Whole Lentiviruses Expressing S1 protein analysis

To evaluate the performance of the immunosensor in terms of detection and quantification of the whole SARS-CoV-2 virus, different tests were performed with a third generation replicating uncompetent lentiviral vector, pseudotyped with SARS-CoV-2 spike glycoprotein. VTM was added to these samples to mimic the collection of nasopharyngeal swabs in clinical samples. Different concentrations, in a range from $6.3 \bullet 10^7$ to $1.9 \bullet 10^6$ transducing units (TU)/ml, were considered. As shown in Figure 4.12, a concentration of $3.9 * 10^6$ is sufficient to generate a signal significantly different from the negative sample, thus showing the ability of the immunosensor to detect the whole virus.

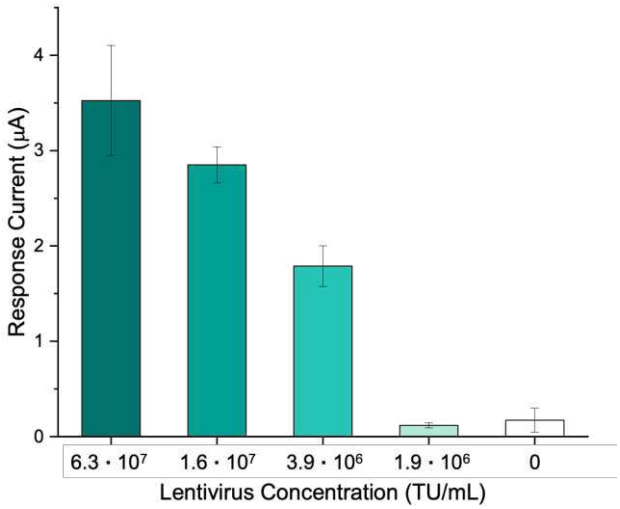

Figure 4.12: Tests of different concentrations of SARS-CoV-2 replicating lentivirus on the developed immunosensor.

4.3.8 Use of Machine Learning techniques for sample classification

The data obtained for the development of the immunosensor were analysed through ML techniques to automatically process the signals generated by the immunosensor and to classify samples as negative or positive, improving the

accuracy of the measurement. This is also essential for the on-site detection of SARS-CoV-2 antigen, making the immunosensor consistent with the PoCT context.
A set of 55 positive and 53 negative samples was acquired for a total of 108 data for training and validation purposes. Different SVM classifiers were evaluated with the main goal of selecting the best SVM kernel and optimal hyperparameters to achieve the highest classification accuracy computed as:

$$accuracy = (TP + TN)/(TP + TN + FP + FN) \quad (2)$$

Where:

- TP: True Positives (i.e., samples that are classified in a class and actually belong to that class)
- TN: True Negatives (i.e., samples that are not classified in a class and actually do not belong to that class)
- FP: False Positives (i.e., the samples that are classified in a class, but actually do not belong to that class).
- FN: False Negatives (i.e., the samples that are not classified in a class, but actually belong to that class)

Data were processed using the MATLAB Classification Learner App and testing Linear, Quadratic, Cubic and Gaussian kernel functions, with and without optimization. Bayesian Optimization[22] was used and 100 iterations were considered. During optimization process, the MATLAB suite computes the best parameters to achieve maximum accuracy in the validation process. The parameters included in the optimization are the Box Constraint Level hyperparameter and the possible selection of the data standardization feature. The Box Constraint of an SVM classifier is a penalty factor that controls the maximum allowable misclassifications, which helps to prevent overfitting: the larger the Box Constraint, the fewer the support vectors in the trained model. In addition, selecting a higher value for this parameter results in a longer training time. To

validate the trained model and ensure generalization of the results, a 10-fold cross-validation was performed. Table 1 summarizes the results in terms of accuracy obtained in the validation phase.

Kernel function	Optimization	Accuracy
Linear	No optimization	94.4%
	Bayesian Optimization	99.1%
Quadratic	No optimization	93.5%
	Bayesian Optimization	99.1%
Cubic	No optimization	94.4%
	Bayesian Optimization	99.1%
Gaussian	No optimization	86.1%
	Bayesian Optimization	95.4%

The best results were obtained using linear, quadratic and cubic kernels. Looking at a future embedded implementation and C code generation with the MATLAB coder app, the linear solution was chosen, as the MCU firmware could benefit from its greater simplicity than the polynomial version. In this case, the optimized model results in a value of 13.94 for the Box Constraint Level hyperparameter with data standardization.

In addition, this configuration was applied to verify the capability of the trained model to classify unknown data. A total of 19 positive and 18 negative solutions were analysed, resulting in a test accuracy of 97.3%, as shown in the confusion matrix reported in Figure 4.13.

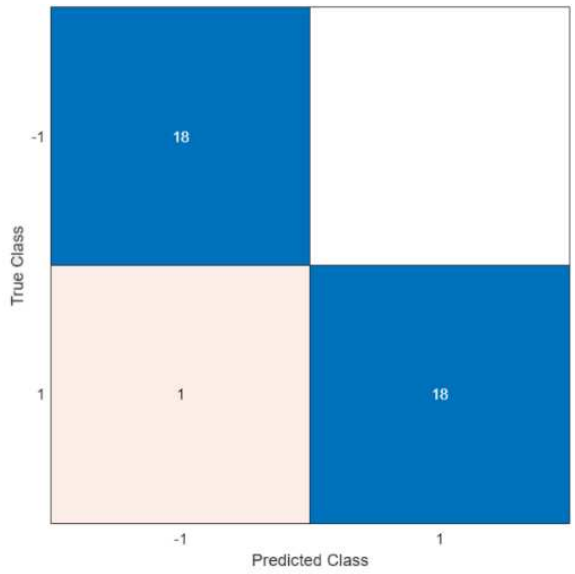

Figure 4.13: Confusion matrix for characterization of positive and negative samples based on ML model

Positive and the negative classes are represented by '1' and '-1', respectively. In this matrix, only in one case a misclassification occurred, leading to a FN indicating the outcome where the model incorrectly predicts the negative class. Instead, all negative samples were correctly classified, and no error was observed (i.e., white square in the upper right of the matrix). This ML algorithm could be easily integrated into the cloud-based portable Wi-Fi device [23], by performing the training phase on the cloud, without the need for any additional external device, improving in this way the ease of use and portability of the device and its introduction in home and PoCT context, outside the clinical settings.

This work led to the publication of a research article:

- Fortunati, S.; Giliberti, C.; Giannetto, M.; Bolchi, A.; Ferrari, D.; Donofrio, G.; Bianchi, V.; Boni, A.; De Munari, I.; Careri, M. Rapid Quantification of SARS-Cov-2 Spike Protein Enhanced with a Machine Learning Technique Integrated in a Smart and Portable Immunosensor. *Biosensors* **2022**, *12*, 426. https://doi.org/10.3390/bios12060426

4.4 REFERENCES

1. (WHO), W. H. O. Testing for SARS-CoV-2 infection and immunity. 30 (2021).
2. Chen, Q. *et al.* Diagnostic technologies for COVID-19: a review. *RSC Adv.* **10**, 35257–35264 (2020).
3. Corman, V. M. *et al.* Detection of 2019 novel coronavirus (2019-nCoV) by real-time RT-PCR. *Eurosurveillance* **25**, (2020).
4. Hsiao, W. W. W. *et al.* Recent advances in novel lateral flow technologies for detection of COVID-19. *Biosensors* **11**, 1–26 (2021).
5. You, M. *et al.* Household Fluorescent Lateral Flow Strip Platform for Sensitive and Quantitative Prognosis of Heart Failure Using Dual-Color Upconversion Nanoparticles. *ACS Nano* **11**, 6261–6270 (2017).
6. Etienne, E. E., Nunna, B. B., Talukder, N., Wang, Y. & Lee, E. S. Covid-19 biomarkers and advanced sensing technologies for point-of-care (Poc) diagnosis. *Bioengineering* **8**, 1–27 (2021).
7. Martín, J., Tena, N. & Asuero, A. G. Current state of diagnostic, screening and surveillance testing methods for COVID-19 from an analytical chemistry point of view. *Microchem. J.* **167**, 106305 (2021).
8. Lino, A., Cardoso, M. A., Gonçalves, H. M. R. & Martins-Lopes, P. SARS-CoV-2 Detection Methods. *Chemosensors* **10**, (2022).
9. Fortunati, S. *et al.* Smart Immunosensors for Point-of-Care Serological Tests Aimed at Assessing Natural or Vaccine-Induced SARS-CoV-2 Immunity. *Sensors* **22**, (2022).
10. Farzin, L., Sadjadi, S., Sheini, A. & Mohagheghpour, E. A nanoscale genosensor for early detection of COVID-19 by voltammetric determination of RNA-dependent RNA polymerase (RdRP) sequence of SARS-CoV-2 virus.

Microchim. Acta **188**, (2021).

11. Sadique, M. A. *et al.* Highly Sensitive Electrochemical Immunosensor Platforms for Dual Detection of SARS-CoV-2 Antigen and Antibody based on Gold Nanoparticle Functionalized Graphene Oxide Nanocomposites. *ACS Appl. Bio Mater.* (2022) doi:10.1021/acsabm.2c00301.

12. Seo, G. *et al.* Rapid Detection of COVID-19 Causative Virus (SARS-CoV-2) in Human Nasopharyngeal Swab Specimens Using Field-Effect Transistor-Based Biosensor. *ACS Nano* **14**, 5135–5142 (2020).

13. Fabiani, L. *et al.* Magnetic beads combined with carbon black-based screen-printed electrodes for COVID-19: A reliable and miniaturized electrochemical immunosensor for SARS-CoV-2 detection in saliva. *Biosens. Bioelectron.* **171**, (2021).

14. Bianchi, V. *et al.* IoT and Biosensors: A Smart Portable Potentiostat with Advanced Cloud-Enabled Features. *IEEE Access* **9**, 141544–141554 (2021).

15. No Title. https://thingspeak.com/ https://thingspeak.com/.

16. B. Magnusson and U. Örnemark. Eurachem Guide: The Fitness for Purpose of Analytical Methods – A Laboratory Guide to Method Validation and Related Topics. in *Eurachem Guide: The Fitness for Purpose of Analytical Methods – A Laboratory Guide to Method Validation and Related Topics* (2014).

17. Donofrio, G. *et al.* A simplified sars-cov-2 pseudovirus neutralization assay. *Vaccines* **9**, 1–12 (2021).

18. Giannetto, M., Bianchi, M. V., Mattarozzi, M. & Careri, M. Competitive amperometric immunosensor for determination of p53 protein in urine with carbon nanotubes/gold nanoparticles screen-printed electrodes: A potential rapid and noninvasive screening tool for early diagnosis of urinary tract

carcinoma. *Anal. Chim. Acta* **991**, 133–141 (2017).

19. Bianchi, V. *et al.* A Wi-Fi Cloud-Based Portable Potentiostat for Electrochemical Biosensors. *IEEE Trans. Instrum. Meas.* **69**, 3232–3240 (2020).

20. Pallesen, J. *et al.* Immunogenicity and structures of a rationally designed prefusion MERS-CoV spike antigen. *Proceedings of the National Academy of Sciences of the United States of America* vol. 114 E7348–E7357 (2017).

21. Sriwilaijaroen, N. & Suzuki, Y. Molecular basis of the structure and function of H1 hemagglutinin of influenza virus. *Proc. Japan Acad. Ser. B Phys. Biol. Sci.* **88**, 226–249 (2012).

22. Zeng, X. T., Zhang, C., Kwong, J. S. W., Sun, X. & Li, Y. P. Software for network meta-analysis: A usage-based comparative study. *Chinese J. Evidence-Based Med.* **14**, 1270–1275 (2014).

23. Bianchi, V. *et al.* IoT and Biosensors: A Smart Portable Potentiostat with Advanced Cloud-Enabled Features. *IEEE Access* **9**, 141544–141554 (2021).

5 *Genosensors for cancer diagnosis by liquid biopsy*

5.1 GENOSENSORS WORKING PRINCIPLE

The study of gene polymorphisms and gene mutations plays an important role in early and accurate disease diagnosis and in predicting disease susceptibility[1]. In this context, genosensors aimed at specific recognition of nucleic acids have been widely exploited in different fields as, for example, early diagnosis, diseases monitoring[2] and detection of genetically modified organisms in food[3]. A DNA biosensor (or genosensor) is characterized by the immobilization of a single-stranded oligonucleotide probe on sensing surface in order to recognize its complementary target DNA sequence via Watson-Crick base pairing, thus generating the so called "hybrid" [4]. This binding event is converted into a measurable analytical signal by the transducer, that can be an optical (fluorescence, surface plasmon resonance), electrical, or electrochemical device. Among them, electrochemical biosensors are often exploited as they enable fast, easy and low-cost detection[5]. Their small size, indeed, make them attractive in the Point-of-Care testing context for early diagnosis, disease monitoring, infectious disease testing, veterinary diagnostics and food testing[6].

As for electrochemical genosensors, a single stranded specific Capture Probe (CP) is immobilized onto the electrode surface to bind the DNA target sequence. In order to improve the selectivity and sensitivity of the genosensor, a labelled detector probe or Signalling Probe (SP) can be exploited to bind the target sequence in a different portion, thus generating the electrochemical signal[7].

5.1.1 Nucleic acids as capture probes

The mainly crucial stage for the development of a genosensor is certainly the design of the CP, as the final hybridization response depends on its features. For the realization of these probes, different parameters have to be taken into account, like

homologies, theoretical melting temperature, dimer formation, and length[8]. Another aspect improving the detection specificity is the prevention of non-specific binding phenomena on the sensor surface[9], especially when dealing with complex matrices such as body fluids. The experimental factors under which the hybridization occurs can also significantly influence the response: among them, the composition of coating buffers employed and the working temperature make a system based on two probes capable of specific recognition of the target genetic material with an acceptable robustness. In this context, DNA sequences have been widely used as capture probes for biosensing applications, although they present different limitations[10] as reduced bioactivity, non-specific interactions, lack of reproducibility and, mainly, their degradability by the nuclease enzymes. Several synthetic alternative nucleic acid analogs or xeno (stands for "alien") nucleic acids (XNAs), so-called because they present modifications in the backbone with respect to DNA, have been developed in the last decades. Among them, peptide nucleic acid (PNA), locked nucleic acid (LNA) and morpholino (MO)[10] were often exploited for genosensing.

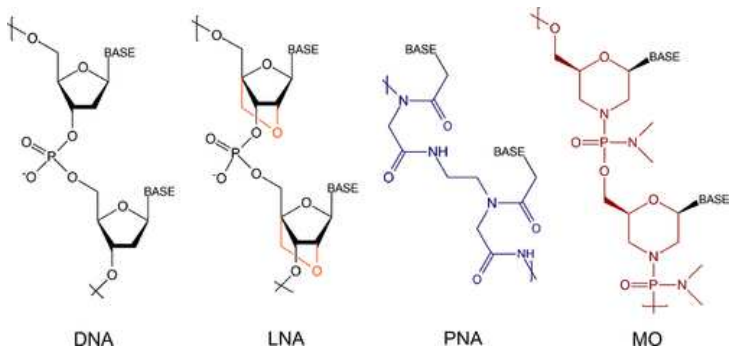

Figure 5.1: Chemical structure of LNA, PNA and MO compared to DNA structure. Reprinted from Ref. 10 with permission from © 2022 American Chemical Society.

LNAs are DNA mimics presenting in the backbone a bicyclic ribose derivative with a bridging methylene group between the 4'-carbon and the 2'-oxygen. LNAs are nuclease-resistant in nature as they are not recognized as substrates[11]. MOs are

other DNA mimics where both the sugar and the phosphodiester bonding are modified [12]. They are composed of morpholino rings, nucleobases and the non-ionic phosphorodiamidates. MOs possess a non-ionic backbone similar to PNA, making them resistant to nucleases and less expensive with respect to other mimics, as they require cheaper ribonucleosides[13].

PNAs are DNA-analogues developed during the 1980s by Peter Nielsen[14]. PNA probes contains a "peptide-like" backbone with repeated units of N-(2-aminoethyl) glycine, linked by amide bonds. This non-ionic, achiral structure makes PNA a highly stable biological molecule, not sensitive to nuclease or protease enzymes[15].

This structure guarantees the correct intra-base distance, allowing for Watson-Crick interactions to occur. Furthermore, due to the absence of negatively charged groups on its backbone and, consequently, of electrostatic repulsion, PNA/DNA hybrids are more stable than DNA-DNA hybrids. Moreover, PNA is not sensitive to ionic force and pH changes and resistant to enzymatic cleavage within living cells. Another important property of PNA/DNA duplexes is their higher sensitivity for the detection of mismatches in the complementary DNA strand, as a single mismatch in PNA/DNA heteroduplex lowers the melting temperature more than in DNA/DNA duplexes (about 15°C compared to 4°C)[16,17]. Given their synthetic nature, PNAs probes are also easily modifiable to include functional groups that can be used, for example, for their covalent immobilization on sensing substrates. These features make PNAs ideal tools for DNA recognition and, in particular, of considerable interest as a probe in different genosensors[18]. As for the synthesis of PNA probes, standard peptide solid-phase synthetic protocols are employed. The first report on PNA oligomer synthesis was based upon Merrifield solid-phase synthesis using Boc/Cbz (tert-butyloxycarbonyl/ carboxybenzyl) protecting group strategy[19]. Subsequently, other strategies, like Fmoc/Bhoc (fluorenylmethyloxycarbonyl/benzhydryloxycarbonyl) were also developed. In

general, the synthesis starts with the monomer loading on the polymeric support[17]. The N-terminal protecting group is then deprotected followed by coupling with another monomer. The elongation process consists of several steps of deprotection of N-terminus of the monomer and coupling to the following N-protected monomer. Finally, the oligomer is cleaved from the solid support to give the final oligomer. The oligomers are then purified by reverse-phase high-performance liquid chromatography and characterised by mass spectrometry.

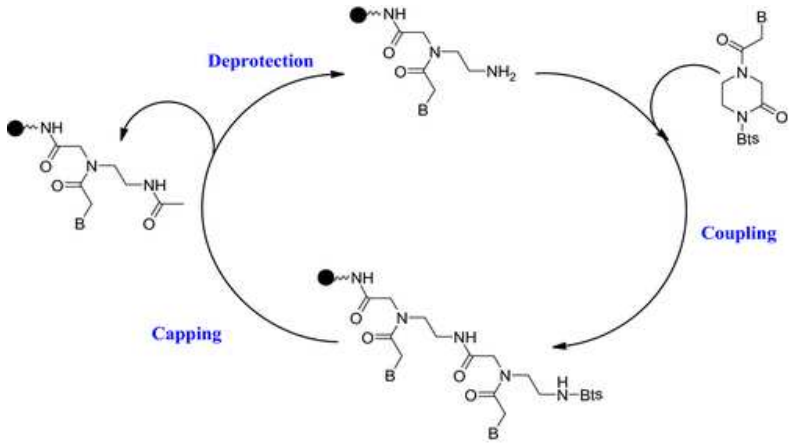

Figure 5.2: General scheme for PNA synthesis Reprinted with permission from Ref. 17 © 2016 John Wiley & Sons A/S. [17]

Customized PNAs are also commercially available, but their cost is still higher than corresponding DNA oligonucleotides. The higher cost is counterbalanced by their peculiar biophysical properties, making them a gold standard for biosensing applications, particularly when used as capture probes. As for the immobilization of oligonucleotide probes on sensing surfaces, different approaches can be pursued:

- Simple adsorption through ionic interactions between the negatively charged probes and positively charged surface.
- Chemisorption of probes modified with thiols moieties, to promote the interaction between sulfur and gold-modified sensing platforms

- Covalent bonding involving amino- functionalities at the 5'-ends and sensing surfaces bearing carboxyl groups, previously activated by coupling reagents as EDC/NHS (S(1-ethyl-3-(3-dimethylaminopropyl)carbodiimide/N-hydroxysuccinimide).
- Avidin/streptavidin- biotin interaction through biotinylated probes.

5.1.2 Electrochemical transduction

Another important issue to consider in the development of genosensors is the selection of transducer elements, since it strongly influences the sensitivity and the overall performance of the sensing devices, depending on the biochemical reaction occurring for the biorecognition.

Based on the transduction principle, genosensors can be divided into electrochemical, optical, calorimetric and mass-based[20].

The need for low-cost, easy-to-use, portable and miniaturised devices led to the development of many electrochemical genosensors, widely used for DNA diagnostics[21] as they are inexpensive, rapid and highly sensitive and specific[22].

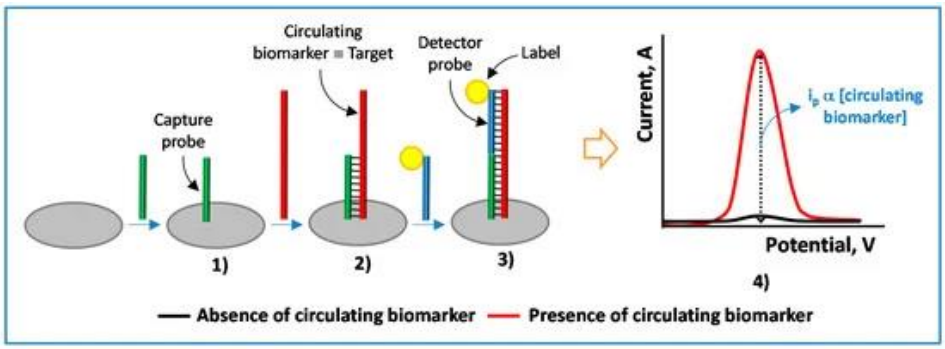

Figure 5.3 : Schematic representation of electrochemical genosensor. Reprinted with permission from Ref. 7 © 2017 MDPI, Basel, Switzerland[7].

For these biosensors, the hybridization between the capture probe and target sequence produces a signal, whose detection can be label-free, based on

modifications occurring at the electrode interface functionalized with CPs, when the hybridization of the target sequence takes place. Conversely, indirect detection exploits a label that reports the hybridization process; electroactive anticancer agents, organic dyes, metal complexes, enzymes or metal nanoparticles are often used as labels[4]. Depending on the capture probe and on the target, different pathways can be used for the signal detection: redox labels or electroactive DNA bases (guanine, adenine), whose changes in the oxidation/reduction peak current can be monitored, or metal nanoparticles probes to monitor the target or enzyme-tagged probes.

Compared to redox labels, which can only transfer a limited number of electrons, probes tagged with enzymes, like alkaline phosphatase (AP) or horseradish peroxidase(HRP), can provide recognition and amplification of the binding event, thus matching the need for high sensitivity when the target availability is low, like for pathogen or cancer DNA detection[9,23].

Several biosensors for early cancer detection and monitoring, indeed, have been developed to avoid invasive, expensive and long-time analysis.

5.2 LIQUID BIOPSY

Cancer is still one of leading causes of death worldwide, accounting for nearly 10 million deaths in 2020, as reported from the Global Cancer Osservatory[24]. Among the most common, there are breast, lung and colorectal cancer according to World Health Organization (WHO). As for cancer therapy, conventional treatments include chemotherapy, radiotherapy and surgery[25] and they strongly depend on the type and stage of the tumour, as well as the health status and age of the patient[26]. Moreover, there are several tumours that can develop resistance to these therapies through drug inactivation, drug target alteration or specific genetic mutations not responding to specific treatments[27]. Therefore, the continuous monitoring of the

diseases as well as early detection, play a paramount importance in the oncological context. The examination of tumour tissue is normally carried out through tissue biopsy, where samples are collected with a needle or open surgery to analyse the molecular and genetic profile of the patient and customize a specific therapy. However, there are different issue regarding this technique: it is strongly invasive, time consuming and painful. In addition, it is not always accessible for all the patients and able to detect the tumour heterogeneity which is crucial for the treatment strategy[25], and it is limited in early and non-symptomatic cancers[28].

To overcome these limitations, liquid biopsy is increasingly employed for cancer molecular profiling and precision oncology. Liquid biopsy is a technique that involves the analysis of biomarkers circulating in the body fluids, especially blood samples of cancer patients to provide information on the genetic profile of patients[29]. It is emerging as an alternative and complementary diagnostic and prognostic tool to surgical biopsy in oncology; it focuses on the detection and isolation of circulating tumour cells, circulating tumour DNA and exosomes. Even though peripheral blood is the main source for liquid biopsy analysis, also other body fluids have been employed, like urine, pleural effusion, saliva, and cerebrospinal fluid. Compared to a classic tissue biopsy, the sampling is significantly less invasive and presents a very low risk, other than a less expensive sample collection. Furthermore, the frequency of liquid biopsies can be higher if compared to tissue biopsies, allowing the continuous monitoring to verify the efficiency of treatment and tumour progression. Therefore, liquid biopsy technology has the potential to provide a more comprehensive understanding of disease and overcome limitations of tissue biopsy[30].

During the last years, several other applications of liquid biopsies in oncology have emerged, like tumour genotyping, precision therapy, monitoring response to

treatment, detection of emergence of treatment resistance and detection of minimal residual disease[31].

5.2.1 Biomarkers for liquid biopsy

Liquid biopsy relies on the analysis of multiple biomarkers, including circulating tumour DNA (ctDNA), circulating tumour cells (CTCs), exosomes and circulating tumour microRNAs (ct-miRNAs).

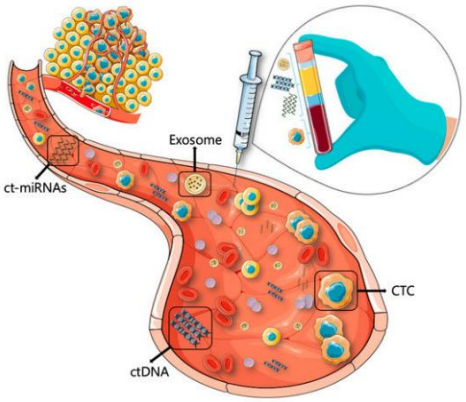

Figure 5.4: Schematic view of liquid biopsy biomarkers: circulating tumour cells (CTCs), circulating tumour DNA (ctDNA), exosomes, and circulating tumour microRNA (ct-miRNA). Reprinted with permission from Ref. 32 © 2023 MDPI, Basel, Switzerland[32].

CTCs are tumour cells present in the bloodstream in low concentrations (1-10 cells/milliliter)[32] and they originates from the primary site of the tumour or from metastasis, giving substantial information about the heterogenicity of the tumour, genetic aberrations and transcriptional dysregulation[33]. Although their concentration can change significantly, they give more information than the small amount of tissue sampled with conventional biopsy. CTCs can give information of metastasis when they are found in peripheral blood and if their levels change over weeks, they can indicate response or resistance to therapies, thus showing their use as prognostic biomarkers[34].

Exosomes are small extracellular vesicles (30-120 nm) covered by a lipid double layer, secreted for intercellular communication; they take part in different cellular

processes and are involved in in tumour mechanisms. They are abundant in the bloodstream, even though it can be difficult to distinguish exosomes deriving from normal and tumoral cells[32,35].

MicroRNA (miRNA) are short non-coding RNA (19-22 nucleotides) molecules involved in the post-transcriptional regulation of gene expression, playing an important role in different cellular processes[36]. They can be secreted into different biological fluids, including blood, cerebrospinal fluid, urine, thus giving the possibility to investigate the condition of their tissue of origin. For example, high expression of different miRNAs (miR-21, miR-17-5p, miR-92a-3P) is strongly associated with colorectal cancer in terms of metastasis, post-treatment relapse[37,38]. Therefore, they are considered valid biomarkers for cancer diagnosis and monitoring as, compared to tissue biopsy, sampling is less invasive and there are no complications. However, limited amounts of analyte, cellular contamination and pre-analytical variables have to be considered for miRNAs detection[36].

Cell-free DNA (cfDNA) comprises circulating nucleic acids not associated with cells, present in plasma and serum; they are released both from normal cells and cancer cells, in which they are called circulating tumor DNA (ctDNA). CtDNA is typically represented by double-stranded DNA molecules between 150 and 200 base pairs. Several processes lead to the release of cfDNA in blood, like passive release (apoptosis, necrosis), hemopoietic cells release, normal tissues after ischemia, trauma, infection's damage, or active secretion via exosomes[39]. Cell-free DNA concentration is not constant in cancer patients blood, but it is usually higher than concentration in healthy people[40]. Moreover, for ctDNA analysis, plasma sample are preferable compared to serum samples, as the latter contain higher levels of DNA from leukocytes, leading to interferences with ctDNA detection.

Variation of ctDNA levels is associated with different features of cancer, like stage, localization, vascularization, and response to therapy. A study on colorectal cancer

(CRC) patients was performed to evaluate the concentration of ctDNA in patients. It was observed that four months after primary resection of the tumour, CRC patients had a significant decrease in plasma cfDNA levels, while in CRC patients with tumor recurrence, cfDNA levels increased[41].

For these reasons, ctDNA is considered a valid tool for molecular profiling in diagnosis, early detection, targeted therapy, monitoring of response to therapy and treatment resistance.

5.2.2 CtDNA detection technologies

Regarding the detection of ctDNA in liquid biopsy, Next Generation Sequencing (NGS), and polymerase chain reaction (PCR) are the main technologies nowadays. Based on the principle of PCR, a series of PCR-related methods have been developed that have also been applied in ctDNA detection[42].

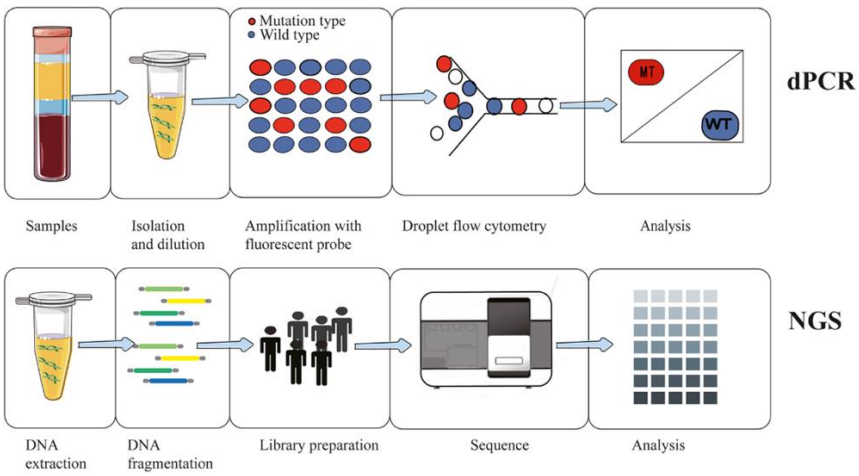

Figure 5.5: Schematic representation of digital PCR and NGS techniques. Reprinted with permission from Ref. 43 © 2021, Springer Nature[43]

Currently, digital PCR (dPCR) is frequently used for the detection of ctDNA because of its high sensitivity and ease of use. This technique enables amplification and quantification of small amounts of mutant sequences, although it can suffer from artifacts and sample contamination[44]. Moreover, this method requires a large

peripheral blood volume when used for ctDNA, so the experimental conditions and reagents need to be optimized[42]. Two common dPCR methods, the droplet digital PCR (ddPCR) and BEAMing (beads, emulsification, amplification, and magnetics) assay, can detect point mutations present at frequencies ≤ 0.1%. NGS-based technologies, on the other hand, are considered the gold standard for the detection of ctDNA as they have high throughput and can screen unknown variants.[45] However, NGS is not compatible with the concept of PoCT, as it is expensive, requires bulky instruments and it is not easy to handle. In addition, it requires advanced bioinformatic systems, fast data processing and large data storage capabilities. Finally, both PCR and NGS based techniques need to be performed in dedicated clinical facilities, so their use in clinical practice in POC contexts can be difficult to afford. These techniques have been widely used for the early detection, treatment response-monitoring and diagnosis of cancer disease through the analysis of ctDNA in liquid biopsy. In particular, they have been also exploited for colorectal cancer, as it requires continuous monitoring and is one of the most common and deadly cancers worldwide[46].

5.3 COLORECTAL CANCER (CRC)

CRC belongs to the top 3 of the most prevalent cancers worldwide, representing, in 2020, 10% of the global cancer incidence and 9.4% of all cancer-related deaths[47]. Globally, it has been observed a decrease in incidence and mortality in the last years, probably due to screening programs implementation and subsequent removal of polyps [48]. On the other hand, it has been observed a higher CRC incidence among the younger population, called early-onset CRC (EO-CRC), compared to the past years, but the reasons are still unknown. Different risk factors are associated with CRC, like Inflammatory Bowel Diseases (IBD), CRC familiarity, lifestyle (smoking, alcol, wrong alimentation), age.

Mutations in specific genes can lead to colorectal cancer, as in other cancers. Such mutations may appear in oncogenes, tumour suppressor genes, and genes related to DNA repair mechanism. Mutated *rat sarcoma virus* (RAS) genes, which represent the most frequently mutated oncogene family, are present in about 22% of human tumours; mutations within the *Kirsten rat sarcoma viral oncogene* (KRAS) account for 90% of all mutations in the RAS family and are associated with the proliferation of various tumours[49].

5.4 G12D Single Nucleotide Variation (SNV)

A common mutation associated with colorectal cancer and other cancers occurs in codon 12 in KRAS gene; it is a missense mutation (Single-Nucleotide Variation: SNV) of guanine in adenine (GGT>GAT), leading to the substitution of glycine into aspartate. It is among the most commonly observed mutations in colorectal adenocarcinomas and has been associated with poor prognosis[50]. KRAS determines the activation of proteins involved in several molecular process regarding cellular growth, differentiation and proliferation. When activated, it is involved in dephosphorylation of guanosine-5'-triphosphate (GTP) to guanosine diphosphate (GDP), after which KRAS is turned off. The substitution of glycine with other aminoacids, like aspartate and valine at codon 12, having larger side chains, cause steric hindrance in GDP/GTP binding pocket of the protein. This determines interferences with GTP hydrolysis, binding and locking the protein in an active, GTP-bound state.

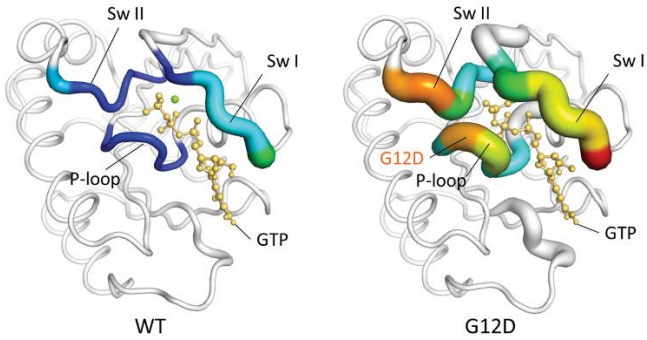

Figure 5.6: Steric hindrance caused by G12D mutation compared to WT protein. Reprinted with permission from Ref. 50 © 2013 PLOS ONE

As a consequence, the epidermal growth factor receptor (EGFR) signalling pathway, that is upstream of the cascade of signals related to the activation of KRAS, is out of control with permanent activation of the KRAS protein.

The aforementioned mechanisms determine resistance to monoclonal antibodies (mAb) directed against EGFR (cetuximab and panitumumab), normally considered as standard components of treatment for colorectal cancer (CRC) patients, either alone or in combination with chemotherapy[51]. The current standard procedure involves the determination of mutations in RAS in all CRC tumours before initiating the treatment, to evaluate the presence of critical biomarkers for the resistance to anti-EGFR. Moreover, it has been observed that also CRC patients that initially respond to anti-EGFR therapy develop resistance, which in 50% of cases is due to the onset of RAS mutations [52]. Currently, RAS mutation determination is carried out in samples from tumour tissue.

Circulating DNA fragments, like ctDNA, offers potential advantages particularly in the metastatic setting as a safe minimally invasive alternative to tissue biopsy. In this context, the detection of KRAS G12D mutation can be a relevant tool both for the diagnosis of CRC and the treatment response monitoring. Several diagnostic tests based on liquid biopsy have been approved for the detection and monitoring of Colorectal Cancer[28,53], but they are still expensive and require long time and

specialized personnel for the execution. For example, a blood test based on 29-gene panel to discriminate patients with colorectal cancer and adenomatous polyps was developed by Novigenix, Switzerland. However, it still requires 1–2 weeks for the response and it is not low-cost ($290)[54].

The concept of using liquid biopsy for disease detection and monitoring is also consistent with the targeted therapy and precision-medicine fields, promoted by technologies enabling molecular profiling, genomic analysis and optimized drug design to tailor treatments for individual patients[55]. The aim is to develop new targeted and efficient therapies with adequate benefits/risks for patients and better molecular understanding for therapy selection. In addition, it could be possible to monitor treatment response, in order to increase the effectiveness and safety of treatments and, therefore, facilitate the elimination of unnecessary therapies, resulting in significant savings on costs of pharmacological treatments for the health system[56].

Therefore, the development of low-cost, rapid and reliable devices is growing to help patients monitoring autonomously the disease and also to improve their compliance. In this context, biosensors could be valuable alternatives due to their characteristics, like small-dimension, easy-handling, low-cost and high sensitivity.

5.5 BIOSENSORS FOR CTDNA ANALYSIS IN LIQUID BIOPSY

In addition to the standard methods for the detection of biomarkers in liquid biopsy, different biosensors with different transduction mechanisms have been developed. For example, a nanoparticle-enhanced plasmonic method was developed for the detection of SNV[57] in CRC patients, without the need for PCR amplification and target labelling. This assay is based on the use of poly-L-lysine (PLL)-based surface layer with a densely immobilized oligopeptide to prevent the non-specific adsorption of plasma components on the sensor surface. On this

surface, PNA probes able to selectively recognize the complementary sequence were immobilized to detect ctDNA. Then, gold nanoparticles conjugated with an oligonucleotide probe complementary to a portion of the target sequence different from the one hybridized with the PNA probe, were used to enhance the assay's performances.

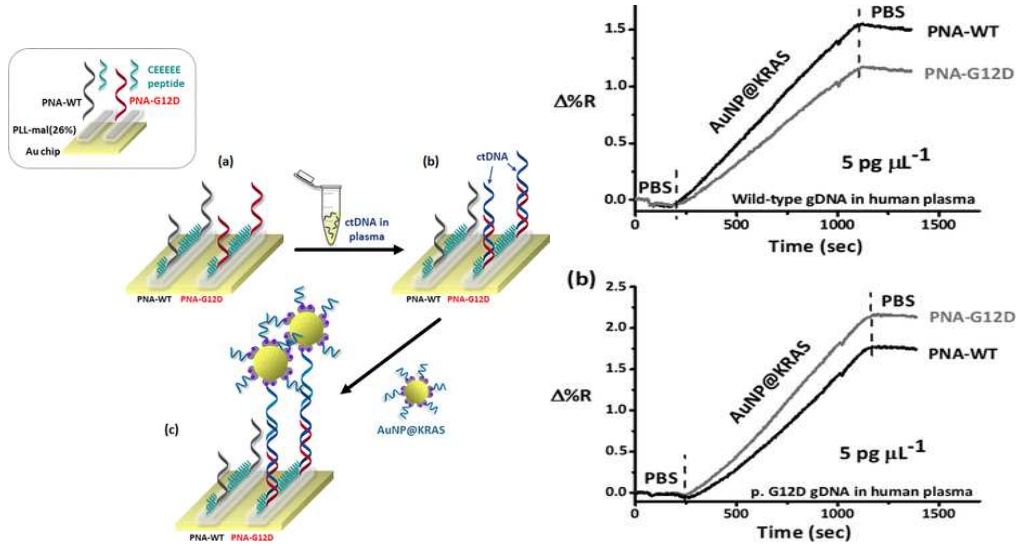

Figure 5.7: Representation of the assay for the detection of the G12D KRAS-mutated ctDNA sequence in human plasma samples. Reprinted with permission from Ref. 57 © 2021, American Chemical Society

The assay reaches a very low limit of detection of ~2.5 aM, with high levels of sensitivity and specificity. However, even though it is very promising, it is difficult to consider in the field of Point-of-Care testing, as surface plasmon resonance can limit the portability of the device.

As for rapid tests, a rapid multiplex strip test that comprises a gold-nanoparticle-based optical DNA biosensor for KRAS screening in cancer[58] was developed for multi-analyte liquid biopsy applications. The wild-type KRAS and three single-point mutations (G12D, G12A, G12V) were simultaneously detected in cfDNA/ctDNA with a single strip test. The strip-type DNA biosensor was tested and optimized in synthetic DNA targets, in colorectal cancer cell lines, in tissue samples and finally applied to blood-derived cfDNA from healthy individuals and ctDNA from patients

with advanced colorectal cancer. However, an amplification step via PCR is required before testing the samples, thus determining long time for the carryout.

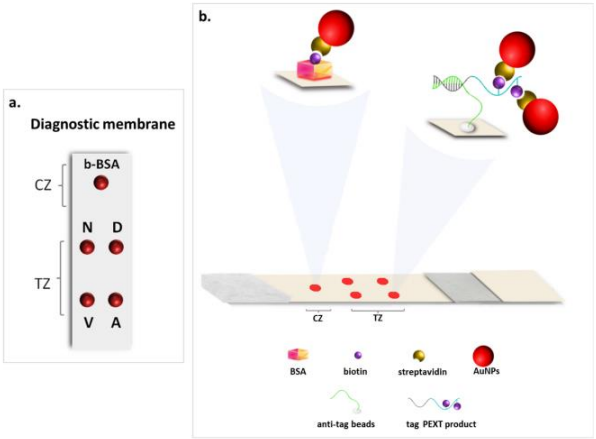

Figure 5.8: Layout of the test and the control spots on the diagnostic membrane of the multiplex strip test. (b) The principle of the multiplex strip test. b-BSA: biotinylated BSA, N: normal allele, D: G12D mutant allele, V: G12V mutant allele, A: G12A mutant allele, TZ: test zone, CZ: control zone, AuNPs: gold nanoparticles. Reprinted with permission from Ref. 58 © © 2022 MDPI, Basel, Switzerland.

A different method for KRAS single nucleotide mutation DNA detection based on Rolling Circle Amplification (RCA) was also reported[59]. The authors exploited a double nucleic acid amplification mechanism in combination with the mutS enzyme for specific binding of point mutations, achieving a LOD of 3.09 aM.

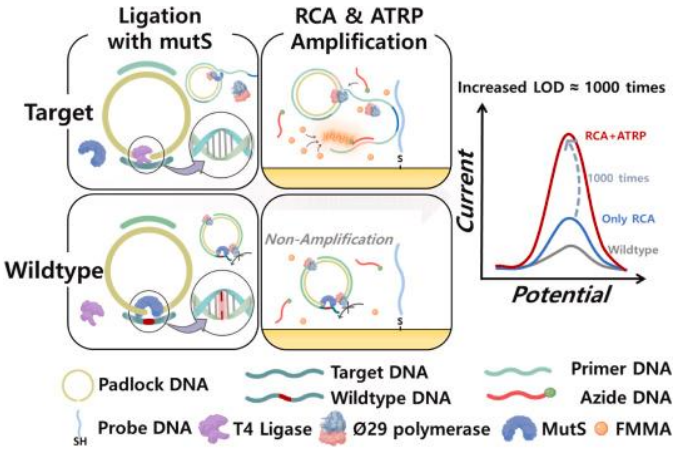

Figure 5.9: Schematic representation of RCA based process. Reprinted with permission from Ref. 59 © 2022 Elsevier B.V. All rights reserved.

In this device, the target DNA and padlock DNA bind complementarily, and circular DNA is formed after T4 ligase is bound to the complex. This determines DNA amplification by polymerase, binding with probe DNA attached to the electrode with a gold-thiol bond, and ATRP reaction due to complementary binding with azide DNA. The presence of SNV was quantitatively determined using square wave voltammetry (SWV) measurements and an electrochemical sensor. As for Wild-Type DNA, a single base mismatch with the padlock DNA occurs. MutS recognizes this single base mismatch, combines with it, and interferes with ligation. In absence of ligation from T4, RCA and ATRP reactions also do not occur, determining a low SWV signal. Despite the outstanding sensitivity and selectivity, analyses were carried out on human serum spiked with synthetic DNA, but no validation on genomic DNA was performed. In addition, the method revealed time-consuming because of the use of amplification systems of nucleic acids.

5.6 AIM OF THE STUDY

In such a context, due to the important role played by genosensors in early detection and therapeutic response and treatment, a novel electrochemical magneto-genosensing assay for the detection of KRAS G12D single nucleotide variation was developed and validated. It is based on the immobilization of PNA capture probes complementary to wild-type or mutated DNA on magnetic microbeads (mMBs) to improve the genoassay performances. The magneto-genosensing assay was integrated with a multichannel smart portable potentiostat with four independent channels, specifically projected by our research team for POC testing. The developed genoassay was validated in human plasma matrix and applied to the analysis of genomic DNA containing wild-type or both wild-type and mutated (G12D) sequences, to prove its applicability in LB clinical diagnostics. To our knowledge, this is the first POC electrochemical magneto-genosensing assay

focused on the specific and highly sensitive detection of G12D SNV mutation of the KRAS oncogene related to tumour DNA, implemented on smart portable instrumentation.

5.7 MATERIALS AND METHODS

5.7.1 Materials

Sodium chloride (NaCl), disodium hydrogen phosphate (Na_2HPO_4), ethylendiaminetetraacetic acid disodium salt dihydrate (Na_2EDTA), sodium bicarbonate ($NaHCO_3$), sodium dodecyl sulfate (SDS), Trizma® Base, magnesium chloride ($MgCl_2$), *N*-(3-dimethylaminopropyl)-*N'*-ethylcarbodiimide hydrochloride (EDC), *N*-hydroxysuccinimide (NHS), 4-morpholineethanesulfonic acid monohydrate (MES), Tween® 20, bovine serum albumin (BSA), hydrochloric acid (HCl, 37%), sodium hydroxide (NaOH) and streptavidin-alkaline phosphatase from Streptomyces avidinii conjugate (ALP-Strp) were purchased from Sigma-Aldrich (Milan, Italy). Human recovered plasma was from Tebu Bio (Magenta, Milano, Italy). Dynabeads™ M-270 carboxylic acid were purchased from Thermo Fischer Scientific (Massachusetts, USA). Hydroquinone diphosphate (HQDP), single-walled carbon nanotubes screen-printed electrodes (SWCNT-SPEs), magnetic support for screen-printed electrodes (DRP-magnet) and support for magnetic separation were supplied by Metrohm Italiana Srl (Origgio, Varese, Italy). Ultrasonic cleaning bath USC300TH was purchased from VWR International (Leuven, Belgium).

The voltammetric readout was performed using a PGSTAT-204 Potentiostat/Galvanostat (Metrohm Italiana Srl, Origgio, Varese, Italy) using NOVA 2.1.6 Advanced Electrochemical Software. The SPEs were connected to a switch box from DropSens (DRP-DSC), allowing their interface with the potentiostat.

To demonstrate the portability of the genoassay, voltammetric measurements were also performed on a custom-made smart portable multichannel

potentiostat[60]. Synthetic DNA targets and Signaling Probe (SP) were purchased from biomers.net GmbH (Ulm, Germany), having the following sequences:

Target KRAS WT DNA: 5'-CTG AAT ATA AAC TTG TGG TAG TTG GAG CTG **G**TG GCG TAG-3'

Target KRAS p.G12D DNA: 5'- CTG AAT ATA AAC TTG TGG TAG TTG GAG CTG **A**TG GCG TAG -3'

Signaling Probe (SP) DNA: 5'-TAC CAC AAG TTT ATA TTC AG -3'.

5.7.2 Buffers composition

Buffer solutions were prepared according to the following compositions:

MES buffer: 0.1 M MES (pH adjusted to 5 using NaOH).

Activation buffer: 0.2 M EDC, 0.05 M NHS in MES buffer

Tris buffered saline (TBS): 0.1 M Trizma® base, 0.02 M $MgCl_2$ (pH adjusted to 7.4 using HCl).

Tris buffered saline-Tween (TBS-T): 0.1 M Trizma® base, 0.02 M $MgCl_2$, 0.05% w/v Tween 20® (pH adjusted to 7.4 using HCl).

Carbonate buffer (CB): 0.1 M $NaHCO_3$, 0.1% w/v SDS (pH adjusted to 9 using NaOH).

Hybridization buffer (HB): 0.3 M NaCl, 0.02 M Na_2HPO_4, 0.1 mM EDTA (pH adjusted to 7.4 using HCl).

Blocking Buffer (BB): 20 mg mL^{-1} BSA in TBS (pH 7.4).

Reading buffer (RB): 0.1 M Trizma® base, 0.02 M $MgCl_2$ (pH adjusted to 9.8 using HCl).

5.7.3 PNA Synthesis

The synthesis of PNA capture probes was performed following previously reported protocols[61].The sequences of the PNA synthesized were (the symbol O represents the spacer 2-(2-aminoethoxy)ethoxyacetyl group) :

Capture Probe complementary to wild-type KRAS DNA (CP_{WT}):

H-OO-CTACGCCACCAGCT-Gly-NH_2

Capture Probe complementary to p.G12D KRAS DNA (CP_{G12D}):

H-OO-CTACGCCATCAGCT-Gly-NH_2

Since CP_{WT} and CP_{G12D} PNA probes used in the present work were stored in water at -20°C for long times, their identity and purity were verified and confirmed using ultra-performance liquid chromatography-mass spectrometry (UPLC/MS) prior to experiments. The Waters Acquity UPLC equipped with Waters™ SQ detector and electrospray (ESI) source was used. The PNA probes were analyzed on the Waters Acquity UPLC BEH C18 300 Å, 50 × 2.1 mm, 1.7 µm column using the following chromatographic conditions:

eluent A: water with 0.2% formic acid (v/v)

eluent B: acetonitrile with 0.2% formic acid (v/v)

Column temperature: 35 °C.

Program: initial isocratic mode at 100% A (0.9 min), then linear gradient to 50% B over 5.7 min. Final wash with 100% B for 1.2 min. Flow rate: 0.25 mL/min.

The UPLC/MS profile of each PNA probe was compared to that of the same stock solutions obtained just after synthesis.

5.7.4 Genoassay procedure

5.7.4.1 Immobilization of CP on mMBs

The aqueous suspension of Dynabeads™ M-270 carboxylic acid was diluted to a concentration of $8 \cdot 10^7$ beads/mL in 100 µL of MES buffer. The beads were washed following a standard protocol comprising suspension in 200 µL of MES buffer, magnetic separation for 2 minutes and discard of the supernatant. After washing with MES buffer, the beads were resuspended in 200 µL of activation buffer for 30 min at 25 °C under shaking at 1500 rpm (Thermomixer C, Eppendorf, Hamburg, Germany), then they were washed with MES buffer and resuspended in a 500 nM solution of CP in CB. The reaction was left for 2h at 25 °C under shaking at 1500 rpm. Finally, the obtained CP@mMBs were washed with CB.

5.7.4.2 Sandwich complex assembling on CP@mMBs

The synthetic target DNA at the desired concentration and 500 nM SP DNA were mixed in HB and left for 10 minutes at 25°C under shaking at 1500 rpm in order to form a first hybrid between the two strands. Then CP@mMBs were resuspended in 200 µL of the DNA/SP solution for 1 h at 50°C under shaking at 1500 rpm. The beads were then washed with HB.

5.7.4.3 Enzyme labelling and electrochemical readout

The beads reacted with the DNA/SP mixture were resuspended in 200 µL of a solution of ALP-Strp 1:100 diluted in BB for 15 min at 25 °C under shaking at 1500 rpm, after which they were washed with TBS-t and then with TBS. The beads were then resuspended in 100 µL of a 1 mg/mL solution of HQDP in RB for 3 min, then 50 µL of the suspension were drop-casted onto the SWCNT-SPE, located on the magnetic support for SPE, to confine the magnetic particles on the working

electrode surface. DPV measurements were recorded by scanning the potential between 0.2-0.5 V with the following waveform parameters:

step potential: 0.005 V

modulation amplitude: 0.05 V

modulation time:100 ms

interval time: 400 ms.

5.7.4.4 Experimental design

A three level, two factor (3^2) Full Factorial Design (FFD) was carried out using both CP_{WT} and CP_{G12D}. The response variable was the rate of signal reduction between complementary and non-complementary sequences, depending on the immobilized CP. The factors examined were *i)* the incubation temperature for the sandwich complex assembling and *ii)* the DNA target concentration. The levels explored were 30, 40 and 50°C for the incubation temperature and 1, 5 and 10 nM for the target DNA concentration. Each of the experiments was replicated twice and acquired under randomized sequence. All statistical calculations were performed using the Statistics for Data Analysis V.28 software package (SPS Srl, Bologna, Italy).

5.7.4.5 Magnetogenoassay validation in human plasma

Validation of the developed magnetogenoassay was performed according to Eurachem Guide[62]. Measurements were carried out performing the sandwich complex assembly in the presence of human plasma diluted 1:10 in HB. Specificity was assessed by calculating the observed signal reduction rates at the same concentration for non-complementary *versus* complementary targets with both CP_{WT} and $CP_{G12D.}$

As for limit of detection (LOD) and limit of quantification (LOQ), 10 replicate measurements of blank samples, i.e., matrices containing no detectable analyte,

were carried out. LOD was calculated as $3 \cdot s_0/\sqrt{n}$ and LOQ as $10 \cdot s_0/\sqrt{n}$, where s_0 is the blank standard deviation and n is the number of replicate measurements. Linearity and precision in terms of repeatability were calculated performing three replicated measurements for each level explored. Concerning the evaluation of linearity, regression residuals were calculated, the mean of which was not significantly different from zero ($p > 0.05$) over the linearity range.

5.7.4.6 Analysis of real samples of genomic DNA

For the analysis of real samples with the magneto-genosensing assay, genomic DNA from two different cell lines were used: LS147T with a heterozygous mutation KRAS c.35G> A (p.G12D) and HT29 with a WT KRAS sequence. The genomic DNA samples containing wild-type DNA or both wild-type and G12D sequences were from UOC Oncological Translational Research, IRCCS-Regina Elena National Cancer Institute, Rome, Italy[40]. Prior to incubation with SP, they were sonicated (5 minutes), denatured by heating (5 minutes at 95 °C) and kept in ice for 5 minutes. Samples were then diluted 1:50 in a solution containing 500 nM SP in HB and kept under shaking for 10 minutes at 1500 rpm at 25 °C for the hybridization. CP@mMBs were then resuspended in 200 µL of these solutions.

5.8 RESULTS AND DISCUSSION

5.8.1 Magneto-genosensing assay setup

The magneto-genosensing assay setup, schematized in figure 5.10, is based on the formation of a sandwich complex between PNA Capture Probe (CP), target DNA and Signaling Probe DNA (SP). CP was immobilized onto the surface of magnetic microbeads (mMBs) to exploit their advantages, like easy separation of the samples through an external magnetic field, higher surface immobilization and low non-specific binding[63]. In particular, two PNA probes complementary to wild-type or G12D mutated sequences were used. They were alternatively immobilized onto the mMBs surface functionalized with carboxylic group, exploiting them through activation with coupling reagents, namely EDC and NHS. As for the SP, it is complementary to a different portion of DNA target maintained in both WT and mutated sequences. In parallel with functionalization of mMBs with CP, a separated solution for the hybridization of target DNA and SP was incubated. This solution is then added to the suspension containing CP@mMMBs to promote the formation of the sandwich complex. As for the generation of the electrochemical signal, SP is labelled with biotin so that it can interact with the ALP-Strp conjugate added in the following step. In this way, upon addition of HQDP, substrate for the enzyme ALP, the electroactive compound hydroquinone is generated, providing a signal proportional to the amount of sandwich complex[61], acquired by DPV.

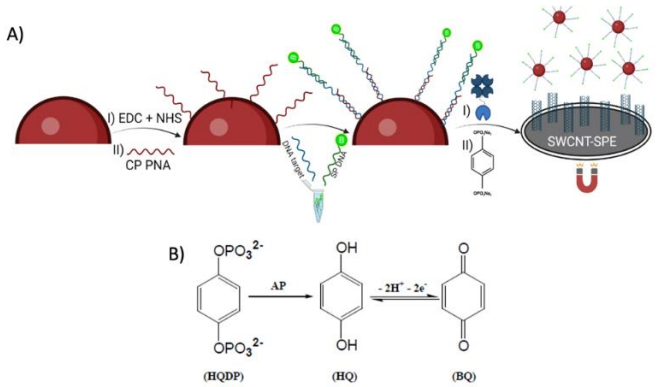

Figure 5.10: A) Genoassay protocol B) HQDP dephosphorylation by AP enzyme and generation of electroactive species

Performing the test with the mutated and WT target DNA, a difference in the intensity of the signals was obtained with complementary and non-complementary sequences, given by the discrimination operated by the PNA CPs

5.8.2 Evaluation of incubation time

Different incubation times were considered for the genoassay development. First, different incubation times were tested for the hybridization between the SP and the target. CP and SP were kept at a concentration of 500 nM, while DNA target concentration was 1 nM. Incubation times ranging from 10 to 120 minutes were evaluated: Figure 5.11 shows that an incubation time of only 10 minutes allows to reach a complete hybridization reaction, as no statistically significant difference *($p > 0.05$)* was observed between 10 and 20 minutes, while higher incubation times determine signal lowering. On the basis of these results, the incubation time was set to 10 min for subsequent experiments.

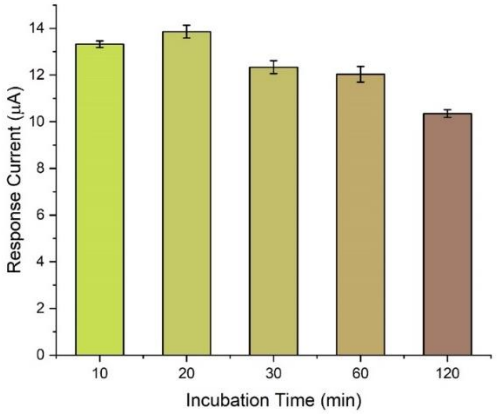

Figure 5.11: Incubation time for DNA target-SP hybrid

Once the first hybridization reaction was evaluated, the incubation time for the sandwich formation between the target DNA-SP hybrid and the CP probes immobilized onto the mmBs was considered. Also in this case, CP and SP were kept at a concentration of 500 nM, while target DNA concentration was 1 nM. Incubation times between 30 min and 120 minutes were tested, reaching the signal saturation after 90 minutes. Based on these findings, even though the highest signal was obtained at 90 min, incubation time of 60 min was considered for the following experiments, as it gives higher signal reduction between complementary and non-complementary target (see Figure 5.12) and keeps the execution times low, resulting in a total of 1 h 30 min for the whole magneto-genosensing assay.

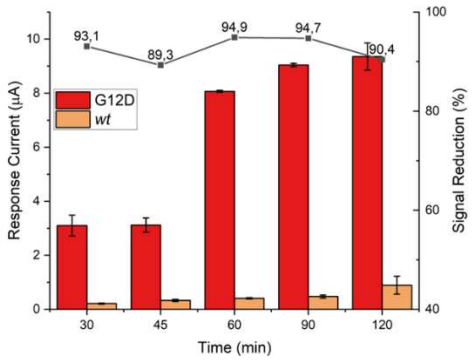

Figure 5.12: Incubation time for sandwich formation between CP@mMBs and DNA target-SP hybrid

5.8.3 Optimization of magneto magneto-genosensing assay

Two different factors were considered for the optimization, determining the discrimination between complementary and non-complementary target: the incubation temperature and the target concentration for the formation of the sandwich between CP, target DNA and SP. Indeed, the hybridization reaction should occur above the melting temperature of the CP-non complementary target duplex and below the melting temperature of the complementary target-CP duplex. To this end, a Full Factorial Design (FFD) with two factors and three levels (3^2) was performed. Factor A and B were respectively the target DNA concentration and the temperature for the hybridization between CP, target DNA and SP. The signal reduction between complementary and non-complementary target was set as response variable. Both CP_{WT} and CP_{G12D} were tested for the FFD. A two-way ANOVA with Bonferonni post-hoc test was performed, showing that both factors and their interactions were statistically significant (*p<0,01* and *p<0,05*, respectively). Moreover, multiple linear regression (MLR) was performed to evaluate the significance of coefficients related to temperature and target concentration as independent variables, self-interaction and interaction between the two factors. The response functions (1) and (2) were obtained with CP_{G12D} and CP_{WT}, respectively, whereas the corresponding response surfaces are reported in Figure 5.13 (A, B) also reporting the voltammograms obtained for complementary and non-complementary target DNA under optimized conditions for CPG12D (D) and CPWT (E)

$$CP_{G12D}: Signal\ Reduction\ (\%) = 140,46 - 15,77*A - 4,15*B + 0,66*A^2 + 0,14*A*B + 0,07*B^2 \quad (1)$$

$$CP_{WT}: Signal\ Reduction\ (\%) = -74,29 - 17,38*A + 7,06*B + 0,73*A^2 + 0,16*A*B - 0,04*B^2 \quad (2)$$

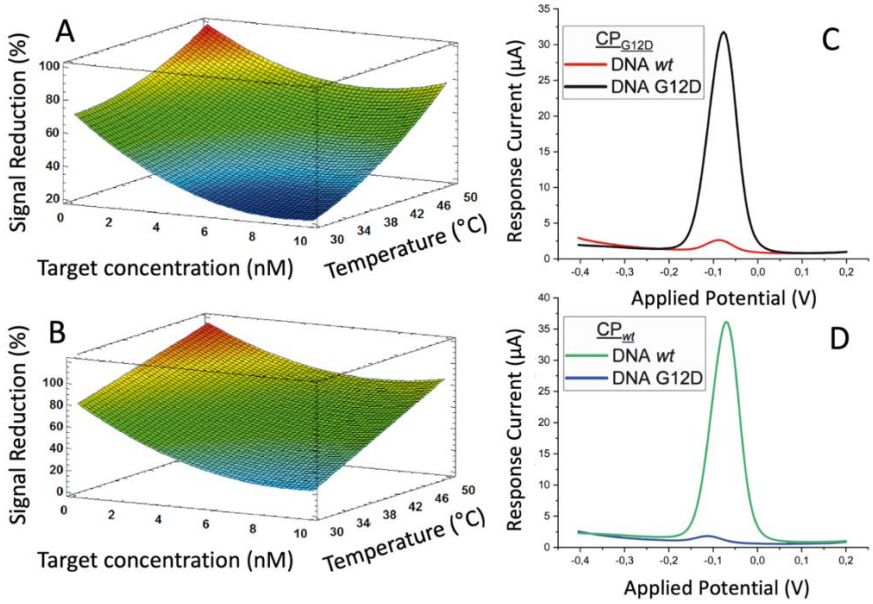

Figure 5.13: Response surfaces obtained by the FFD for CPG12D (A) and CPWT (B) and voltammograms obtained for complementary and non-complementary target DNA under optimized conditions for CPG12D (C) and CPWT (D)

The optimal conditions found, clearly detectable also in the response surfaces, were 1 nM for DNA target concentration and 50 °C for the hybridization temperature between target DNA -SP hybrid and CP. Under these conditions, the highest signal suppression was obtained both for CP_{G12D} (94%) and CP_{WT} (97%).

5.8.4 Linearity assessment

The analytical performance of the magneto-genosensing assay was evaluated in human plasma. To this end, matrix effect was tested spiking with target DNA human plasma diluted with different factors, i.e., 10%, 20% 30%, 50% and comparing the results obtained in absence of matrix. As shown in Figure 5.14, a significant signal suppression was observed for plasma concentrations higher than 10%.

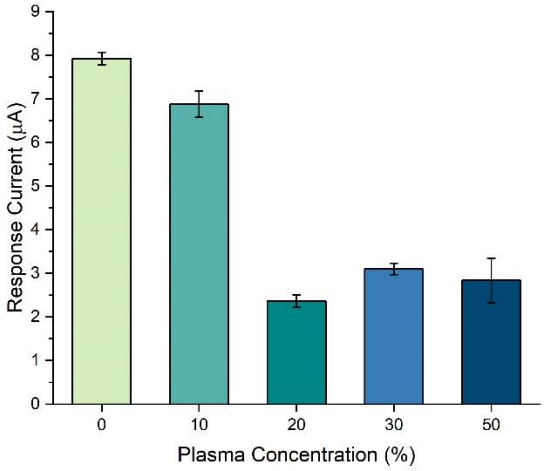

Figure 5.14: Evaluation of different plasma dilution factors

Based on these findings, calibration lines both for CP_{WT} and CP_{G12D} were acquired in 1:10 diluted plasma (10% concentration). Figure 5.15 shows as for CP_{WT}, a linear response ranging from 50 to 2000 pM was obtained, thus giving very low limit of detection and quantification, i.e. 1.98 pM (LOD) and 6.6 pM (LOQ). Regarding CP_{G12D}, a linear response between 50 and 1000 pM was observed, with very good LOD and LOQ levels of 818 fM and 2.72 pM, respectively.

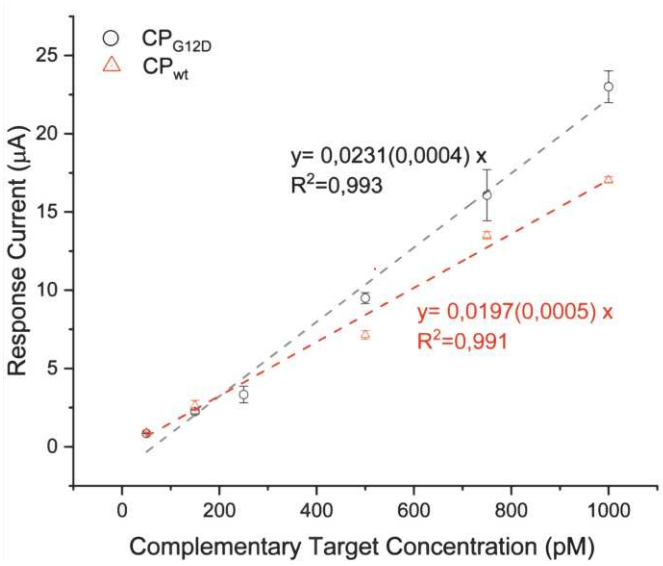

Figure 5.15: Calibration curves obtained in 10% human plasma for CP_{G12D} and CP_{WT}. The error bars represent the standard deviation between three replicate response current measurements (RSD<5%).

To assess the specificity of the genoassay, voltammetric measurements on multichannel smart portable potentiostat in 1:10 diluted plasma were performed. The following samples were tested: CP_{G12D} and G12D DNA target (Channel,1 CH1); CP_{G12D} and WT target DNA (Channel 3, CH3); CP_{WT} and WT target DNA (Channel 2, CH2); CP_{WT} and G12D target DNA (Channel 4, CH4). The magneto genoassay resulted highly specific also in plasma-diluted samples, as shown in Figure 5.16.

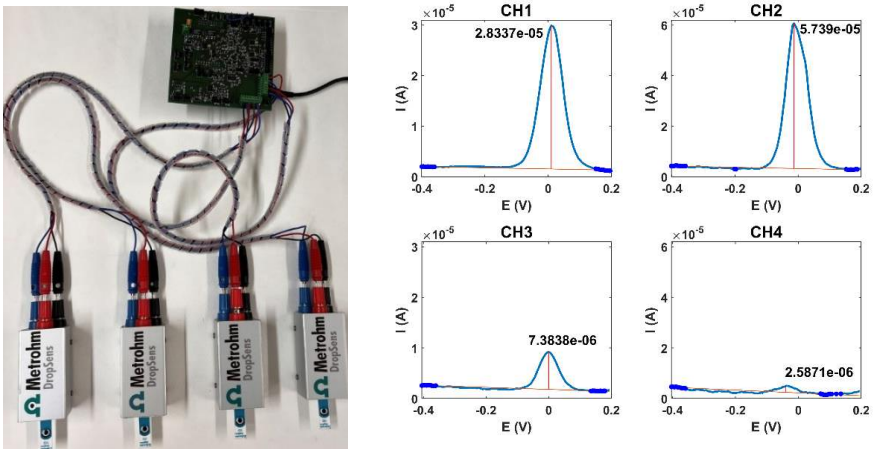

Figure 5.16: Representation of portable potentiostat with 4 independent channels (left) Voltammograms acquired on a multichannel smart portable potentiostat (right)

One of the advantages of using CP-PNA probes is their chemical and enzymatic stability, leading to long-term storage of the stock solution needed for sensor and kit fabrication. Their identity and purity were assessed using mass spectrometry prior to experiments. The target compound's identity was confirmed using molecular ion in the MS spectrum, shown in Supplementary material (Fig.S1 and S2) comparable to data previously recorded on the same stock solution of CP-PNA probes[2]. Taking into account that the stock solutions of the PNAs used in the present study were stored in aqueous solutions at −20 ◦C for several years after their synthesis, no sign of degradation was observed, thus proving that the shelf-life of these probes is extremely long.

Finally, to evaluate the stability of PNA probes on mmBs, CP_{G12D} was immobilized on mMBs and tested the same day, after 45 days and 90 days. Signals obtained were comparable and no signal lowering was observed, thus showing the high stability of the genoassay and a shelf-life of at least 90 days, as shown in Figure 5.17

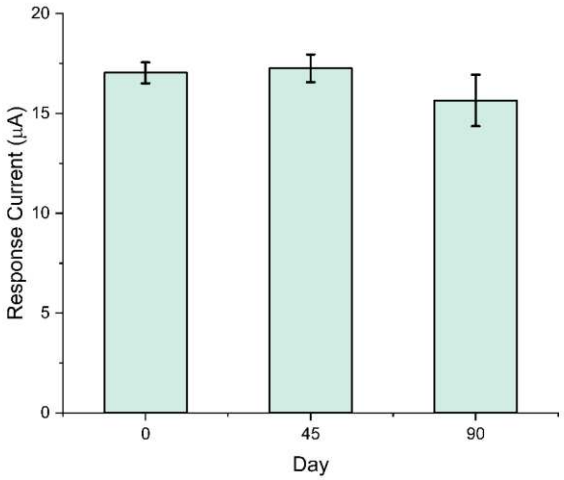

Figure 5.17: Shelf-life evaluation of CP_{G12D} at 0, 45 and 90 days

5.8.5 Performance of the readout instrumentation

The good analytical performance of the magneto-genosensing assay, combined with the signal readout carried out with multichannel smart portable potentiostat enable the suitability of the developed device for the POC context. In fact, the battery-powered device includes four independent channels, operating in parallel, that can be conditioned with different voltage ranges[60]. The smart potentiostat is equipped with a Wi-Fi section for the connection to cloud analytics for data storage and processing, and with different users for data sharing without the need for other external tools such as personal computers or smartphones. These features, combined with the versatility of the portable device, allow for widespread screening programs, paving the way to POC devices for non- invasive ultra-sensitive detection of the most frequent KRAS mutation.

5.8.6 Validation on gDNA samples

To validate the genoassay performance also in real samples, genomic DNA (gDNA) from two different cell lines was tested under the optimized conditions: LS147T cell line contains both mutated and WT DNA, while HT29 only contains WT DNA. A sample pre-treatment was carried out to obtain single-stranded DNA fragments from gDNA, so that they can hybridize with CP and SP probes. Samples were subjected to sonication for 5 min, denaturation at 95 °C for 5 min, followed by rapid cooling in ice bath together with SP to promote hybridization between SP and target DNA and block the strand reassociation. After sample treatment, binding with both CPs was tested using the aforementioned multichannel smart portable potentiostat.

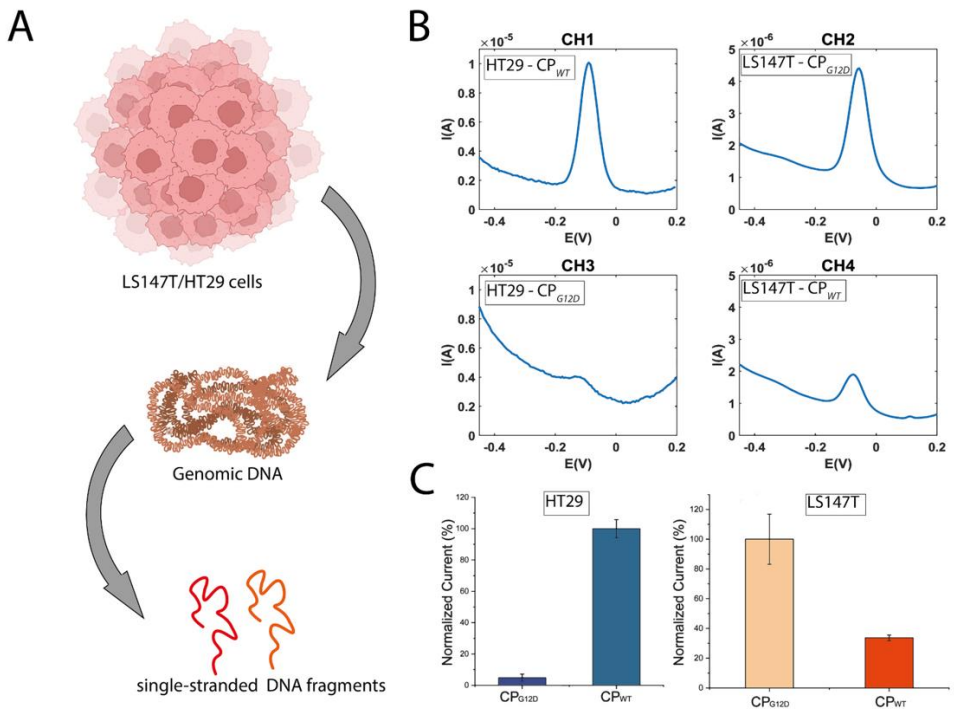

Figure 5.18: (A) Schematic representation of sample treatment to obtain single-stranded DNA fragments from cells, (B) voltammograms acquired on smart portable multichannel potentiostat and (C) current responses normalized on signal attributable to complementary target for CP_{WT} and CP_{G12D}.

As for LS147T cell line, a more intense signal was obtained with CP_{G12D}, while CP_{WT} gives a 67% lower signal. In the case of HT29, CP_{G12D} provides a signal practically negligible (95% lower) with respect to CP_{WT}. The results obtained (see Figure 5.18) were consistent with the composition of the samples, previously tested by qPCR (Fig.S3) at IRCSS-Regina Elena National Cancer Institute. These results show the ability of the magneto-genosensing assay to recognize the presence of the G12D mutation with high sensitivity and selectivity. Moreover, the full integration of the assay with a smart portable electrochemical set-up makes it suitable for POC contexts for both early detection and personalized medicine applications.

This work led to the publication of the following research article:

S. Fortunati, C. Giliberti, M. Giannetto, A. Bertucci, S. Capodaglio, E. Ricciardi, P. Giacomini, V. Bianchi, A. Boni, I. De Munari, R. Corradini, M. Careri, *A highly sensitive electrochemical magneto-genosensing assay for the specific detection of a single nucleotide variation in the KRAS oncogene in human plasma,* **Biosensors and Bioelectronics: X**, Volume 15,2023,100404.

5.9 SUPPLEMENTARY MATERIALS

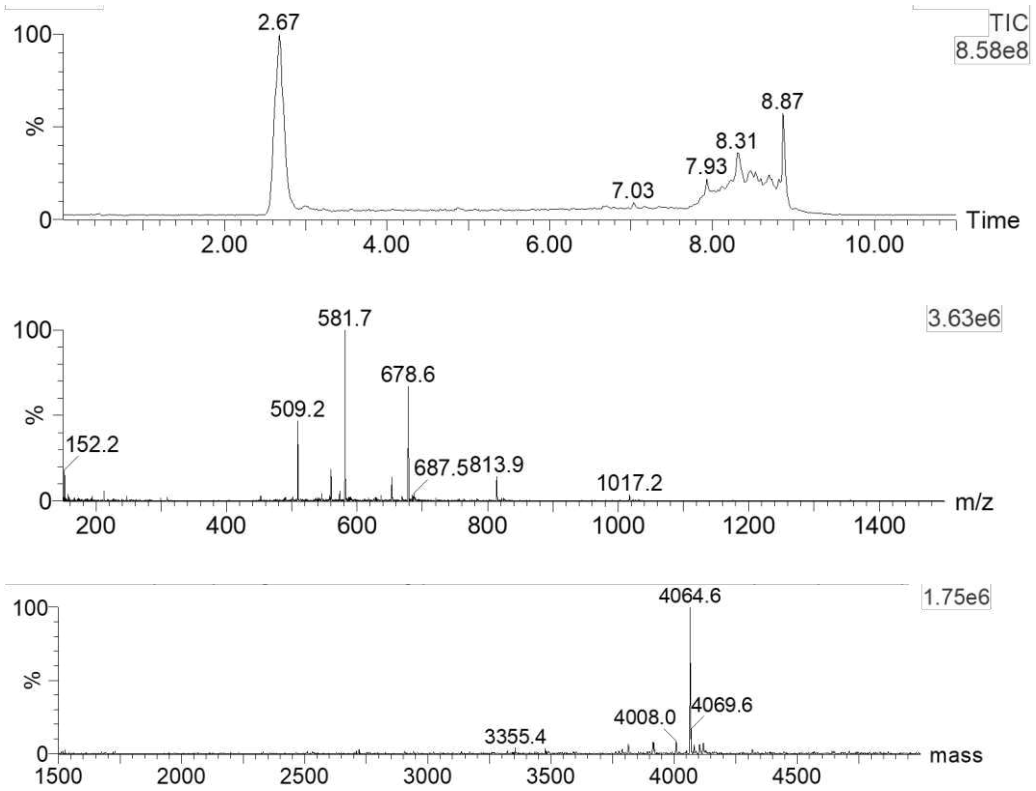

Figure S1: *UPLC-MS analysis of solution of the CP_{WT} PNA probe 6 years after synthesis: sequence H-OOCTACGCCACCAGCT-Gly-NH2. Upper panel: UPLC/MS chromatogram. Middle panel: ESI-MS spectrum of the peak at 2.67 min; m/z found (calculated): 1017.2 (1017.0) $[MH_4]^{4+}$, 813.9 (813.8) $[MH_5]^{5+}$, 678.6 (678.3) $[MH_6]^{6+}$, 581.7 (581.6) $[MH_7]^{7+}$, 509.2 (509.0) $[MH_8]^{8+}$. Lower panel: reconstructed molecular mass spectrum; MW: calculated 4064.0 Da, found 4064.6 Da.*

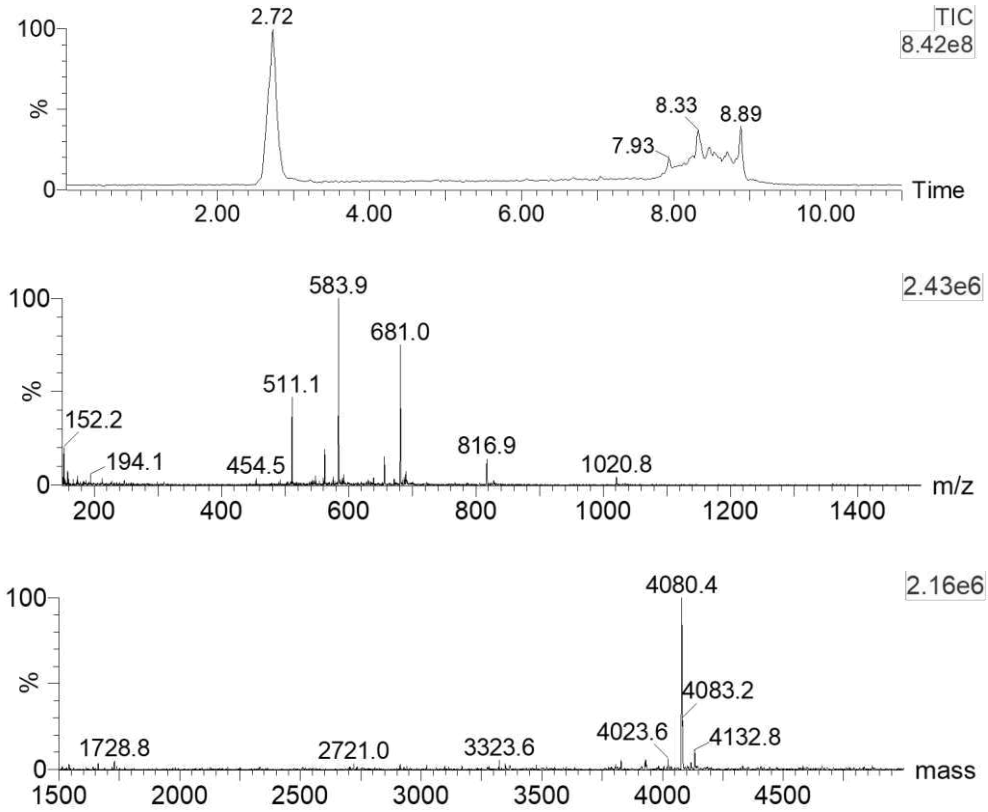

***Figure S2**: UPLC-MS analysis of solution of the CP_{G12D} PNA probe 6 years after synthesis: sequence H-OOCTACGCCATCAGCT-Gly-NH2. Upper panel: UPLC/MS chromatogram. Middle panel: ESI-MS spectrum of the peak at 2.72 min: m/z found (calculated): 1020.8 (1020.8) $[MH_4]^{4+}$, 816.9 (816.8) $[MH_5]^{5+}$, 681.0 (680.8) $[MH_6]^{6+}$, 583.9 (583.7) $[MH_7]^{7+}$, 511.1 (510.9) $[MH_8]^{8+}$, 454.5 (454.2) $[MH_9]^{9+}$. Lower panel: reconstructed molecular mass spectrum; MW: calculated 4079.0 Da, found 4080.4 Da.*

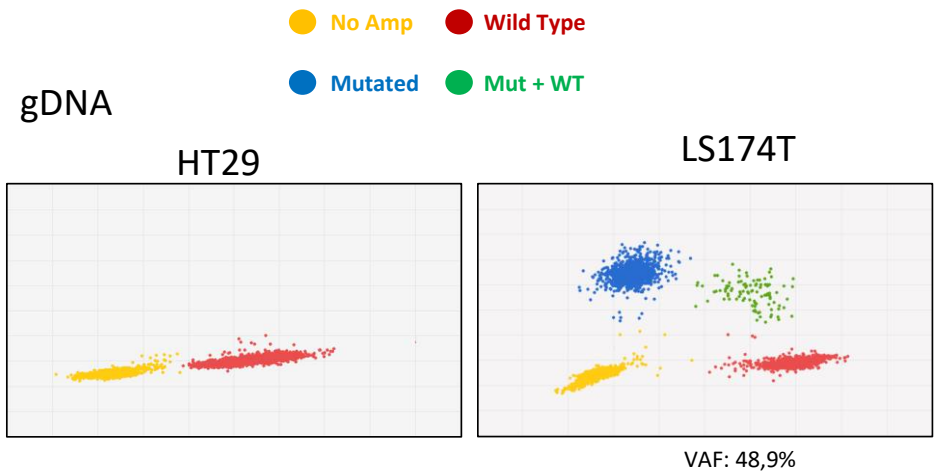

Figure S3: *dPCR analysis carried out on HT29 (left) and LS147T (right) cell lines showing the presence of WT and Mutated sequences*

5.10 REFERENCES

1. Lahiri, H., Mishra, S. & Mukhopadhyay, R. Nanoscale Nucleic Acid Recognition at the Solid-Liquid Interface Using Xeno Nucleic Acid Probes. *Langmuir* **35**, 8875–8888 (2019).
2. D'Agata, R. *et al.* Direct plasmonic detection of circulating RAS mutated DNA in colorectal cancer patients. *Biosens. Bioelectron.* **170**, (2020).
3. Fortunati, S. *et al.* Novel amperometric genosensor based on peptide nucleic acid (PNA) probes immobilized on carbon nanotubes-screen printed electrodes for the determination of trace levels of non-amplified DNA in genetically modified (GM) soy. *Biosens. Bioelectron.* **129**, 7–14 (2019).
4. Kerman, K., Kobayashi, M. & Tamiya, E. Recent trends in electrochemical DNA biosensor technology. **15**, 1–11 (2004).
5. Zhang, Y. & Zhou, N. Electrochemical Biosensors Based on Micro-fabricated Devices for Point-of-Care Testing: A Review. *Electroanalysis* **34**, 168–183 (2022).
6. Trotter, M., Borst, N., Thewes, R. & von Stetten, F. Review: Electrochemical DNA sensing – Principles, commercial systems, and applications. *Biosens. Bioelectron.* **154**, (2020).
7. Campuzano, S., Yáñez-Sedeño, P. & Pingarrón, J. M. Electrochemical genosensing of circulating biomarkers. *Sensors (Switzerland)* **17**, 1–20 (2017).
8. Kulkarni, M. B., Ayachit, N. H. & Aminabhavi, T. M. A Short Review on Miniaturized Biosensors for the Detection of Nucleic Acid Biomarkers. *Biosensors* **13**, 1–15 (2023).
9. Zhu, C., Yang, G., Li, H., Du, D. & Lin, Y. Electrochemical sensors and

biosensors based on nanomaterials and nanostructures. *Anal. Chem.* **87**, 230–249 (2015).

10. Mana, T., Bhattacharya, B., Lahiri, H. & Mukhopadhyay, R. XNAs: A Troubleshooter for Nucleic Acid Sensing. *ACS Omega* **8**, (2022).

11. Vester, B. & Wengel, J. LNA (Locked Nucleic Acid): High-affinity targeting of complementary RNA and DNA. *Biochemistry* **43**, 13233–13241 (2004).

12. Fortunati, S. *et al.* A highly sensitive electrochemical magneto-genosensing assay for the specific detection of a single nucleotide variation in the KRAS oncogene in human plasma. *Biosens. Bioelectron. X* **15**, 100404 (2023).

13. Karkare, S. & Bhatnagar, D. Promising nucleic acid analogs and mimics: Characteristic features and applications of PNA, LNA, and morpholino. *Appl. Microbiol. Biotechnol.* **71**, 575–586 (2006).

14. Nielsen, P. E. Peptide nucleic acid (PNA). A structural DNA mimic. *Mater. Res. Soc. Symp. - Proc.* **330**, 3–6 (1994).

15. Saadati, A. *et al.* Recent advances on application of peptide nucleic acids as a bioreceptor in biosensors development. *TrAC - Trends Anal. Chem.* **114**, 56–68 (2019).

16. Park, H. *et al.* Kinetic and affinity analyses of hybridization reactions between peptide nucleic acid probes and DNA targets using surface plasmon field-enhanced fluorescence spectroscopy. *Biointerphases* **1**, 113–122 (2006).

17. Sharma, C. & Awasthi, S. K. Versatility of peptide nucleic acids (PNAs): role in chemical biology, drug discovery, and origins of life. *Chem. Biol. Drug Des.* **89**, 16–37 (2017).

18. D'Agata, R., Giuffrida, M. C. & Spoto, G. Peptide Nucleic Acid-Based Biosensors for Cancer Diagnosis. *Molecules* **22**, 1–15 (2017).

19. Nielsen, P. E., Egholm, M., Berg, R. H., & Buchardt, O. Sequence-selective recognition of DNA by strand displacement with a thymine-substituted polyamide. *Sci. (New York, N.Y.),* **254**, 1497–1500 (1991).

20. Babaei, A. *et al.* Genosensors as an alternative diagnostic sensing approaches for specific detection of virus species: A review of common techniques and outcomes. *TrAC - Trends Anal. Chem.* **155**, (2022).

21. Drummond, T. G., Hill, M. G. & Barton, J. K. Electrochemical DNA sensors. *Nat. Biotechnol.* **21**, 1192–1199 (2003).

22. Pänke, O., Kirbs, A. & Lisdat, F. Voltammetric detection of single base-pair mismatches and quantification of label-free target ssDNA using a competitive binding assay. *Biosens. Bioelectron.* **22**, 2656–2662 (2007).

23. Tsaloglou, M. N. *et al.* Handheld isothermal amplification and electrochemical detection of DNA in resource-limited settings. *Anal. Biochem.* **543**, 116–121 (2018).

24. WHO. The Global Cancer Observatory - All cancers. *Int. Agency Res. Cancer - WHO* **419**, 199–200 (2020).

25. Hirahata, T. *et al.* Liquid Biopsy: A Distinctive Approach to the Diagnosis and Prognosis of Cancer. *Cancer Inform.* **21**, (2022).

26. Glatzer, M., Panje, C. M., Sirén, C., Cihoric, N. & Putora, P. M. Decision Making Criteria in Oncology. *Oncol.* **98**, 370–378 (2020).

27. Timar, J. & Kashofer, K. Molecular epidemiology and diagnostics of KRAS mutations in human cancer. *Cancer Metastasis Rev.* **39**, 1029–1038 (2020).

28. Cowling, T. & Loshak, H. An Overview of Liquid Biopsy for Screening and Early Detection of Cancer. *CADTH Issues Emerg. Heal. Technol.* (2016).

29. Mathai, R. A. *et al.* Potential utility of liquid biopsy as a diagnostic and

prognostic tool for the assessment of solid tumors: Implications in the precision oncology. *J. Clin. Med.* **8**, 1–17 (2019).

30. Vacante, M., Ciuni, R., Basile, F. & Biondi, A. The liquid biopsy in the management of colorectal cancer: An overview. *Biomedicines* **8**, (2020).

31. Siravegna, G., Marsoni, S., Siena, S. & Bardelli, A. Integrating liquid biopsies into the management of cancer. *Nat. Rev. Clin. Oncol.* **14**, 531–548 (2017).

32. Ricciardi, E. *et al.* Metastatic Melanoma: Liquid Biopsy as a New Precision Medicine Approach. *Int. J. Mol. Sci.* **24**, (2023).

33. Rupp, B., Ball, H., Wuchu, F., Nagrath, D. & Nagrath, S. Circulating tumor cells in precision medicine: challenges and opportunities. *Trends Pharmacol. Sci.* **43**, 378–391 (2022).

34. Sparano, J. *et al.* Association of Circulating Tumor Cells With Late Recurrence of Estrogen Receptor-Positive Breast Cancer: A Secondary Analysis of a Randomized Clinical Trial. *JAMA Oncol.* **4**, 1700–1706 (2018).

35. Xie, F., Xu, M., Lu, J., Mao, L. & Wang, S. The role of exosomal PD-L1 in tumor progression and immunotherapy. *Mol. Cancer* **18**, 1–10 (2019).

36. Valihrach, L., Androvic, P. & Kubista, M. Circulating miRNA analysis for cancer diagnostics and therapy. *Mol. Aspects Med.* **72**, 100825 (2020).

37. Tsukamoto, M., Iinuma, H., Yagi, T., Matsuda, K. & Hashiguchi, Y. Circulating Exosomal MicroRNA-21 as a Biomarker in Each Tumor Stage of Colorectal Cancer. *Oncol.* **92**, 360–370 (2017).

38. Fu, F., Jiang, W., Zhou, L. & Chen, Z. Circulating Exosomal miR-17-5p and miR-92a-3p Predict Pathologic Stage and Grade of Colorectal Cancer. *Transl. Oncol.* **11**, 221–232 (2018).

39. Arisi, M. F., Dotan, E. & Fernandez, S. V. Circulating Tumor DNA in Precision

Oncology and Its Applications in Colorectal Cancer. *Int. J. Mol. Sci.* **23**, (2022).

40. Gasparello, J. *et al.* Liquid biopsy in mice bearing colorectal carcinoma xenografts: Gateways regulating the levels of circulating tumor DNA (ctDNA) and miRNA (ctmiRNA). *J. Exp. Clin. Cancer Res.* **37**, 1–11 (2018).

41. Frattini, M. *et al.* Quantitative analysis of plasma DNA in colorectal cancer patients: A novel prognostic tool. *Ann. N. Y. Acad. Sci.* **1075**, 185–190 (2006).

42. Wen, X., Pu, H., Liu, Q., Guo, Z. & Luo, D. Circulating Tumor DNA—A Novel Biomarker of Tumor Progression and Its Favorable Detection Techniques. *Cancers (Basel).* **14**, 1–36 (2022).

43. Li, Y. *et al.* Correction to: Current status of ctDNA in precision oncology for hepatocellular carcinoma (Journal of Experimental & Clinical Cancer Research, (2021), 40, 1, (140), 10.1186/s13046-021-01940-8). *J. Exp. Clin. Cancer Res.* **40**, 13046 (2021).

44. Nazir, S. Medical diagnostic value of digital PCR (dPCR): A systematic review. *Biomed. Eng. Adv.* **6**, 100092 (2023).

45. Chen, M. & Zhao, H. Next-generation sequencing in liquid biopsy: cancer screening and early detection. *Hum. Genomics* **13**, 34 (2019).

46. Mauri, G. *et al.* Liquid biopsies to monitor and direct cancer treatment in colorectal cancer. *Br. J. Cancer* **127**, 394–407 (2022).

47. Xi, Y. & Xu, P. Global colorectal cancer burden in 2020 and projections to 2040. *Transl. Oncol.* **14**, 101174 (2021).

48. Saraiva, M. R., Rosa, I. & Claro, I. Early-onset colorectal cancer: A review of current knowledge. *World J. Gastroenterol.* **29**, 1289–1303 (2023).

49. Prior, I. a, Lewis, P. D. & Mattos, C. UKPMC Funders Group UKPMC Funders Group Author Manuscript A comprehensive survey of Ras mutations in

cancer. *Cancer Res.* **72**, 2457–2467 (2012).

50. Chen, C. C. *et al.* Computational Analysis of KRAS Mutations: Implications for Different Effects on the KRAS p.G12D and p.G13D Mutations. *PLoS One* **8**, 6–13 (2013).

51. Vidal, J. *et al.* Plasma ctDNA RAS mutation analysis for the diagnosis and treatment monitoring of metastatic colorectal cancer patients. *Ann. Oncol.* **28**, 1325–1332 (2017).

52. Van Emburgh, B. O. *et al.* Acquired RAS or EGFR mutations and duration of response to EGFR blockade in colorectal cancer. *Nat. Commun.* **7**, 1–9 (2016).

53. Ciarloni, L. *et al.* Development and clinical validation of a blood test based on 29-gene expression for early detection of colorectal cancer. *Clin. Cancer Res.* **22**, 4604–4611 (2016).

54. Connal, S. *et al.* Liquid biopsies: the future of cancer early detection. *J. Transl. Med.* **21**, 1–18 (2023).

55. Manzari, M. T. *et al.* Targeted drug delivery strategies for precision medicines. *Nat. Rev. Mater.* **6**, 351–370 (2021).

56. Martins, I. *et al.* Liquid biopsies: Applications for cancer diagnosis and monitoring. *Genes (Basel).* **12**, 1–20 (2021).

57. Bellassai, N. *et al.* Detection of Tumor DNA in Human Plasma with a Functional PLL-Based Surface Layer and Plasmonic Biosensing. *ACS Sensors* **6**, 2307–2319 (2021).

58. Kalligosfyri, P. M. *et al.* Rapid Multiplex Strip Test for the Detection of Circulating Tumor DNA Mutations for Liquid Biopsy Applications. *Biosensors* **12**, 1–19 (2022).

59. Lee, S. *et al.* Synergistic enhanced rolling circle amplification based on mutS

and radical polymerization for single-point mutation DNA detection. *Biosens. Bioelectron.* **210**, 114295 (2022).

60. Boni, A. *et al.* A Stand-Alone Portable Potentiostat With Parallel Channels for Smart Electrochemical Analyses. *IEEE Trans. Instrum. Meas.* **72**, 1–12 (2023).

61. Fortunati, S., Giannetto, M., Rozzi, A., Corradini, R. & Careri, M. PNA-functionalized magnetic microbeads as substrates for enzyme-labelled voltammetric genoassay for DNA sensing applied to identification of GMO in food. *Anal. Chim. Acta* **1153**, 338297 (2021).

62. B. Magnusson and U. Örnemark. Eurachem Guide: The Fitness for Purpose of Analytical Methods – A Laboratory Guide to Method Validation and Related Topics. in *Eurachem Guide: The Fitness for Purpose of Analytical Methods – A Laboratory Guide to Method Validation and Related Topics* (2014).

63. Yáñez-Sedeño, P., Campuzano, S. & Pingarrón, J. M. Magnetic particles coupled to disposable screen printed transducers for electrochemical biosensing. *Sensors (Switzerland)* **16**, (2016).

6 *Micropore nanoelectrodes*

6.1 INTRODUCTION

Blood cells counting provides important information about people general health status and can be used to diagnose illnesses and determine the exact treatment[1]. In particular, Coulter counters are widely used in the hospital settings for the complete blood counts (CBC), used for the analysis of white and red blood cells in patients[2]. These techniques are based on Coulter Counter principle, stating that non-conductive cells suspended in an electrolyte, determine changes in electrical resistance[3]. They aim at detecting individual molecules passing through a pore giving changes in ionic pore current. Among the different advantages, they are label-free and do not require immobilization of the analytes on the surface. Coulter counters are typically composed of two electrolyte-filled chambers connected through a microscale aperture.

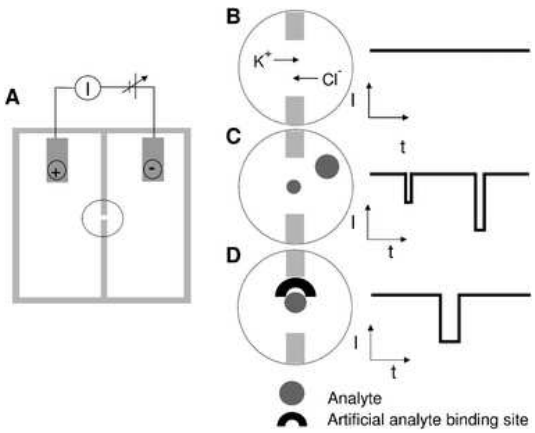

Figure 6.1: General scheme of Coulter Counter principle and nanopore analytics. Reprinted with permission from Ref. 1 © Royal Society of Chemistry

Two electrodes and a potentiostat give a transmembrane potential which drives an ionic current through the opening. When microparticles or eukaryotic cells are added and pass through the pore, they can cause short pulses of altered resistance. The number and amplitude of pulses detected are proportional to the number and

volume of particles, respectively. Also other techniques, as for example nanopore sequencing[4], are based on a nanoscale protein pore, or “nanopore” working as a biosensor embedded in an electrically resistant membrane.

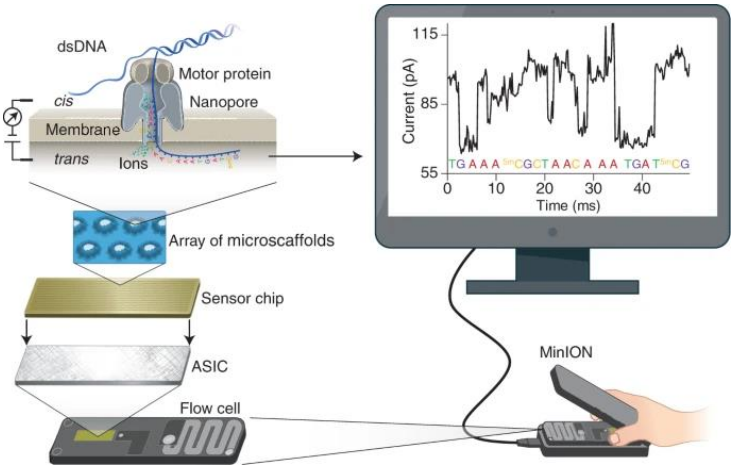

Figure 6.2: General scheme of nanopore sequencing. Reprinted with permission from Ref.2 © 2008, Springer Nature America, Inc.

Here, a constant voltage is applied in an electrolytic solution, to obtain an ionic current through the nanopore[5]. In this way, negatively charged single-stranded DNA or RNA molecules are driven through the nanopore from the negatively charged side to the positively charged side. Changes in the ionic current during translocation correspond to the nucleotide sequence present in the sensing region decoded using computational algorithms, allowing real-time sequencing of single DNA strands. Moreover, the motor protein has helicase activity, to obtain single-stranded sequences that pass through the nanopore. These techniques have been commonly applied for DNA, RNA, peptide identification and biosensing pathological biomarkers. In particular, several nanopore biosensors have been developed with different systems, like biological nanopores and solid-state nanopores[6]. However, to date, little attention has been paid to the detection of whole cells in the micron scale. The importance of continuous blood analysis that can be performed outside the hospital settings has determined the need for easy-to-use, low-cost and reliable

devices, consistent with the Point-of-Care concept. Several devices have been developed as a miniaturization of Coulter Counter instruments[1,6,7].

In the context of the research activity carried out at Catalan Institute of Nanoscience and Nanotechnology (ICN2), the fabrication of nanoelectrodes with a micropore for the detection of different-size cells was studied. The aim of this project was to create low-cost, miniaturized and possibly implantable Coulter Counters to monitor different-size cells, as red blood cells or macrophages. The initial part of this project involved the evaluation of different parameters for the preparation of micropore nanoelectrodes. A protocol was developed by the hosting research group regarding the fabrication of nanoelectrodes with clean-room free, rapid and cheap methods with respect to the traditional methods that are expensive and time-consuming[8]. Specifically, this protocol involves the deposition of metallic thin films using a sputter-coater. These metallic films are deposited onto a substrate and covered with a capping layer. Finally, they are cut at the edge to obtain a nanoband electrode. Starting from this protocol, the aim of this project was to create micropore nanoelectrodes, consisting of a single device with two gold nanoelectrodes and a pore between them to detect the molecules passing through it by means of changes in current, depending on their dimensions.

6.2 MATERIALS AND METHODS

6.2.1 Materials and chemicals

Sputter coater Quorum SC7620 and gold target were purchased from ANAME Instrumentaciòn Cientifica (Madrid, Spain). Polyethylene terephthalate (PET), Polyethylene naphthalate (PEN) and Kapton were purchased from GoodFellow GmbH (Spain). Kapton tape 5413 was purchased from DigiKey, Acrylic Varnish Clear Brilliant was purchased from RS Components Spain. Polystyrene microbeads (1,8,25 µm diameter) were purchased from Sigma Aldrich (Germany), PRESCH Drilling Clamp was purchased from Amazon, needles were purchased from Presch (Germany) and Rapid-Core Sampling Punches were purchased from TedPella Inc. (USA). Potassium hexacyanoferrate (III) ($K_3[Fe\ (CN)_6]$) and potassium hexacyanoferrate (II) 3-hydrate ($K_4[Fe\ (CN)_6]\cdot 3H_2O$), 3,4-Ethylenedioxythiophene (EDOT), Lithium Perchlorate ($LiClO_4$) 2-propanol (IPA), acetone and Phosphate Buffered Saline (PBS) were purchased from Merck (Milan, Italy and Germany).

6.2.2 Equipment

Masks were created using AutoCAD Software, 2021 and produced using a GraphTec ce6000-40 plotter. Gold screen-printed electrodes Dropsens C220 (DRP-C220 BT) were purchased from Metrohm SRL (Origgio, Italy). Ag/AgCl reference electrodes and platinum wire counter electrodes were purchased from Dropsense, Spain. Screen-printed Gold Electrode (DRP-220BT) were purchased from Metrohm (Origgio, Italy). All solutions were prepared in distilled water and deionized water from a Milli-Q Advantage A10 Water Purification System with 0.22 µm filters MPGP04001 (18.2 MΩ cm, Merck Millipore, Spain). Electrochemical measurements were performed using a benchtop Potentiostat Autolab PGSTAT 204 (Metrohm, Origgio, Italy) with NOVA 2.1.6 in University of Parma, Italy and a Metrohm Autolab

PGSTAT 12 with NOVA 2.1 Software in ICN2, Spain. Olympus IX71 Inverted Microscope was used to characterize nanoelectrodes, Scanning Electron Microscope (SEM) Fei Quanta 200 was used for characterization of DRP-220BT coated with electropolymerized EDOT (PEDOT).

6.2.3 Micropore nanoelectrodes preparation

Nanoelectrodes were prepared according to previously optimized and described methods[8] (Experimental Section- Nanoelectrode Fabrication) with several changes in the final part to obtain micropores.

6.2.3.1 Sputtering

The substrate was cut to obtain squares with dimensions compatible with both the masks and the sputter coater. Substrates were washed keeping them in acetone for 5 min, IPA for 5 min and finally rinsing with water. They were subsequently placed into the sputter-coater already equipped with the gold target and a vacuum was applied to reach a pressure lower than 0.8 mbar. The chamber was flushed with Argon three times. Then potential was applied to begin sputtering. 10 mA current and a deposition rate of 5 nm/min were chosen. For this project, a thickness of 80 nm was chosen, determining a duration of 16 minutes for sputtering.

6.2.3.2 Capping layer

After removing devices from sputter-coater, capping layer was prepared testing adhesive Kapton tape and Varnish Spray. The former was applied by hand-fixing the electrodes on a surface and pushing to avoid bubble formation. For the latter, the area that had to be covered was isolated with a plastic mask and spray was applied and left to dry for about 20 min.

6.2.3.3 Punching

To create the pore, different techniques were tested. As for Drilling Clamp, the electrodes were placed onto the disk to create the pore and punched with the smaller dimension of the clamp (2.0 mm). As for needles and sampling punches, electrodes were placed upside down onto a pad, then needles and punches were pushed by hand to create the pore.

6.2.3.4 Electropolymerization

Electropolymerization of PEDOT was carried out on DRP-C220BT and micropore nanoelectrodes with a solution of 0.01 M EDOT- 0.1 M $LiClO_4$ in water. Cyclic voltammetry was performed from -0.2 V to +1.1 V for different number of cycles at a scan rate of 0.05 V/s, with Ag as Reference Electrode and Pt Wire as counter electrode.

6.2.3.5 Micropore nanoelectrodes characterization

After preparation, nanoelectrodes were characterized with Olympus IX71 Inverted Microscope at different magnifications. They were then tested with electrochemical measurements in a solution containing 0.05 M potassium ferricyanide, 0.05 M potassium ferrocyanide in PBS. CV were performed from -0.1 to 0.45 V at a scan rate of 0.01 V/s using Ag/AgCl reference electrode and Pt wire counter electrode. As for characterization of SPE after electropolymerization, SEM images were acquired to study the morphology of PEDOT deposed on the surface.

6.2.3.6 Tests with beads

To mimic real samples, tests with different-size beads (1,8,25 µm) were performed. Chronoamperometry (CA) measurements were carried out at 0.2 V for 400 seconds in 0.05 M potassium ferricyanide, 0.05 M potassium ferrocyanide in PBS. Beads

were 1000-fold diluted in water and pushed through the micropore with the help of a micropipette every 60s to evaluate the change in current.

6.3 *RESULTS AND DISCUSSION*

6.3.1 Fabrication protocol

The aim of this project is to create micropore nanoelectrodes consisting in a single device composed of two separated gold electrodes with a pore between them. Therefore, the sensing surface is represented from the exposed gold between the two electrodes, thus giving the possibility to measure the change in current when different-size molecules are passing through the pore. In particular, it could be considered for the detection of micron scale biomarkers in blood. These analytes, such as red blood cells or macrophages, can give a different change in current when they are passing through a pore depending on their dimensions. Besides, red blood cells can have different dimensions in people affected by sickle anaemia[9], while macrophages are important to evaluate the inflammatory process. To prepare these nanoelectrodes, three different steps were required (Figure 6.3):

- Gold-deposition on substrate with sputter-coating techniques and sputtering masks
- Covering with insulating materials to create the capping layer
- Pore punching to create the micropore.

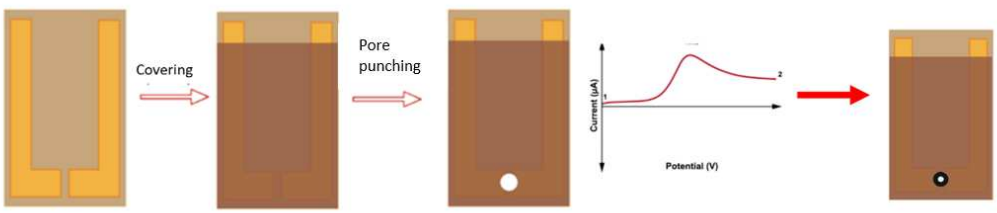

Figure 6.3: Schematic representation of fabrication of Micropore nanoelectrode

Moreover, to control the pore dimension, electropolymerization of PEDOT was carried out in order to generate, starting from nanoelectrodes with the same pore dimension, different-size pores to make them suitable for the detection of different-size biomarkers. Electropolymerization appears to be a promising approach as it only requires a further step, without the need of creating different-size pores during the nanoelectrodes' fabrication. For example, different-diameters pores could be prepared in order to improve red blood cells detection (8 µm diameter) or macrophages detection (about 20 µm diameter).

During the research period spent in ICN2, the fabrication process was studied and the best solutions for different aspects were found. The first considered aspect was the dimension of the pore and, therefore, the distance between the two electrodes. To this end, different sputtering masks were designed and prepared with different distances (2 mm- 0,5 mm- 0,3 mm-0.16mm) as shown in Figure 6.4.

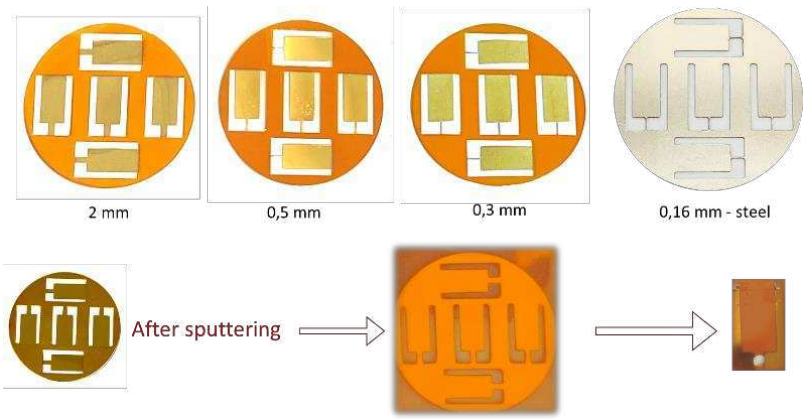

Figure 6.4: Designed mask for different distances between electrodes.

These masks were tested in combination with different capping layers and punching techniques. Taking into account that the aim is to detect molecules in the order of micrometers, masks with lower distances were preferable as they also give the possibility to create pores with smaller diameters.

6.3.2 Pore punching methods

To control the size of the pores, different techniques were evaluated, determining different diameters' pores. In combination with the designed mask, in particular, three methods were considered:

- Drilling clamp in combination with 2mm mask
- Needles in combination with 0,5 mm mask
- Sampling punches with 0,3 mm and 0,16 mm masks.

For all the three methods, working electrodes were obtained and characterization with CV was performed. CVs were performed testing separately the two electrodes with external RE (Ag/AgCl) and CE (Pt wire). However, drilling clamps and needles did not give a homogeneous cut, thus causing different exposed gold surface between the two electrodes resulting in different levels of current when performing CV measurements and, consequently, not reproducible data, as shown in Figure 6.5.

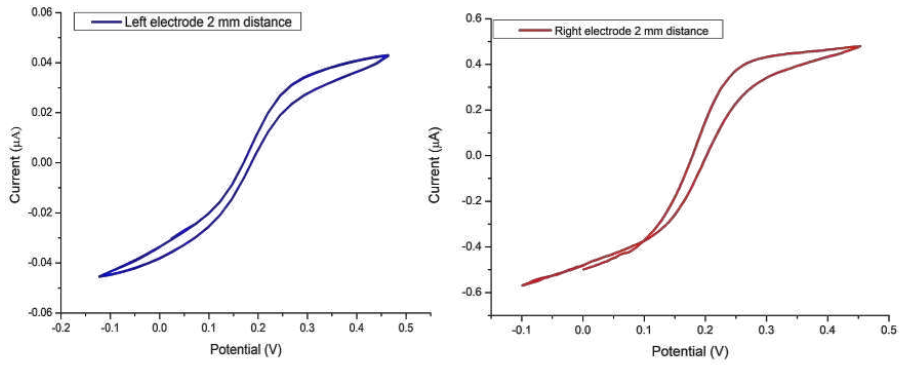

Figure 6.5: Electrochemical characterization of micropore nanoelectrodes sputtered with 2mm mask and punched with drilling clamp.CV performed in 0.05 M ferrocyanide/ferrycianide solution in 1x PBS (RE: Ag/AgCl; WE: Pt wire) from -0.1 V to 0.45 V. Scanrate 0.01 V/s

The best conditions were found with the last combination, in particular with 0,16 mm as smaller pore size and reproducible results were obtained, as shown in Figure

6.6. In fact, considering that the diameter of the sampling punches is 0,3 mm with 0,16 mm distance, it resulted more practical to create a homogeneous pore for the two electrodes. Under these conditions, it is also easier to obtain an efficient polymerization on both the electrodes, thus giving the possibility to control and tune the pore size.

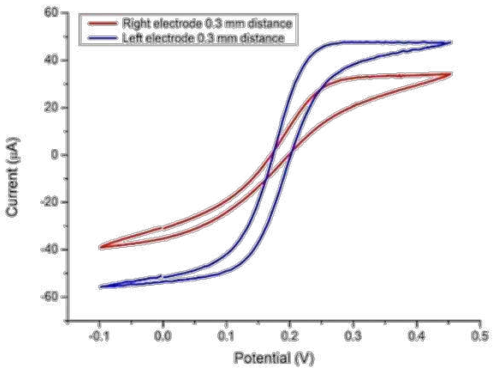

Figure 6.6: Electrochemical characterization of micropore nanoelectrodes sputtered with 0.3 mm mask and punched with sampling punches. CV performed in 0.05 M ferrocyanide/ferrycianide solution in 1x PBS (RE: Ag/AgCl; WE: Pt wire) from -0.1 V to 0.45 V. Scanrate 0.01 V/s.

6.3.3 Capping layer methods

After testing different punching and sputtering methods, different capping layers were evaluated. Electrodes were covered and tested with Kapton adhesive tape and acrylic varnish spray. Good performance was obtained in all cases, but the acrylic varnish gave a better response as shown from the characterization at the microscope and with electrochemical measurements with respect to Kapton adhesive tape. Probably, the punching step has less impact on electrodes with acrylic varnish that remains homogeneous, while Kapton tape can be damaged, as shown in figure 6.7.

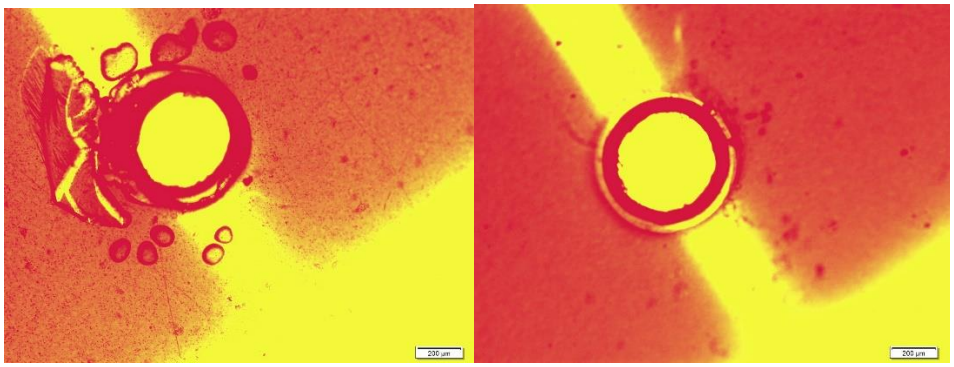

Figure 6.7: Images from Olympus IX71 Microscope: micropore nanoelectrodes covered with Kapton adhesive tape (left) and acrylic varnish spray (right).

Therefore, the conditions for fabrication of micropore nanoelectrodes in the following experiments were: 0,16 mm sputtering mask acrylic varnish spray as capping layer and sampling punches for the pore. To further improve the performances of these nanoelectrodes, measurements were carried out exploiting them as a three-electrode system: in particular, one gold electrode was connected with RE and CE, while the other electrode was used as WE. CV measurements were performed, giving good results and showing their suitability as complete systems without the need for external RE and CE. In this way, they can be adapted also for the measurement of small volumes, as shown in figure 6.8.

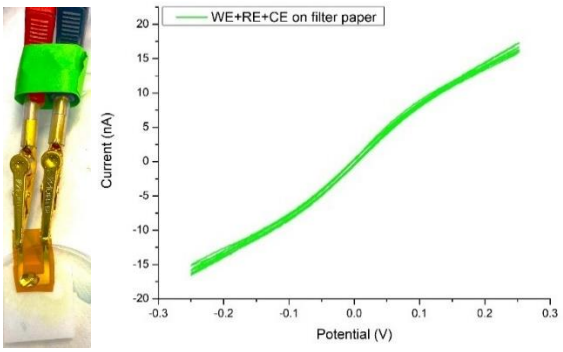

Figure 6.8: (Left) Representation of three-electrode system micropore nanoelectrodes tested on filter paper with 50 µl of solution. (Right) CV performed in 0.05 M ferrocyanide/ferrycianide solution in 1x PBS from -0.25 V to 0.25 V. Scanrate 0.01 V.

6.3.4 Electropolymerization

In order to make the pore size tuneable, electropolymerization of EDOT was considered with the aim of regulating the dimension of the pore with electrochemical techniques and to improve the flexibility of the device for multiple applications. Several issues have arisen for this process, as it was difficult to reach the proper direction of polymerization and direct it through the pore. To tackle this issue, electropolymerization was first tested on SPEs taking into account previously described procedures[10,11]. The best results were obtained with CV, as shown in Figure 6.9.

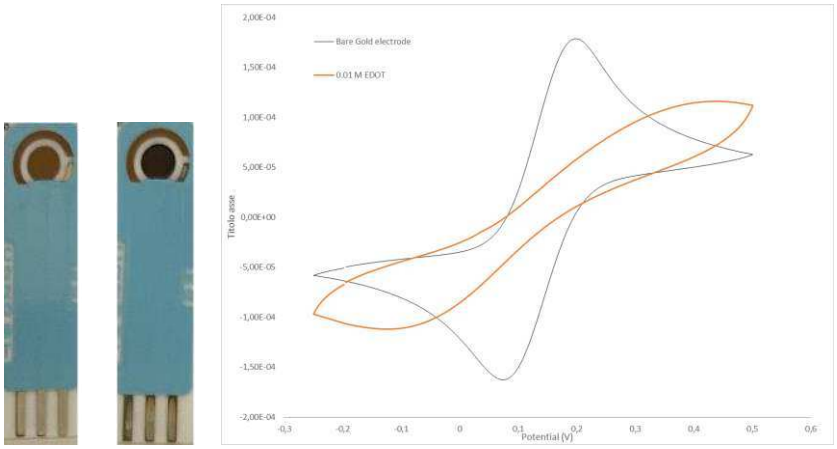

Figure 6.9: SPEs before and after electropolymerization (left); CV before & after polymerization performed in 0.05 M ferrocyanide/ferrycianide solution in 1x PBS from -0.25 V to 0.25 V. Scanrate 0.01 V.

Both SPEs and micropore nanoelectrodes were characterized with SEM, as shown in figure 6.10.

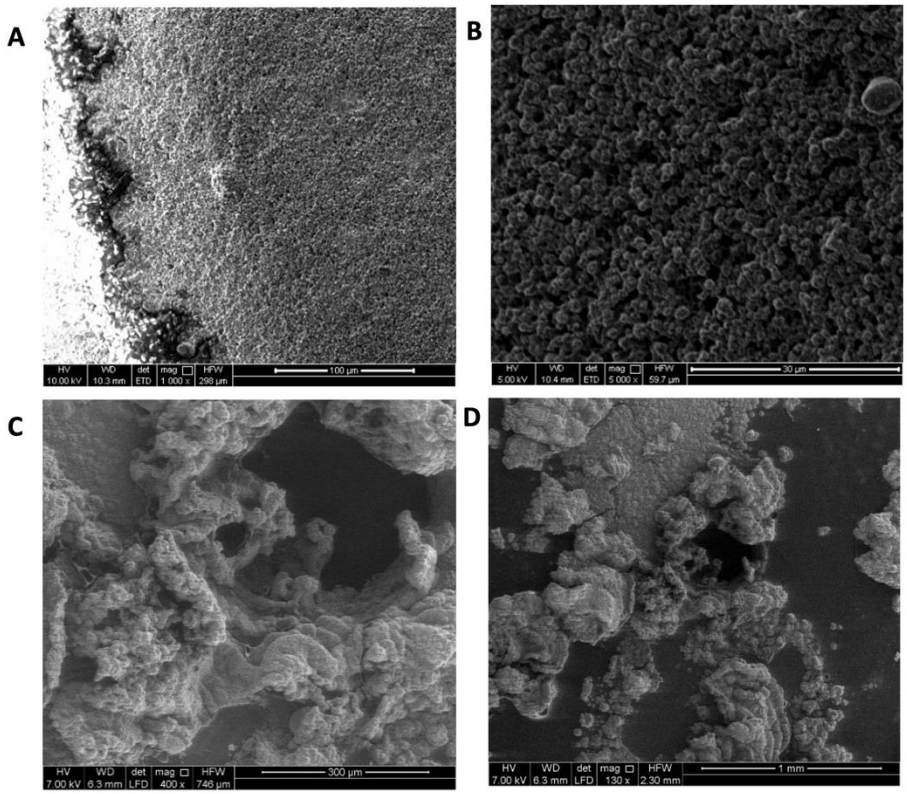

Figure 6.10: SEM characterization of SPEs electrodes after electropolymerization of PEDOT (A-B) and micropore nanoelectrodes after electropolymerization (C-D).

As shown in Figure 6.10 C-D, the direction of polymerization in micropore nanoelectrodes did not allow to manage the pore dimension as polymer was not directed into it. To this aim, new electrodes were prepared and with the same conditions used for SPEs, the pore was completely closed. Therefore, by managing CV parameters it will be possible to have different pore dimensions also for nanoelectrodes. Figure 6.11 shows the nanoelectrode after electropolymerization.

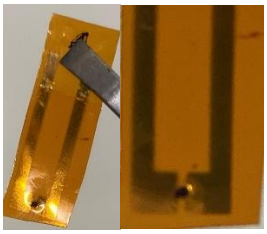

Figure 6.11: Micropore nanoelectrodes after electropolymerization with EDOT

6.3.5 Tests with beads

In order to mimic the real samples, tests with different-size beads were performed. In particular, three different diameters were considered: 1 µm to evaluate the minimum detectable, 8 and 20 µm to mimic red blood cells and macrophages, respectively. These tests were performed in chronoamperometry, by passing the beads through the micropore with the help of a micropipette. Beads were 1000-fold diluted in water and added to solution every 60s.

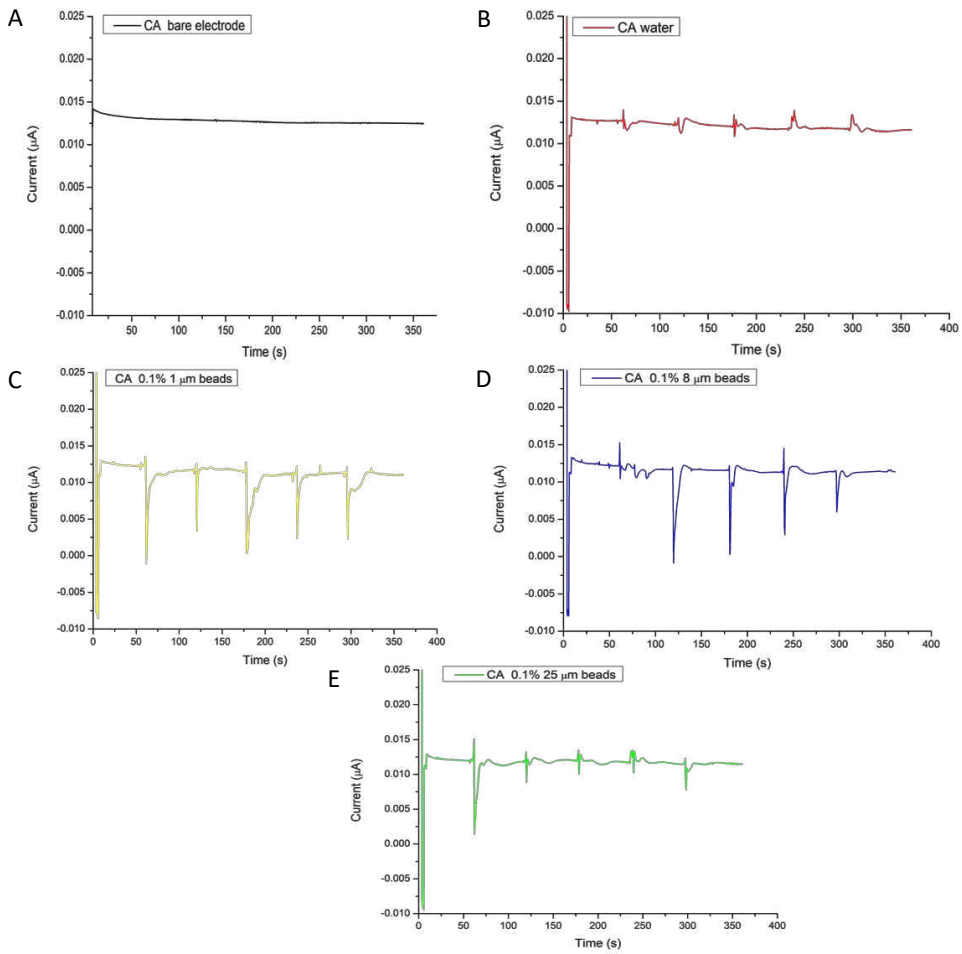

Figure 6.12: CA at 0.2 V performed in 0.05 M ferrocyanide/ferrycianide solution in 1x PBS for 400s, with addition of beads every 60s. Tests were performed with A) bare electrode B) addition of water (tested as blank sample) C) 0.1 % 1 µm beads- D) 0.1 % 8 µm beads E) 0.1 % 25 µm beads

Figure 6.12 shows the changes in current when beads are passing through the pore, showing a noticeable difference with water solution. However, there is still not a clear differentiation among the three different sizes of beads. To this end, the combination between different sizes of beads and micropores obtained through electropolymerization could be advantageous and provide a better discrimination.

6.4 CONCLUSION AND FUTURE OUTLOOKS

During my period in ICN2, the initial part of this project was approached. Further studies will be carried out to optimize the pore dimension through electropolymerization. In particular, different-size beads will be combined with different-size pores to monitor the response to different-size molecules and mimic the real sample. Moreover, the system will be integrated into a microfluidic system to control the flow of the samples that will be tested. Finally, validation on real samples will be carried out to monitor the presence of different-size molecules, as red blood cells in sickle anaemia or macrophages in inflammation, as a proof-of-principle that these devices could be also used to monitor continuously the patients.

6.5 REFERENCES

1. Chen, Y. *et al.* Portable Coulter counter with vertical through-holes for high-throughput applications. *Sensors Actuators, B Chem.* **213**, 375–381 (2015).

2. Howorka, S. & Siwy, Z. Nanopore analytics: Sensing of single molecules. *Chem. Soc. Rev.* **38**, 2360–2384 (2009).

3. Hurley, J. Sizing Particles with a Coulter Counter. *Biophys. J.* **10**, 74–79 (1970).

4. Branton, D. *et al.* The potential and challenges of nanopore sequencing. *Nat. Biotechnol.* **26**, 1146–1153 (2008).

5. Wang, Y., Zhao, Y., Bollas, A., Wang, Y. & Au, K. F. Nanopore sequencing technology, bioinformatics and applications. *Nat. Biotechnol.* **39**, 1348–1365 (2021).

6. Lenhart, B. *et al. Nanopore fabrication and application as biosensors in neurodegenerative diseases*. *Critical Reviews in Biomedical Engineering* vol. 48 (2020).

7. Merchant, C. A. *et al.* DNA translocation through graphene nanopores. *Nano Lett.* **10**, 2915–2921 (2010).

8. Storm, A. J., Chen, J. H., Zandbergen, H. W. & Dekker, C. Translocation of double-strand DNA through a silicon oxide nanopore. *Phys. Rev. E. Stat. Nonlin. Soft Matter Phys.* **71**, 51903 (2005).

9. Santos, A., Kumeria, T. & Losic, D. Nanoporous anodic aluminum oxide for chemical sensing and biosensors. *TrAC - Trends Anal. Chem.* **44**, 25–38 (2013).

10. Maroli, G., Abarintos, V., Piper, A. & Merkoçi, A. The Cleanroom-Free, Cheap, and Rapid Fabrication of Nanoelectrodes with Low zM Limits of Detection. *Small* **2302136**, 1–11 (2023).

11. Sundd, P., Gladwin, M. T. & Novelli, E. M. Pathophysiology of Sickle Cell Disease. *Annu. Rev. Pathol. Mech. Dis.* **14**, 263–292 (2019).

12. Giannetto, M., Mori, G., Terzi, F., Zanardi, C. & Seeber, R. Composite

PEDOT/Au Nanoparticles Modified Electrodes for Determination of Mercury at Trace Levels by Anodic Stripping Voltammetry. *Electroanalysis* **23**, 456–462 (2011).

13. Bello, A. *et al.* Optimization of the DPV potential waveform for determination of ascorbic acid on PEDOT-modified electrodes. *Sensors Actuators, B Chem.* **121**, 430–435 (2007).